Prediction-based power management strategy and optimum capacity design of a battery and hydrogen system for DC grid with photovoltaic power generation

著者	NGUYEN THI HOAI THU
year	2017
その他のタイトル	太陽光発電連系直流系統のための蓄電・水素システムに関する予測を基にした出力制御方策ならびに最適容量設計
学位授与大学	筑波大学 (University of Tsukuba)
学位授与年度	2016
報告番号	12102甲第8094号
URL	http://hdl.handle.net/2241/00148267

Prediction-based power management strategy and optimum capacity design of a battery and hydrogen system for DC grid with photovoltaic power generation

March 2017

NGUYEN THI HOAI THU

Prediction-based power management strategy and optimum capacity design of a battery and hydrogen system for DC grid with photovoltaic power generation

Graduate School of Systems and Information Engineering
University of Tsukuba

March 2017

NGUYEN THI HOAI THU

ABSTRACT

In the context of energy crisis and the environmental concerns, the integration of distributed energy resources from renewable energy (RE) and storages in the form of Microgrid (MG) is becoming a promising solution for power generation. The advantages of MG have motivated numerous researches in order to develop and broaden its application into the normal life. The purpose of almost all studies on RE based generation MG is to guarantee and improve its feasibility in both technical and economical issues. In this study, both these aspects in the short-time as well as in the long-time operation of a MG based on photovoltaic (PV) generation and storages are considered for the stable and sustainable operation.

Power management strategy (PMS) plays an important role in the operation of the system. In this research, a PMS based on the dynamic characteristics of the devices and the trend-prediction of the power is proposed. Firstly, the system components' dynamic characteristics are measured and modeled. The transient characteristic of fuel cell (FC) is slow while that of battery is fast. Secondly, based on the results, we propose a new trend-prediction PMS using Kalman Filter (KF) for the system including PV, FC and Lithium-ion battery (LiB). In the case of shortage power, the trend of power for storages calculated by the difference of PV power and load power will be predicted and designated to FC. LiB will cover the rest fluctuated power. KF parameter can be suitably selected for the predicted value satisfying the limited power changing rate of FC. The effectiveness of the new control method will be evaluated through simulation using real data of PV power and the load demand and compared with conventional PMS. The proposed PMS can give more economically effective performance than the conventional PMS.

Another issue that needs to be solved is the required capacity of battery for an existing PV/hydrogen system which includes FC, hydrogen tank and electrolyzer (EL). Due to the high cost, the estimation of the least battery capacity requirement for compensating any potential fluctuations becomes necessary. Therefore, in this part, we aim at downsizing the battery capacity requirement in the hybrid PV/hydrogen system by the trend-prediction PMS when the allowed maximum power changing rate of hydrogen system and the charge/discharge process efficiency are also taken into

consideration. The results reveal that using KF with suitable noise covariance Q can reduce the necessary energy of battery in comparison with no-prediction PMS of up to 56%. The PMS is then improved by combining KF and the power adjustment based on the state of charge of the battery. The simulation results show that the improved PMS achieves better effectiveness in decreasing the required capacity of battery than using the KF-PMS of about 14%.

When the economic criteria and the operation over the project lifetime are considered, it is essential to define the proper sizing of the system in order to use the RE more efficiently and economically. So far, there has been no common formula showing the dependence of the system reliability on the weather conditions and the devices capacity. We optimize the size of the system based on minimizing the levelized cost of energy (*LCE*) subjected to a required grid dependency (*GD*). Firstly, we establish an empirical formula showing the dependence of the *GD* on weather conditions and devices capacity. The formula will give a simple way to rapidly calculate the *GD* for any other location in Japan. The results illustrate that the *GD* depends on the annual total solar insolation without taking the waveform of the weather data into consideration and inconsiderably depend on the locations in Japan. The verification results show that the formula can be applied in estimating the *GD* of the system quickly and precisely. Secondly, the optimal capacity of the PV and storages can be rapidly estimated using a simple iterative method based on the required *GD* and the lowest *LCE*. In addition, the sensitivities analysis is conducted to investigate how the *LCE* changes when the parameters change. The results indicate that the *LCE* is more sensitive with the variation of the PV cost, the battery cost, the battery lifetime and the interest rate than the variation of the EL/FC cost. Thirdly, we examine the effect of the PMS proposed in the previous chapter and the fluctuated waveform of load on the *GD* and compare it with the *GD* calculated by the formula.

In conclusion, some issues of the PV-based generation MG are considered in this research for the stable and economical performance of the system during the short-term as well as long-term operation of the system: power management strategy based on dynamic characteristics using trend-prediction and the optimal sizing of devices in the system. As for each problem, the solution is proposed and proves its effectiveness in the application.

TABLE OF CONTENTS

LIST OF FIGURES

LIST OF TABLES

Chapter 1: Introduction

1.1 General introduction on Renewable Energy – based DC Microgrid

Energy plays an important role in the development of the world due to its necessity for every living requirement of humankind [1~4]. Energy is currently mainly supplied by the conventional energy sources, for example from coal, petroleum, natural gas, crude oil, etc. Figure 1 shows the total primary energy supply by resources in the world in 1993, 2011 and estimation for 2020 [5]. The fossil fuel was estimated to supply up to about 80% of the total energy. However, fossil fuel is nowadays more and more exploited, which in turn leads to various problems, for example, its depletion, the increasing price [1,2,6~9] and the political instabilities in the regions of energy sources [7]. Meanwhile, the nuclear power has another problem of the public opponents that concern the occurrence of the hazardous accidences [10]. In addition, the conventional energy can produce the greenhouse gas emissions or air pollutions, which may be one of the main causes of the global warming. Therefore, an urgent need for the renewable and sustainable energy sources is required [1-11].

A sustainable energy system is regarded as a cost-efficient, reliable, and environmentally friendly system [12]. Renewable energy (RE) such as wind, solar, water, sea, biomass and geothermal energy may be attracting attention as a promising alternative of the conventional power [1,2,6,12,13]. RE technologies show many advantages which include energy security, non-greenhouse gas emissions, and especially, the sustainable development. RE sources can create more job and business opportunities [1,2,6~13]. According to IEA statistic data of CO_2 emissions from Combustion [14], up to 44% of the global CO_2 emissions was produced from coal while only 1% from non-fossil fuel (Figure 1.2). Being considered as clean and safe power generation, RE is also easily adopted from the social viewpoint [10, 15].

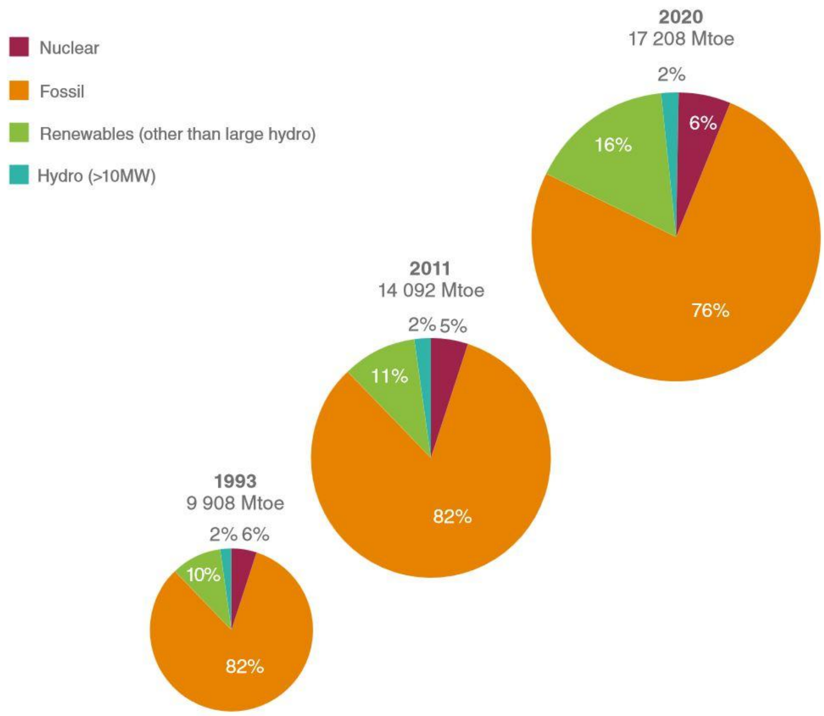

Figure 1.1: Total primary energy supply by resources in 1993, 2011 and estimation in 2020 [5]

Additionally, RE is an attractive option for supplying loads in remote area [6, 7]. Along with the advantages, there are still some associated drawbacks which are their intermittent nature depending on the locations and the seasons, and the high capital cost of implementation [1,2,6,7,15,16] . The fluctuated output power from RE may lead to the difficulty in satisfying the load at any instant. To overcome these obstacles, RE sources are always integrated with other energy storages in order to meet the load demand during the varying natural conditions and the fluctuation of the load [4, 16~25].

Energy storage can be categorized into short-term and long-term storage. Hydrogen system, as long-term storage, which includes fuel cell (FC), water electrolyzer (EL) and hydrogen storage tanks, uses hydrogen as alternative form of

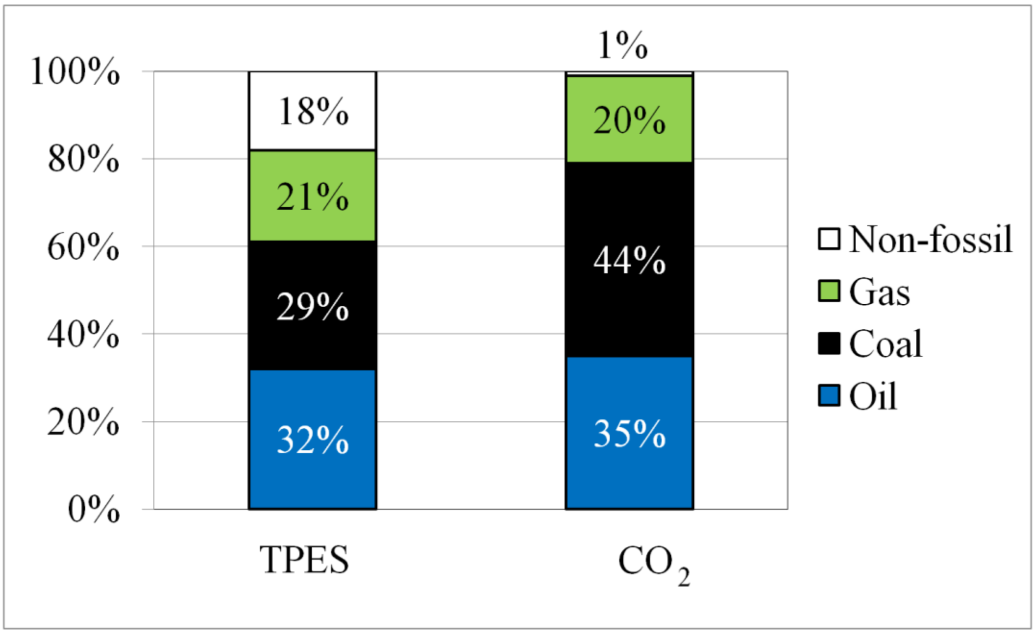

Figure 1. 2: World primary energy supply and CO_2 emissions shares by fuel in 2011[14]

energy [18~23] . Because of its high energy density, it can provide a viable, efficient energy for a long time. However, its slow dynamic characteristics make it difficult to effectively respond to the fluctuation of the RE or the load. Battery, as one of short-term energy storages, which has advantages of fast charging/discharging capacity and high round-trip efficiency, but also has disadvantages of low energy density, self-discharge and leakage, can be used to cover the sudden change of RE and load [19,21~23] .

The integration of RE sources and storages in the form of Microgrid (MG) have been recently developed and implemented in various locations around the world [26]. A MG can be defined as a local power generation which may either be based on renewable energy or fossil, combined with storages and loads, and operate as a single controllable system. It can work in either grid-dependent or stand-alone mode by connecting or disconnecting from the utility [27~30]. The operation of MG can decrease the stress on transmission and distribution system of the centralized electrical grid [30]. The advantages of MG have motivated extensive researches to develop and broaden its application into the normal life [30, 31]. Numerous studies on these systems have been conducted on various aspects, for example, the characteristics of the devices, their modeling, control method, optimal operation, optimal sizing, etc. The purpose of almost all studies on RE-based generation MG is to guarantee and improve its feasibility in both technical and economical issues. As for short-time operation, the system will be controlled in order to secure the stability against the sudden fluctuation of supply and demand. Meanwhile, for the long-time operation, along with the technical criteria, the economic effectiveness is also taken into consideration.

Figure 1.3 illustrates the image of a RE generation-based Microgrid [32] (a) and the scheme in the case of DC grid with PV/Hydrogen system and battery (b). The use of DC bus is popular in the RE generation based Microgrid due to its advantages over AC energy distribution [28, 33-35]. The electrical energy produced and consumed by PV, hydrogen system and battery is in the form of the DC electrical energy while all the load demand are consumed in AC form. Hence it is compulsory to convert DC into AC for consumers by DC/AC converter [34]. The number of DC/AC converters in AC network will be high corresponding to the generators and storages. Meanwhile, using DC distribution network inside the system will decrease these DC/AC converters, thus reducing some problems involving in DC/AC converter such as harmonics, the loss of energy, the cost, etc. [34, 35]. Additionally, if a short circuit occurs at the load side, it will not affect the remaining parts of the system [35].

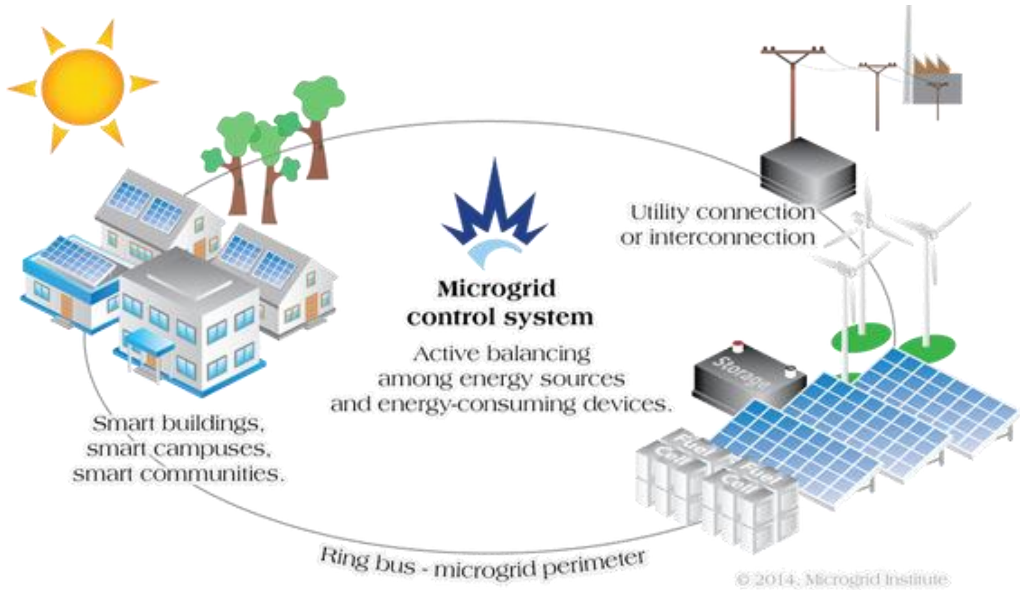

(a)

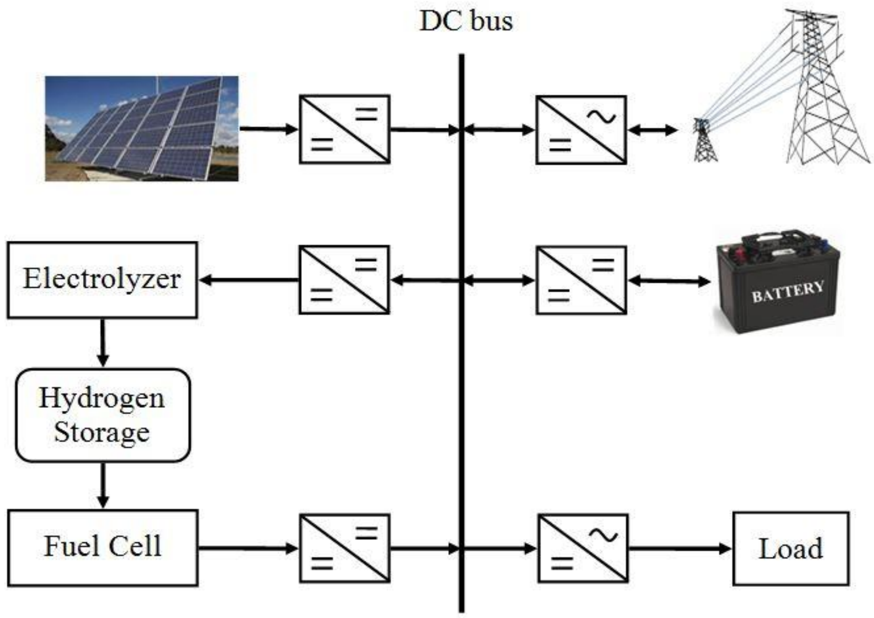

(b)

Figure 1.3: The image of a Renewable Energy generation – based Microgrid [32] (a) and the scheme in the case of DC grid with PV/Hydrogen system and battery (b).

1.2 Motivation of the research

In order to widely implement and apply the RE-based MG into the energy sector to support the conventional main grid, numerous studies have been carried out. Many aspects of the system were considered such as the modeling, the control method including both supervisory and local control, the interconnection to the grid, optimal sizing, etc.

The most important problem for the system is the control strategy to ensure the equality between the supply and the demand against the fluctuation of the Load and the RE source at any instant. Significant efforts have been devoted to the power management strategy (PMS), which is the algorithm to allocate the power and control the performance of the devices [18,19,22,23,36-38]. The main objective of a PMS is to ensure the load satisfaction under power sources' fluctuations. However, because almost all the PMS were based on the power and the state of charge (SOC) of the battery to make decision which storage would operate, the sampling time must be long enough for the FC being able to work without error. In addition, many researches are based on the theoretical model due to the high capital cost of the system design and implementation. So far, the dynamic characteristics of the devices in a big-scale system have not been considered.

Another problem motivated the researches for the feasibility of the system is the optimal sizing of the system. Sizing optimization of the RE-based MG is very important because in fact, the cost of energy produced from such a system is quite expensive in comparison with conventional energy, reducing the energy cost will make it feasible to any application in industrial as well as in domestic sector. Numerous studies on sizing optimization have been conducted in literatures. Most of the researches solved the problem by examining the optimization functions which were based on minimizing an economic criterion such as the cost of the system [39,40], the levelized cost of energy (*LCE*) [41-43] or maximizing the net present value (*NPV*) of the system [44] subjected to the required system reliability such as loss of power supply probability (*LPSP*) [39,41,42], loss of load expected (*LOLE*), loss of energy expected (*LOEE*) or Expected Energy not Supplied (*EENS*), etc. [45]. However, almost all the existing researches assessed the system reliability using the weather data in a typical year or supposed solar irradiance waveform for a certain location. With the different weather data at a different location, the optimization process must be reconducted. So far, there has been no empirical formula showing the dependence of the system reliability on the weather conditions and the devices capacity. Such empirical formula not only shows the relationship between them but also makes the optimization problem become simpler and easier.

Therefore, in this study, we consider both technical and economical issues in the short-time as well as in the long-time operation of a MG based on photovoltaic (PV) generation and storages by solving 2 important problems of the RE-based MG that are: i) to develop a new power management strategy based on the real dynamic characteristics of the devices and the trend-prediction of the power and ii) to design the optimal size of the system based on minimizing the levelized cost of energy and satisfying a required grid dependency which is calculated by an established empirical formula.

1.3 Target of the dissertation

The target of this research is to study and develop a stable, sustainable and economical MG including renewable energy system and storages which can be connected to or disconnected from the main grid to work dependently or off-grid mode, respectively. For the purpose of the stable and economical operation of the system, this research will solve 2 aspects of the MG as mentioned in the previous section.

The targets can be summarized as follows:

- R&D the control methods for RE systems with storages for stable and economical operation in short time:
  - Study the transient response of the system components in which not only the devices but also the DC/DC converters are taken into account.
  - Enhance the efficiency and the stability in supplying power to the load demand despite the intermittent and stochastic RE power.
  - Downsize the battery capacity needed to cover the fluctuation in an existing system.
- Optimize the size of all devices in the system for the stable and economical operation in a long time:
  - Establish an empirical formula of the system reliability, namely the grid dependency (*GD*), depending on the weather condition and the capacity of the devices. The empirical formula is to estimate the *GD* in a rapid and highly accurate way.
  - Minimize the economic index, namely the levelized cost of energy (*LCE*) to find out the optimal configuration.

1.4 Outline of the dissertation

Here we outline the structure of the subsequent chapters of this thesis and highlight the contributions:

- Chapter 2 provides the background and literature reviews on the previous study of the control methods for the renewable energy sources based Microgrid. The experiments on the dynamic response of the storages, namely the battery and fuel cell are conducted. Based on the experimental results, we develop their dynamic models. The efficiencies of the energy conversion and of the DC/DC converters for each device are calculated as well. Moreover, the data of the photovoltaic power of the system over 1 year is also analyzed. A new control method which is based on the dynamic characteristics and the trend-prediction of the supply-demand power is proposed. The algorithm of the power management strategy is also presented in this chapter. The implementation of the proposed control method to the test systems is tested by simulation. The effects of the controller parameter on the performance are investigated to achieve the most effective and stable operation of the system. In addition, the effectiveness of the method is evaluated and discussed through comparison with the performance of the system using other control methods. The main reason for the effectiveness is explained in this chapter as well.

Moreover, this chapter also considers the method to downsize the required battery capacity to cover the fluctuation component of the power. The proposed trend-prediction PMS is applied to find out the sizing requirement of battery for an existing system. When the distribution of the fluctuation component is asymmetric and the efficiency of the charging/discharging process is included, the PMS will be improved by using *offset* to adjust the power for battery while the changing rate of hydrogen system is still kept within the limited range. The algorithm of the battery input/output control in the improved PMS is described. The comparison of battery capacity requirement using no-prediction PMS, trend-prediction PMS and improved trend-prediction PMS is also carried out to prove the effectiveness of the proposed PMS in decreasing the needed sizing of battery.

- Chapter 3 studies the sizing optimization of the PV/hydrogen/battery system in order to use the RE more efficiently and economically. Firstly, we summarize the studies on sizing optimization in literatures from the optimal sizing problems to the methods to solve them. Then we try to establish the grid dependency, which represents for the system reliability, depending on the weather and system configurations. We carry out the calculation of the *GD*, using the 25 – year weather data of 9 locations throughout Japan, aiming to find out the general relationship between the *GD* and other parameters. The fitting process using regressive model is conducted to establish the function between the *GD* and annual total PV energy and storages capacity. The accuracy of the fitting as well as the application of the developed *GD* formula is demonstrated by applying in other location and compared with the normal calculation. Hence, the optimal capacity of the PV and storages can be rapidly estimated using simple iterative method based on the required *GD* and the minimum *LCE*. In addition, the sensitivities analysis is conducted to investigate how the *LCE* changes when the parameters take other values. However, the PMS used in the establishment of formula is the conventional one with the time interval of 1 hour and the demand is smooth, the dynamic process is not considered. Therefore, finally we examine the effect of the PMS proposed in the previous chapter and the fluctuated waveform of load on the *GD* and compare it with the *GD* calculated by the formula.

- Chapter 4 concludes the dissertation.

1.5 References

[1] O. Erdinc, M. Uzunoglu, Optimum design of hybrid renewable energy systems: Overview of different approaches, Renewable and Sustainable Energy Reviews 16 (2012) 1412-1425.

[2] R. Banos, F. Manzano-Agugliaro, F.G. Montoya, C.Gil, A. Alcayde, J. Gómez, Optimization methods applied to renewable and sustainable energy: A review, Renewable and Sustainable Energy Reviews 15 (2011) 1753-1766

[3] S. Upadhyay, M.P. Sharma, A review on configurations, control and sizing methodologies of hybrid energy systems, Renewable and Sustainable Energy Reviews 38 (2014) 47–63

[4] A. Chauhan, R.P. Saini, A review on Integrated Renewable Energy System based power generation for stand-alone applications: Configurations, storage options, sizing methodologies and control, Renewable and Sustainable Energy Reviews 38 (2014) 99–120

[5] World Energy Resources 2013 Survey, World Energy Council http://www.worldenergy.org/wp-content/uploads/2013/09/Complete_WER_2013_Survey.pdf

[6] Prabodh Bajpai, Vaishalee Dash, Hybrid renewable energy systems for power generation in stand-alone applications: A review, Renewable and Sustainable Energy Reviews 16 (2012) 2926– 2939

[7] Engin Cetin, Ahmet Yilanci, H. Kemal Ozturk, Metin Colak, Ismail Kasikci, Serdar Iplikci, A micro-DC power distribution system for a residential application energized by photovoltaic–wind/fuel cell hybrid energy systems, Energy and Buildings 42 (2010) 1344–1352

[8] Pervez Hameed Shaikh, Nursyarizal Bin Mohd Nor, Perumal Nallagownden, Irraivan Elamvazuthi, Taib Ibrahim, A review on optimized control systems for building energy and comfort management of smart sustainable buildings, Renewable and Sustainable Energy Reviews 34 (2014) 409–429

[9] Siang Fui Tie, Chee Wei Tan, A review of energy sources and energy management system in electric vehicles, Renewable and Sustainable Energy Reviews 20 (2013) 82–102

[10] T.N. Srinivasan, T.S. Gopi Rethinaraj Fukushima and thereafter: Reassessment of risks of nuclear power, Energy Policy 52 (2013) 726–736

[11] O. Alsayegh, S. Alhajraf, H. Albusairi, Grid-connected renewable energy source systems: Challenges and proposed management schemes, Energy Conversion and Management 51 (2010) 1690–1693

[12] Arif Hepbasli, A key review on exergetic analysis and assessment of renewable energy resources for a sustainable future, Renewable and Sustainable Energy Reviews 12 (2008) 593–661

[13] Mine Tükenmez, Erhan Demireli, Renewable energy policy in Turkey with the new legal regulations, Renewable Energy 39 (2012) 1-9

[14] CO_2 emissions from fuel combustion ©OECD/IEA2013, IEA Publishing. License: http://www.iea.org/termsandconditionsuseandcopyright/

[15] Annika Skoglund, Mats Leijon, Alf Rehn, Marcus Lindahl, Rafael Waters, "On the physics of power, energy and economics of renewable electric energy sources - Part II", Renewable Energy 35 (2010) 1735–1740

[16] Pragya Nema, R.K. Nema, Saroj Rangnekar, A current and future state of art development of hybrid energy system using wind and PV-solar: A review, Renewable and Sustainable Energy Reviews 13 (2009) 2096–2103

[17] J.E. Paiva, A.S. Carvalho, Controllable hybrid power system based on renewable energy sources for modern electrical grids, Renewable Energy 53 (2013) 271-279

[18] Manuel Castaneda, Antonio Cano, Francisco Jurado, Higinio Sanchez, Luis M. Fernandez, Sizing optimization, dynamic modeling and energy management strategies of a stand-alone PV/hydrogen/battery-based hybrid system, International Journal of Hydrogen Energy 38 (2013) 3830-3845

[19] K. Zhou, J.A. Ferreira, S.W.H. de Haan, Optimal energy management strategy and system sizing method for stand-alone photovoltaic-hydrogen systems, International Journal of Hydrogen Energy 33 (2008) 477– 489

[20] Roberto Carapellucci, Lorena Giordano, Modeling and optimization of an energy generation island based on renewable technologies and hydrogen storage systems, International Journal of Hydrogen Energy 37 (2012) 2081-2093

[21] Rihab Jallouli, LotfiKrichen, Sizing, techno-economic and generation management analysis of a stand-alone photovoltaic power unit including storage devices, Energy 40 (2012) 196-209

[22] Dimitris Ipsakis, Spyros Voutetakis, Panos Seferlis, Fotis Stergiopoulos, Costas Elmasides, Power management strategies for a stand-alone power system using renewable energy sources and hydrogen storage, International Journal of Hydrogen Energy 34 (2009) 7081-7095

[23] Giorgio Cau, Daniele Cocco, Mario Petrollese, Søren Knudsen Kær, Christian Milan, Energy management strategy based on short-term

generation scheduling for a renewable microgrid using a hydrogen storage system, Energy Conversion and Management 87 (2014) 820–831

[24] Erkan Dursun, Osman Kilic, Comparative evaluation of different power management strategies of a stand-alone PV/Wind/PEMFC hybrid power system, Electrical Power and Energy Systems 34 (2012) 81–89

[25] M.S. Ismaila, M. Moghavvemi, T.M.I. Mahlia, K.M. Muttaqi, S. Moghavvemi, Effective utilization of excess energy in standalone hybrid renewable energy systems for improving comfort ability and reducing cost of energy: A review and analysis, Renewable and Sustainable Energy Reviews 42 (2015) 726–734

[26] Little M, Thomson M, Infield D., Electrical integration of renewable energy into stand-alone power supplies incorporating hydrogen storage, International Journal of Hydrogen Energy 32 (2007) 1582–1588

[27] Eklas Hossain, Ersan Kabalci, Ramazan Bayindir, Ronald Perez, Microgrid testbeds around the world: State of art, Energy Conversion and Management 86 (2014) 132–153

[28] G. Bruni, S. Cordiner, V. Mulone, V. Rocco, F. Spagnolo, A study on the energy management in domestic micro-grids based on Model Predictive Control strategies, Energy Conversion and Management 102 (2015) 50–58

[29] Linfeng Zhang, Nicolae Gari, Lawrence V. Hmurcik, Energy management in a microgrid with distributed energy resources, Energy Conversion and Management 78 (2014) 297–305.

[30] Ramon Zamora, Anurag K. Srivastava, Controls for microgrids with storage: Review, challenges, and research needs, Renewable and Sustainable Energy Reviews 14 (2010) 2009–2018

[31] Prasenjit Basak, S. Chowdhury, S. Halder nee Dey, S.P. Chowdhury, A literature review on integration of distributed energy resources in the perspective of control, protection and stability of Microgrid, Renewable and Sustainable Energy Reviews 16 (2012) 5545–5556

[32] http://www.microgridinstitute.org/about-microgrids.html

[33] Phatiphat Thounthong, Viboon Chunkag, Panarit Sethakul, Suwat Sikkabut, Serge Pierfederici and Bernard Davat, Energy management of fuel cell/solar cell/supercapacitor hybrid power source, Journal of Power Sources 196 (2011) 313–324.

[34] Engin Cetin, Ahmet Yilanci, H. Kemal Ozturk, Metin Colak, Ismail Kasikci and Serdar Iplikci, A micro-DC power distribution system for a residential application energized by photovoltaic-wind/fuel cell hybrid energy systems, Energy and Buildings 42 (2010) 1344–1352

[35] Hiroaki Kakigano, Yushi Miura, Toshifumi Ise and Ryohei Uchida, A DC micro-grid for superhigh-quality electric power distribution, Electrical Engineering in Japan 164 (1) (2008), 34–42

[36] Abdelkafi, Lotfi Krichen, Energy management optimization of a hybrid power production unit based renewable energies, Electrical Power and Energy Systems 62 (2014) 1–9

[37] M. Hattia, A. Meharrarb, M. Tioursi, Power management strategy in the alternative energy photovoltaic/PEM Fuel Cell hybrid system, Renewable and Sustainable Energy Reviews 15 (2011) 5104– 5110

[38] Erkan Dursun, Osman Kilic, Comparative evaluation of different power management strategies of a stand-alone PV/Wind/PEMFC hybrid power system, Electrical Power and Energy Systems 34 (2012) 81–89

[39] Yang Hongxing, Lou Chengzhi, Optimal design and techno-economic analysis of a hybrid solar–wind power generation system, Applied Energy 86 (2009) 163–169

[40] Xiongwen Zhang, Siew-Chong Tan, Guojun Li, Jun Li, Zhenping Feng, Components sizing of hybrid energy systems via the optimization of power dispatch simulations, Energy 52 (2013) 165-172

[41] Diaf, G. Notton, M. Belhamel, M. Haddadi, A. Louche, Design and techno-economical optimization for hybrid PV/wind system under various meteorological conditions, Applied Energy 85 (2008) 968–987.

[42] Zachariah Iverson, Ajit Achuthan, Pier Marzocca, Daryush Aidun, Optimal design of hybrid renewable energy systems (HRES) using hydrogen storage technology for data center applications, Renewable Energy 52 (2013) 79-87

[43] Benjamin Guinot, Benedicte Champel, Florent Montignac, Elisabeth Lemaire, Didier Vannucci, Sebastien Sailler, Techno-economic study of a PV-hydrogen-battery hybrid system for off-grid power supply: Impact of performances' ageing on optimal system sizing and competitiveness, International Journal of Hydrogen Energy 40 (2015) 623- 632

[44] Rodolfo Dufo-Lopez, Jose L. Bernal-Agustın, Franklin Mendoza, Design and economical analysis of hybrid PV–wind systems connected to the grid for the intermittent production of hydrogen, Energy Policy 37 (2009) 3082–3095

[45] A. Kashefi Kaviani, G.H. Riahy, SH.M. Kouhsari, Optimal design of a reliable hydrogen-based stand-alone wind/PV generating system, considering component outages, Renewable Energy 34 (2009) 2380–2390

Chapter 2: Trend prediction – based power management strategy (PMS) for PV system based on dynamic characteristics of system components

2.1 Introduction

As previously introduced, in the context of increasing concerns regarding the energy crisis and the environmental pollution, RE is becoming more and more attractive as alternative of the conventional energy sources due to its advantages of environmental friendliness and free availability [1-2]. The use of the RE-based Microgrid in power generation can contribute to the protection of the environment from the green house gas or air pollutants emissions [3-6]. However, the problems of most RE sources are the fluctuating and unpredictable characteristics depending on meteorological conditions of the installation site, and consequently the impossibility for the RE output power to synchronize with the energy consumption. The integrated RE system with energy storage systems, therefore, can be the solution of the problem and enhance the reliability of the system in satisfying the demand [1-10]. The storage systems usually include both short-term and long-term storages, such as battery and hydrogen system. Because the transient response of hydrogen system is slow while that of battery is faster, battery is used to cover the fluctuation. Aiming at stable and sustainable operation of such a hybrid system, one of the most important problems is the control strategy to ensure the equality between the supply and the demand against the fluctuation of the RE source at any instant. Depending on the objectives of the controlling, the power management strategies were studied and simulated in both short-term and long-term. The simplest power management strategies (PMSs) in which the key decision factors were the power delivered by the RE sources and the SOC of the battery were proposed [12-18]. Abdelkafi et al. [12] considered the PMS for hybrid power production unit made up of wind/fuel cell/electrolyzer/ supercapacitor (SC) and supplying a three-phase load. The proposed PMS was simple which was only based on the difference of wind power and load and the nominal power of fuel cell/electrolyzer. The FC/WE will generate/consume the lack/excess power while SC has the only role of compensating the difference power during the transient time of FC/WE. In the case of over-charged SC, a dumping load was added and vice versa, in the case of deep-discharged SC, the lower priority loads would be disconnected. In order to make the most of the capacity of battery/capacitor, Ipsakis et al. [13] proposed three power management strategies for a hybrid PV/Wind/Battery and hydrogen system. The authors used the power delivered by the RE sources and the SOC of the batteries as the key control parameters. A similar PMS was studied in Ref. [14-18]. The PMS was further developed by using hysteresis band to prevent fuel cell from frequent start – up and shut – down. Initially studied by Ulleberg et al. [19], the double hysteresis bands which were the upper and lower thresholds for the on/off switching of FC/WE were introduced and applied in various PMSs [20-25]. However, because the PMS was based on the power and the SOC of battery to make decision which storage will operate, the sampling time must be long enough for the hydrogen system, which has slow dynamic characteristics, being able to work without error. Another approach for studying the PMS is based on optimization of power cost and the life time of storage devices [26~34]. In Ref. [26], Dufo-Lopez et al. presented a strategy to optimize the control of a hybrid system considering the lowest total cost during the lifetime the system. They calculated the power below which it is more economical to store energy in batteries than in the hydrogen tank. In a similar way, Castaneda et al. [28] and Torreglosa [29] also calculated and based on the power limits depending on economic criteria for the master control. Although the PMSs were also based on the economic approach, Tascikaraoglu et al. [30] and Wang et al. [31] allocated the power in a different way by optimizing the objective function of the operating cost of the system. Similarly, Cau et al. [32] also based on cost function to make decision which storages would operate. However, the authors took into account the uncertainty of the both forecast weather and load by using probabilities in a stochastic approach instead of deterministic one. In Ref. [33], 3 different energy management strategies based on optimization of utilization cost, efficiency and lifetime were compared. In general, the cost optimization-based PMSs gained the economic benefit in the long run. However, most of the studies used an hourly time interval for simulation [26, 28, 30-34], they had not taken into consideration the dynamic process of the system which is the behavior of the system when there is a sudden change of supply or demand. Some other researches considered the simulation of the system in the short-time [27, 29]. The system behavior was simulated in 160s [27] or 120s [29]. However, it can be seen that although the dynamic process was taken into account, the real dynamic model of devices were not examined. Due to the high capital cost of the system design and implementation, the previous researches were mainly based on theoretical models.

The description of the conventional method to use the actual power and the SOC to make decision of allocating power was illustrated in Figure 2.1 and Figure 2.2. As seen in Figure 2.1, the actual power (black line), which is the difference between PV power and the load, is used to make reference to allocate for hydrogen system (blue line) [12]. In this case, battery was used as a compensator to cover the deviation of the actual power and the power generated/consumed by hydrogen system. In general, battery has high capacity; therefore it is used not only as a compensator but also as storage. Then the allocation of power also depended on SOC of battery as shown in Figure 2.2 with the use of hysteresis band to prevent the frequent start-ups and shut-downs [20-25]. In the case of shortage power, fuel cell will generate power when the SOC of battery is smaller than SOC_{on} and will not operate when SOC is higher than SOC_{off}. When SOC is within a range of (SOC_{on}, SOC_{off}), the operation of FC or not depending on the previous status, it will continue its operation if it is working and continue not to work if it is off.

It can be noted that using the actual power to designate to hydrogen system will result in large energy for battery. In the shortage of power, battery energy may decrease quickly, making it deeply discharged or requiring higher energy of battery to be back – up for this situation. The use of trend-prediction which can smooth the

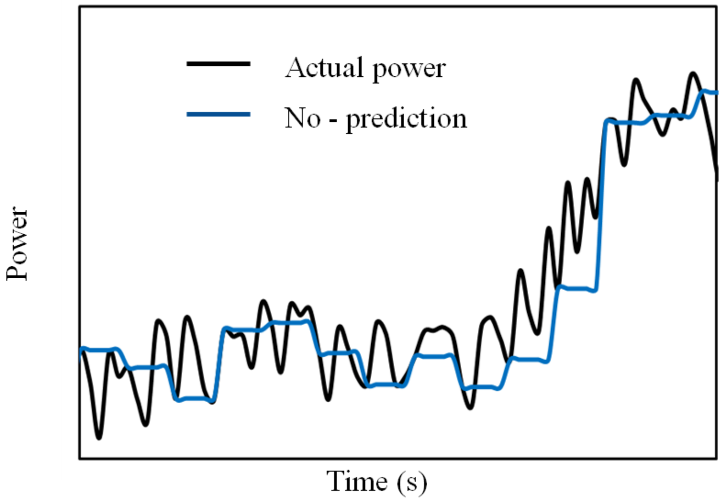

Figure 2.1: The allocation of power to hydrogen system based on the actual power [12].

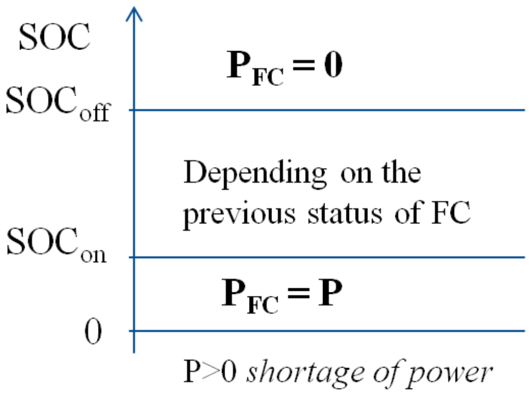

Figure 2.2: Algorithm of making decision with the use of hysteresis band for the fuel cell operation in case of shortage power [20-25]

reference power for hydrogen system and adapt to their dynamic characteristics may be a possible solution which results in the smaller needed energy of battery for covering the fluctuation.

In this chapter, we proposed a new PMS considering the dynamic response of the components of the system and trend- prediction of supply-demand power that can work with real time power using short time interval. Based on experimental results, we modeled the dynamic characteristics of devices. Due to its slow response, FC will operate with little change power which is predicted while LiB with its ability of fast changing will work to compensate the deviation. The trend of the power will be predicted satisfying the dynamic response of the fuel cell, allowing the use of shorter sampling time. For trend-predicting, Kalman Filter is used due to its ability to recursively estimate the state of a dynamic system without considering all the past data and easy adaptation to any alteration of the observations [35-36]. Moreover, the changing rate of predicted time series can be adjusted by changing the parameter used in KF algorithm. The effectiveness of this new control method will be evaluated through simulation. In addition, the comparison between the performance of the system under KF-based PMS and conventional one was also carried out.

As mentioned above, battery with high capacity would work as both a compensator and energy storage. In the first part, the trend-prediction PMS was applied to an existing RE system with high capacity battery. Therefore, the proposed PMS considered the operation of battery including its function of storage along with the function of compensator. The second part of this chapter is to consider the required capacity of battery to compensate the fluctuation when it works as a compensator only and method to downsize it. For an existing PV/Hydrogen system, the estimation and the downsizing of battery used for covering the fluctuation becomes necessary. KF can predict the trend which is smooth component, adapt the required slow changing rate of hydrogen system and filter the symmetrical fluctuation part as expected; therefore it can decrease the required capacity of battery. However, when the fluctuation distribution is asymmetric, which leads to the unsymmetrical charging and discharging power of battery, the evolution of energy in battery may increase or decrease continuously, consequently stopping the operation of battery when it is fully charged or deeply discharged or requiring higher capacity. Therefore, in order to secure the stable operation of the battery as well as the system and use battery with smaller capacity, the energy in battery needs to be successively fluctuated around the value corresponding to SOC of 50%, especially in the case of asymmetric variations and taking into account the converter efficiency. This can be achieved by controlling the power for battery as symmetrical as possible. The proposed trend-prediction PMS was improved by combining KF with the adjustment of power allocated to battery using offset to control the SOC around a reference value. The effectiveness in decreasing the battery capacity will be evaluated by simulation and comparison of the required battery energy using conventional, trend-prediction PMS and improved trend-prediction PMS.

2.2 Trend prediction based PMS for stable and economical operation of the PV/FC/Battery system

2.2.1 Dynamic characteristics of devices in the system

A system consisting of solar energy with LiB and hydrogen system is currently installed at University of Tsukuba in Japan. The block diagram of the system is shown in Figure 2.3. The system, which is designed for the commercial utility, is composed of PV-arrays with nominal capacity of 15kW. When the PV is unable to meet the load, a PEM FC rated at 10kW will operate as alternative power source. In addition, in order to quickly respond to the PV and Load fluctuation, a Lithium Battery with the capacity of 7.5kWh and 15kW is used together with the operation of FC or WE. All the devices are combined together to a DC bus of 380V through DC/DC converters. The system also connects to the utility through AC/DC converter. The utility is responsible for supplying to auxiliary equipments.

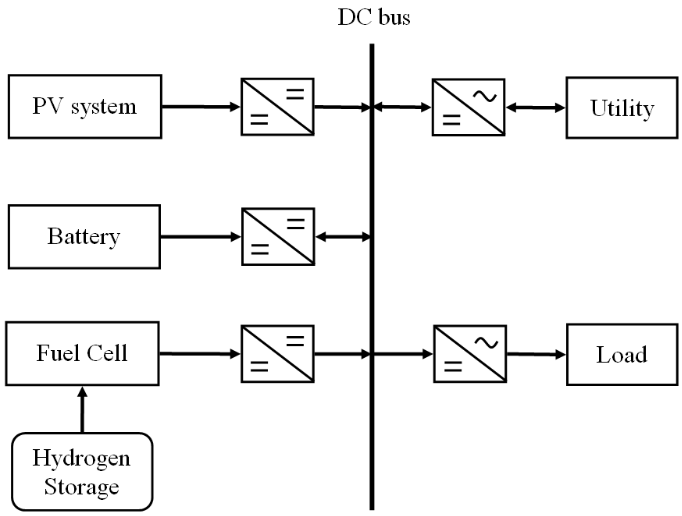

Figure 2.3: A system model composed of PV, LiB and FC for supply-demand adjustment in CNES.

In order to evaluate the integrated system's dynamic performance by simulation, the models of all components play important roles and should be developed. In this study, dynamic models of all components including DC/DC converter which are based on the experimental data have been created.

2.2.1.1. Photovoltaic system:

As introduced above, solar PV is available in abundance and considered as clean energy source over the conventional one. It becomes a potential energy source for power generation and the subject of commercial as well as academic interest.

The PV system in the study is of 15 kW for medium – scale business including 84 panels typed NU-180LW wiring in 12 series × 7 parallel. Figure 2.4 shows the I-V and P-V characteristics of 1 PV panel. Other technical specifications of the PV panel, PV module and DC/DC converter were shown in Table 2.1 and 2.2, respectively.

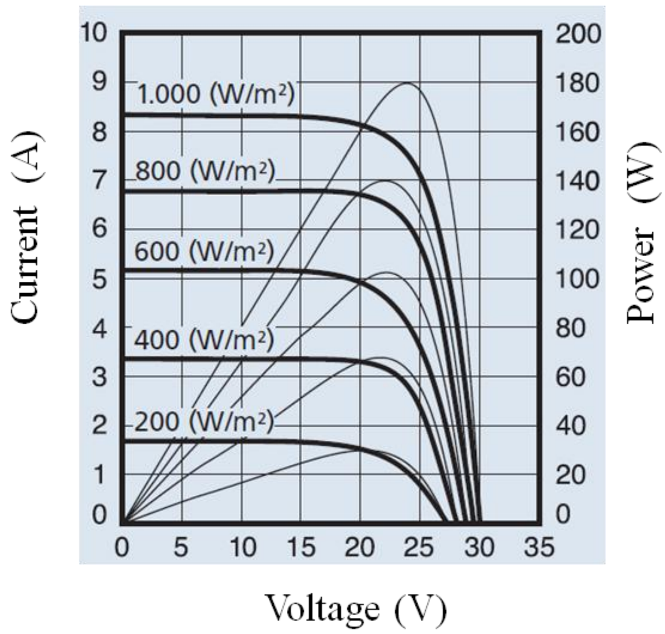

Figure 2.4: I-V and P-V Characteristics of PV panel (NU – 180LW) used in CNES at 25^0C

PV output data were collected in CNES in 1 year and analyzed to investigate the changing rate. The result of histogram and accumulative distribution of the changing rate of PV output in 1 year were shown in Figure 2.5. It can be noted that the distribution of PV power changing rate is asymmetric.

Table 2.1: Specifications of NU – 180LW PV panel.

Maximum power	P_{max}, W	180
Open-circuit voltage	V_{oc}, V	30
Short-circuit current	I_{sc}, A	8.37
Voltage at MPP	V_{MPP}, V	23.7
Current at MPP	I_{MPP}, A	7.6
Temperature coefficient – short circuit current	K_I,%/C	0.053

Table 2.2: Specifications of PV module and DC/DC converter for PV in CNES.

	PV Module	DC/DC converter
Operating Voltage range	DC0 ~ 420V	DC 380 ± 40V
Operating Current range		0 ~ 37.5A
Rate efficiency	13.7%	85%

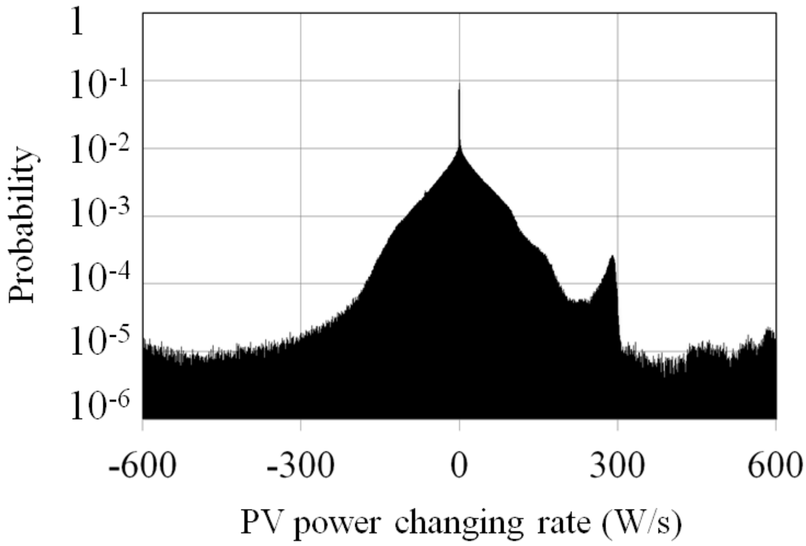

(a)

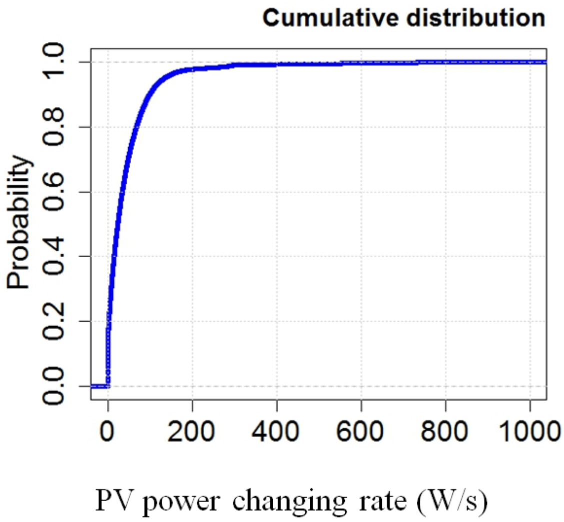

(b)

Figure 2.5 The histogram (a) and cumulative distribution (b) of the changing rate PV output in 1 year

2.2.1.2. Load

Assuming that the system is to supply to a domestic load, the load pattern data is collected from several households on the basis of minute and shown in Figure 2.6.

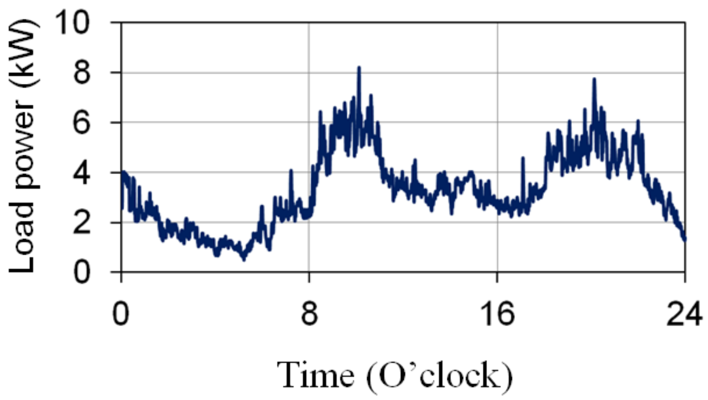

Figure 2.6: Household load pattern.

2.2.1.3. Fuel cell

Fuel cell is a device which uses hydrogen to generate electrical power. The principle operation of FC can be illustrated in Figure 2.7 [37]. Among many kinds of fuel cells, proton exchange membrane (PEM) fuel cells are widely regarded as one of the most one of the most promising energy – conversion devices for automotive, stationary and portable power systems due to its advantages of low temperature, high power density and fast response in comparison with other type of fuel cells [38-40]. Most studies on the dynamic characteristics of PEMFC were based on the modeling and considered the chemical reactions and the affected conditions such as humidity and temperature into the fuel cell operation [41-46].

In this section, we carried out the experiments on the PEMFC to obtain the dynamic characteristics of FC, namely the dynamic response of fuel cell power vs. time when the power reference to FC changes and the consumed hydrogen mass flow vs. fuel cell power. These characteristics would be used in modeling the transient response of fuel cell when power was allocated to it and to calculate the amount of hydrogen as well as the energy conversion efficient of using fuel cell.

The PEMFC with the power rating of 10kW has been used in the system as shown in figure 2.8. Other specifications of this FC are in Table 2.3.

A numerous experiments on dynamic characteristics of FC were carried out by changing the setting output power of the FC stack and DC/DC converter and then

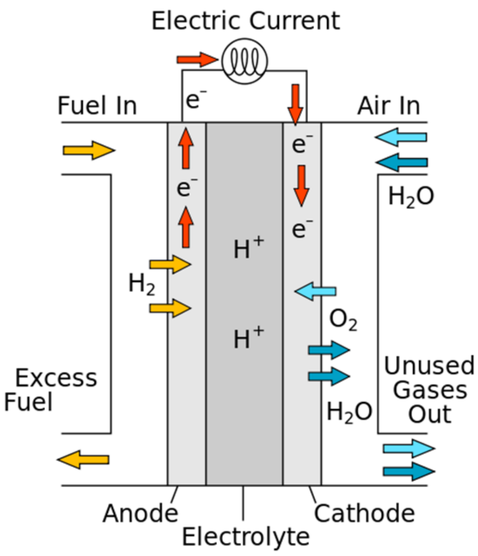

Figure 2.7: Principle operation of a fuel cell [38]

Figure 2.8: The PEMFC 10 kW used in CNES under the study.

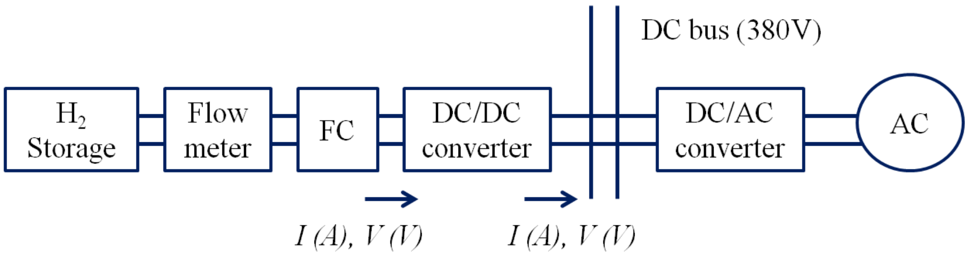

Figure 2.9: The scheme of devices in the experiment on the dynamic characteristics of FC.

Table 2.3: Specifications of PEMFC stack and DC/DC converter.

	FC stack	DC/DC converter
Input	Hydrogen	DC 90 ~ 146V
	Rate max. 124LPM, Pressure 5barg.	
Output	DC 100~150V	DC 380V ± 40V
	94~100A	0~25A

measuring the real responsiveness of the FC, namely the voltage, current and the flow rate of hydrogen. The scheme of the experiment devices were shown in Figure 2.9.

Figure 2.10 shows the measurement and simulation result of the transient response of FC when the required power is 0 kW – 5 kW – 3 kW. The experimental results show that the transient response of FC is linear with the rate of about 100 W/s when FC stack changes the status from ON to OFF or vice versa or changes its generated power.

The results of experiment on the hydrogen mass flow were shown in Figure 2.11

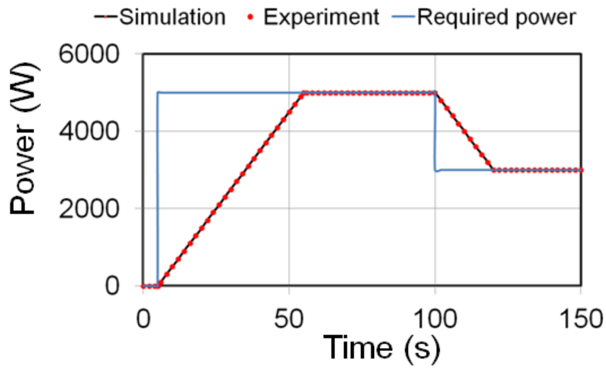

Figure 2. 10: Simulation result for dynamic process of FC power in the case of changing power from 0 to 5 kW and then down to 3 kW.

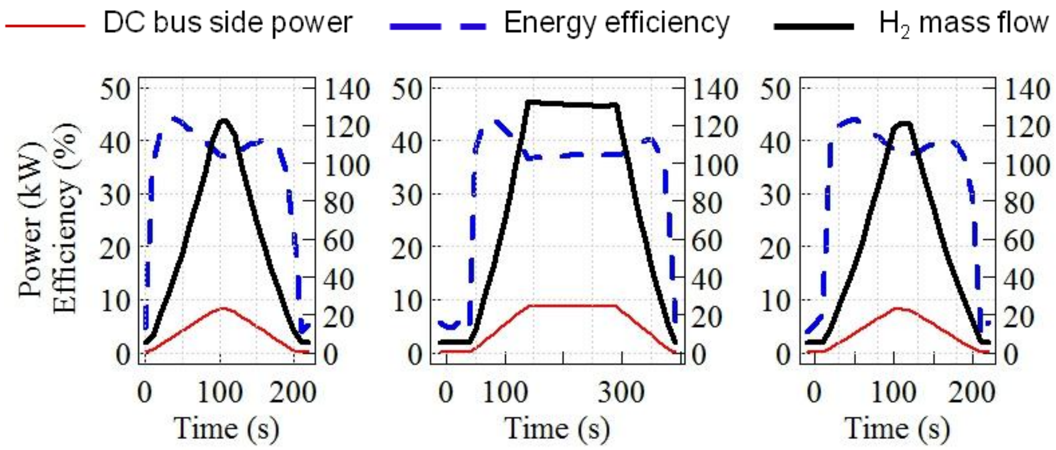

Figure 2.11: The experimental results of the mass flow of hydrogen and the calculated energy efficiency to time when the fuel cell power at the DC bus side changes.

for both dynamic and steady state. In this figure, the hydrogen mass flow and the efficiency of energy conversion during dynamic and steady state corresponding to the change of FC power at DC bus side were illustrated. The efficiency was calculated through experimental results as following function:

$$\eta_{\Delta E} = \frac{P_{DC} \times \Delta t}{\Delta E_{H_2 equi}} \times 100 \qquad (2.1)$$

where $\eta_{\Delta E}$ is energy conversion efficiency in Δt, P_{DC} is power at DC bus side of the converter at t and ΔE_{H2equi} is equivalent power of hydrogen in Δt, which can be calculated as below:

$$\Delta E_{H_2 equi} = \frac{m_{H_2} \times \Delta t \times p}{\mathrm{R} \times T} \times \mathrm{M} \times \mathrm{LHV} \times 10^{-3} \tag{2.2}$$

where m_{H_2}, p, T is mass flow, pressure and temperature of H_2 respectively, LHV is lower heating value of H_2 (33kWh/kg), M is molar mass of H_2 (2.016g/mol), R is gas constant, 0.0821 atm/(mol.K).

The amount of hydrogen needed to supply to FC depending on the power was approximated using fitting curve as shown in Figure 2.12:

$$m_{H_2} = 0.4951 P_{DC(FC)}^2 + 10.066 P_{DC(FC)} + 5.0687 \tag{2.3}$$

where $P_{DC(FC)}$ is power at DC bus side of the converter.

It can be seen that in Figure 2.12, the hydrogen mass flow is nonlinear with the power due to the losses in a fuel cell which can be categorized as fuel crossover and internal currents, activation losses, Ohmic losses and concentration losses [40, 46, 47]. Instead of ions transporting, in some cases, the fuel also diffuses in the electrolyte, which causes the fuel crossover and internal current losses [48]. Mean while, the irreversibility intrinsic in the electrochemical reaction causes the activation loss [49]. The Ohmic losses are associated with the resistance to the flow of electrical charges. The concentration losses result from the diffusion of the reactant and product [49, 50].

Using the measured hydrogen mass flow and equation (2.2), we calculated the energy conversion efficiency of both fuel cell and the DC/DC converter which is shown in Figure 2.13. The efficiency was estimated of approximately 40% including the efficiency of DC/DC converter. The efficiency from the experimental results

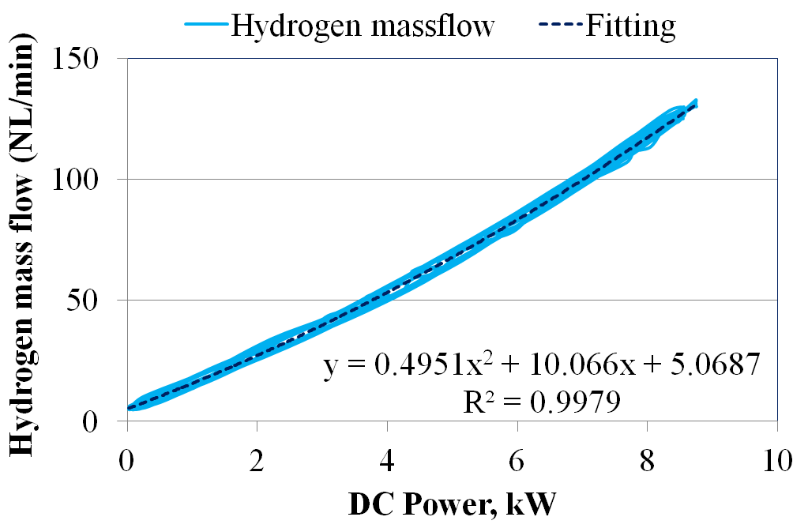

Figure 2.12: Experiment and fitting result of the hydrogen mass flow depending on FC power at the DC bus side.

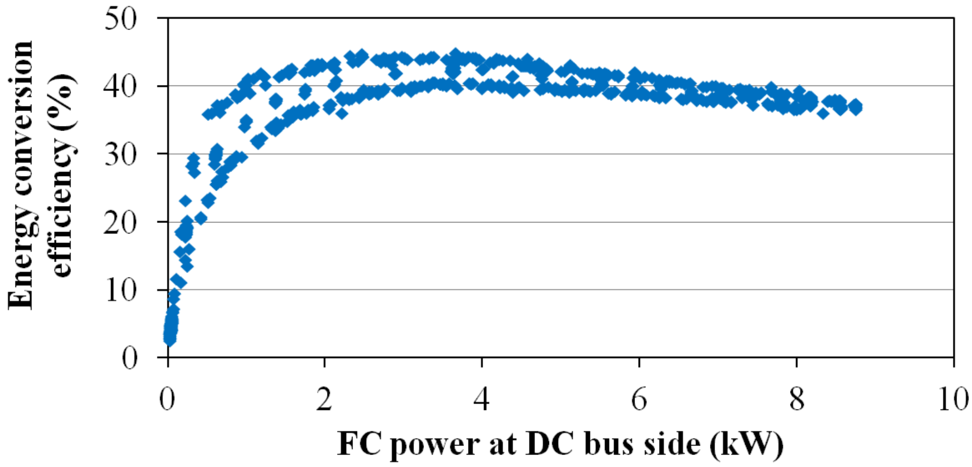

Figure 2. 13: Dependence of energy conversion efficiency on the FC power at DC bus side.

separates into 3 curves because in fact when the efficiency in the steady state and dynamic state, namely the increase and decrease of fuel cell power, slightly changes.

2.2.1.4. Lithium-ion Battery

Batteries are the most common choice of short-term storage for RE based – Microrgird [1-10]. Among the batteries, LiB has been widely used to smooth out the output power fluctuations due to its ability of fast charging/discharging, high round-trip efficiency, long – cycle life, etc. [51]. The LiB used in the research is SLPB60460330H module with the capacity of 7.5 kWh and maximum power of 15 kW as shown in Figure 2.14 and other specifications in Table 2.4.

Figure 2. 14: Lithium – ion Battery 15 kW – 7.5 kWh in the CNES under study.

Table 2.4: Technical specification of the DC/DC converter used for LiB in the system.

	LiB side	DC bus side
Voltage range	DC 200 ~ 225V	DC 380 ± 40V
Current range	0 ~ 72.5A	0 ~ 37.5A

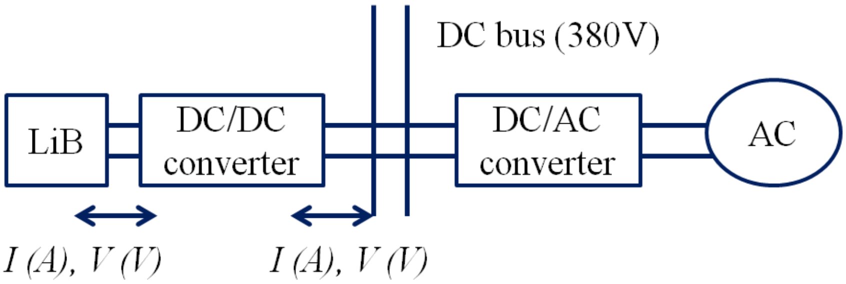

Figure 2. 15: Scheme of the experiment on the dynamic characteristics of battery.

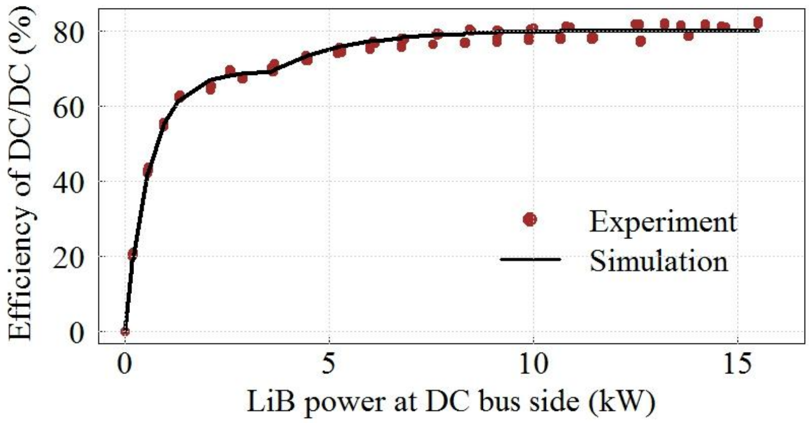

Figure 2. 16: Efficiency of energy conversion for LiB stack depending on the power.

The scheme of experiment on the dynamic characteristics of LiB was depicted in Figure 2.15. State of charge of LiB is a critical parameter using in PMS which is defined as the ratio of the remaining energy in the battery and its nominal capacity and can be estimated as a function of power generated or consumed by the following equation:

$$SOC(t) = SOC(t-1) - \frac{P_{DC}(t-1)\times \Delta t}{E} \times \eta \tag{2.4}$$

where $SOC(t)$ is the SOC at time t, $P_{DC}(t-1)$ is the power at the DC bus side of the converter at time $t-1$, E is the capacity of LiB, η is the efficiency of the energy conversion, considering both charging/discharging efficiency of DC/DC converter which is estimated as in Figure 2.16 according to the fitting function:

$$
\begin{array}{ll}
P_{DC}(t\text{-}1) < 2.9\ \text{kW} & \eta = 0.69 \times \left(1 - e^{-\frac{P_{DC}(t-1)}{0.6}}\right) \\
P_{DC}(t\text{-}1) \geq 2.9\ \text{kW} & \eta = 0.8 \times \left(1 - e^{-\frac{P_{DC}(t-1)}{1.8}}\right)
\end{array}
\qquad (2.5)
$$

Based on the experimental results, an approximated curve of the LiB combined with DC/DC converter's dynamic characteristics was shown in Figure 2.17. It can be realized that the transfer function of the dynamic response of LiB and DC/DC stack is exponential decay in discharging process and combination of exponentially – decaying cosine and sine wave in charging process. This might be due to the characteristics of the current control system inside the DC/DC converter using to connect LiB with the DC bus.

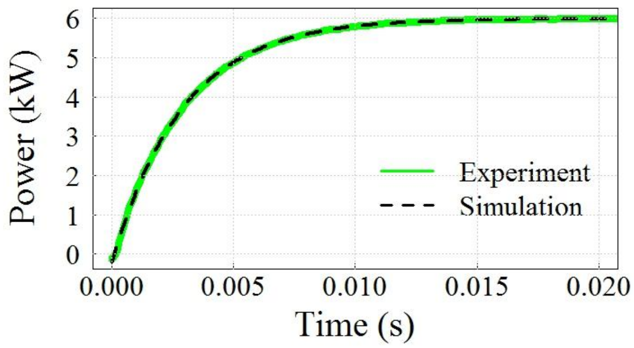

(a)

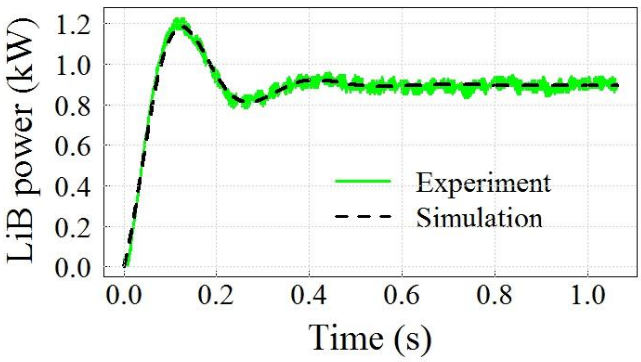

(b)

Figure 2. 17: Transient response of LiB when discharging (a) and charging (b).

The dynamic process of LiB with DC/DC converter when there is a required power change was obtained as:

For the discharging transient process:

$$P = \Delta P_{required} \times (1 - e^{-\frac{t}{0.0029}}) \tag{2.6}$$

And for the charging transient process:

$$P = \Delta P_{required} \times \left(1 - e^{-8.5t}\cos(21.86t) + 0.023e^{-8.5t}\sin(21.86t)\right) \tag{2.7}$$

2.2.2 Trend-prediction PMS based on KF – Autoregressive model

2.2.2.1. Trend-prediction PMS

Control method of the MG based on renewable energy sources and storages in both short-term and long-term plays an important role for the stable operation of the system in supplying the power to the demand. Considering the analyzed PV power changing rate, it can be seen that PV power changes intermittently within a wide range. While the dynamic characteristic of the FC is slow, that of the LiB is considerably faster. Therefore, the allocation of power to the FC needs to satisfy its limit changing rate. In literatures, almost all the PMS was based on the actual power and the SOC to make decision of power allocation [20-25] which is shown in Figure 2.18.

In this research, we proposed a new PMS based on the trend-prediction of the power that can adapt to the dynamic characteristic of the FC (Figure 2.19). In this method, the power is allocated to storages as following:

- The power for storages, which is the difference of load and PV power, $P = P_L - P_{PV}$, will be predicted P_{pre}.

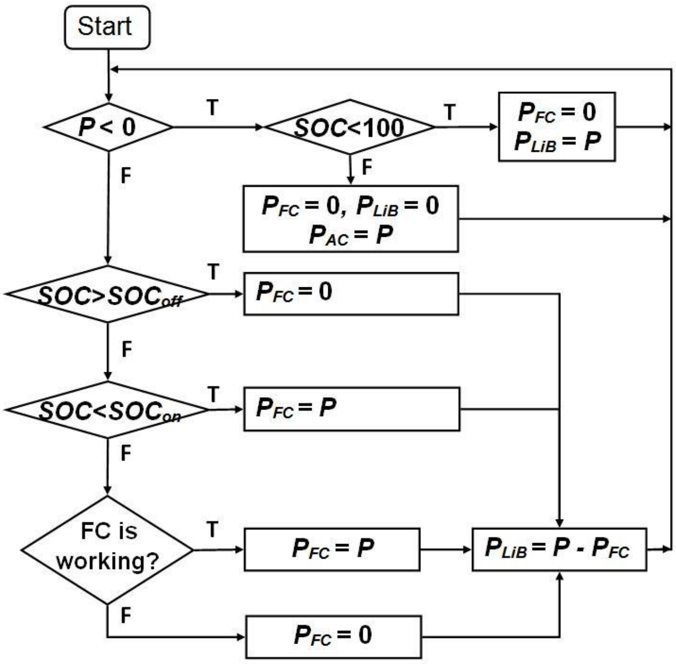

Figure 2. 18: Conventional PMS (no – prediction PMS) [20-25]

- When P_{pre} is positive meaning the predicted shortage of power, the FC will generate this prediction value P_{pre} with or without *offset* depending on the SOC of the LiB. the FC will operate with P_{pre} power minus *offset* when the SOC is high and plus *offset* when it is too small (Figure 2.19a).

- LiB takes the passive role to cover the deviation between the FC power and the actual *P*.

Offset is introduced because the efficiency of DC/DC converter can make LiB to be deeply discharged during the operation if it only works to cover the fluctuation in a long time. The advantage of the proposed PMS is that it allocates the power to FC and LiB according to their dynamic characteristics. Therefore, the system can operate stably.

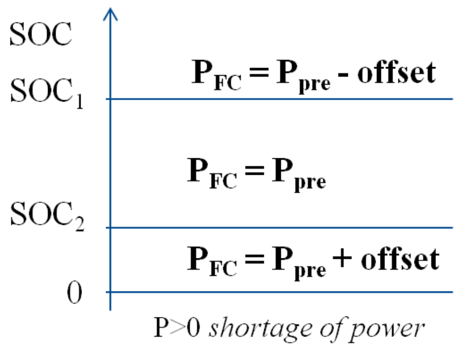

(a)

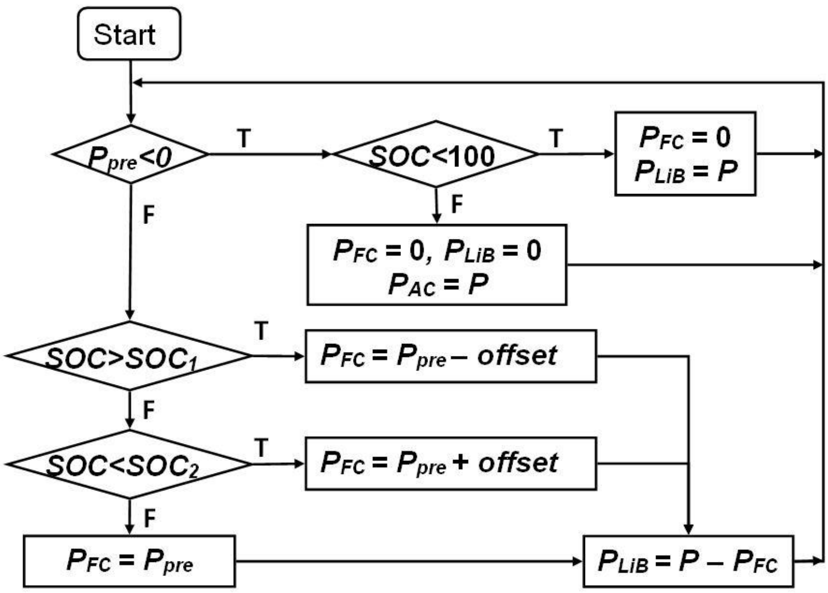

(b)

Figure 2. 19: Algorithm of the trend-prediction PMS for a PV/FC/battery system

2.2.2.2. Kalman Filter algorithm

An important issue needed to be considered in PMS2 is the forecasting tool. In order to predict the stochastic time series, there have been numerous approaches proposed in literatures, ranging from the traditional time series analysis such as

ARMA (autoregressive moving average) models to recent approaches using ANN (artificial neural networks) [52-56]. These methods have the drawback of using numerous known data to determine and validate the model structural coefficients. Additionally, moving average method can predict the trend but slower to respond to rapid change, then it is difficult to adjust the slope of trend. Meanwhile the ANN method predicts the fluctuate value but can not predict the trend. With the presence of random disturbance in PV output as well as the limitation of power changing rate of FC, the use of an adaptive controller becomes necessary. For this reason, Kalman Filter, which has advantages of having simple and optimal algorithm working online for linear systems with Gaussian noise, easy adaptation to any alteration of the observations and ability to change to parameter to obtain the slope of trend as expected [35,36], is chosen for predicting in this study.

The state and measurement equations for the linear stochastic discrete – time system using state – space model (Figure 2.20) are given by:

$$x_n = Fx_{n-1} + Gw_n \tag{2.8}$$

$$y_n = Hx_n + v_n \tag{2.9}$$

where x_n and y_n represent state and the measurement (observation) at the moment n, respectively. w_n and v_n denote process and measurement noises, which are assumed to be zero mean Gaussian white noise with covariance Ro and Q, respectively. F and H are state transition matrix and measurement matrix of appropriate dimensions.

In this study, 2-dimension trend-Autoregressive (AR) model [36] was used for modeling to predict the little changed part of time series with assumption that y contains trend t as:

$$y_n = t_n + v_n \tag{2.10}$$

$$t_n = 2t_{n-1} - t_{n-2} + w_n \tag{2.11}$$

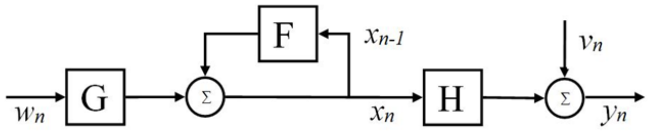

Figure 2. 20*:* State space model using in Kalman Filter.

$$x_n = \begin{pmatrix} t_n \\ t_{n-1} \end{pmatrix} \qquad F = \begin{pmatrix} 2 & -1 \\ 1 & 0 \end{pmatrix} \qquad G = \begin{pmatrix} 1 \\ 0 \end{pmatrix} \qquad H = (1\ 0) \tag{2.12}$$

The algorithm of KF including 2 stages can be illustrated as following:

Time Update: x_n^-, priori state estimate and P_n^-, priori estimate error covariance at step *n* based on the previous time step values can be calculated as:

$$x_n^- = Fx_{n-1} \tag{2.13}$$

$$P_n^- = FP_{n-1}F^T + GQG^T \tag{2.14}$$

Measurement Update: when the new observation value y_n is known, the estimate of x_n at time *n* will be:

$$x_n = x_n^- + K_n(y_n - Fx_n^-) \tag{2.15}$$

The KF gain K_n and the estimate covariance P_n at *n*:

$$K_n = P_n^- H^{\mathrm{T}} (HP_n^- H^T + R_o)^{-1} \tag{2.16}$$

$$P_n = (\mathrm{I} - K_n H)P_n^- \tag{2.17}$$

2.2.3 Simulation

2.2.3.1. Selection of KF parameter

The simulation of the proposed trend-prediction PMS applying to a PV/FC/LiB system in CNES project was carried out using PV data in 1 year and with the assumption that the initial SOC of LiB is of 25%. We calculated the effectiveness of the proposed PMS for all days in the considered year. However, we chose 3 typical days to illustrate the performance of the proposed PMS. These 3 days was typical with the PV output as shown in Figure 2.21 and some analytical data in Table 2.5, namely 1 day with high PV energy and average changing rate of PV power (the 1st day), 1 day with small PV energy and small PV changing rate (the 2nd day), 1 day with average PV energy and fast PV changing rate (the 3rd day).

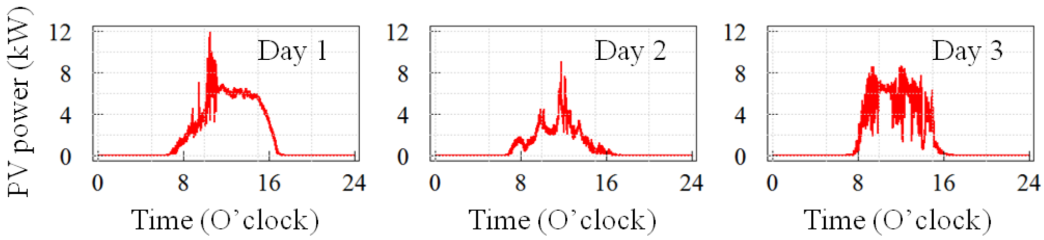

Figure 2. 21 The PV output of 3 typical days for illustration of the system performance.

Table 2.5: Analytical data for the PV power changing rate in 3 typical days.

Day	PV energy (kWh)	P_{PVrate} max (W/s)	P_{PVrate} min (W/s)	P_{PVrate} average (W/s)		P_{PVrate} (W/s) at accumulate probability of 99.5%
				Plus	Minus	
1st	43.21	619	-612	48	-51	288
2nd	18.14	256	-226	41	-41	155
3rd	36.59	607	-609	56	-58	407

First, we selected the suitable parameter of KF. The measurement noise covariance *Ro* was estimated of 0.1 using the maximum log – likelihood [36] and based on the real past PV power series. The selection of KF parameter, e.g. the process noise covariance *Q*, were carried out to guarantee the FC power changing rate smaller than the limit of 100 W/s that FC can operate. Figure 2.22 shows the fluctuation of allocated FC power with different *Q* ($Q = 10^{-3}$, $Q = 10^{-5}$, $Q = 10^{-9}$). The result indicated that the larger the *Q* is, the more strongly the FC power fluctuates. For each day, we can calculate the maximum and minimum power changing rate of FC depending on different *Q*.

Figure 2.23 presents the maximum, minimum FC power changing rate of all days in 1 year corresponding to the *Q*. It can be noted that the power changing rate will decrease when the *Q* decreases. When the *Q* is smaller than 10^{-9}, the FC power will moderately fluctuate with the rate of smaller than 100 W/s. Therefore, 10^{-9} was chosen as the suitable value of the *Q* that the FC can operate with the maximum changing rate close to its real maximum ability of changing power of 100 W/s.

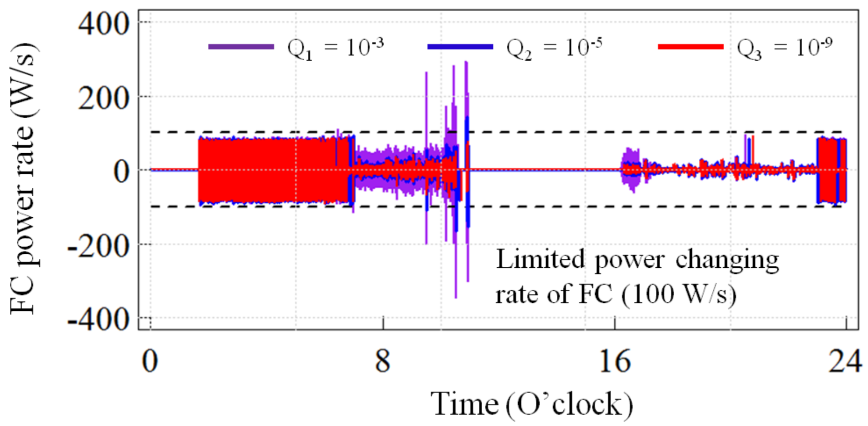

Figure 2. 22: The changing rate of allocated FC power with different *Q* in the 1st day.

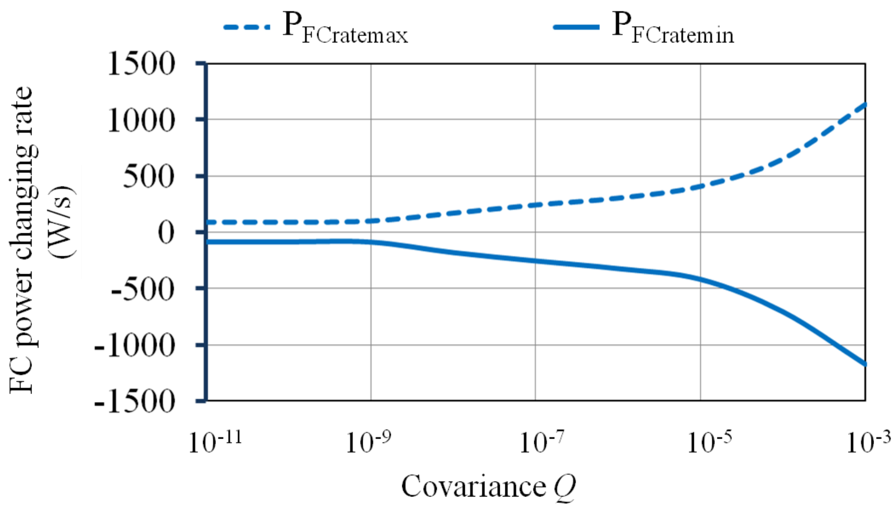

Figure 2. 23: The dependence of maximum and minimum FC power changing rate of all days on the covariance *Q*.

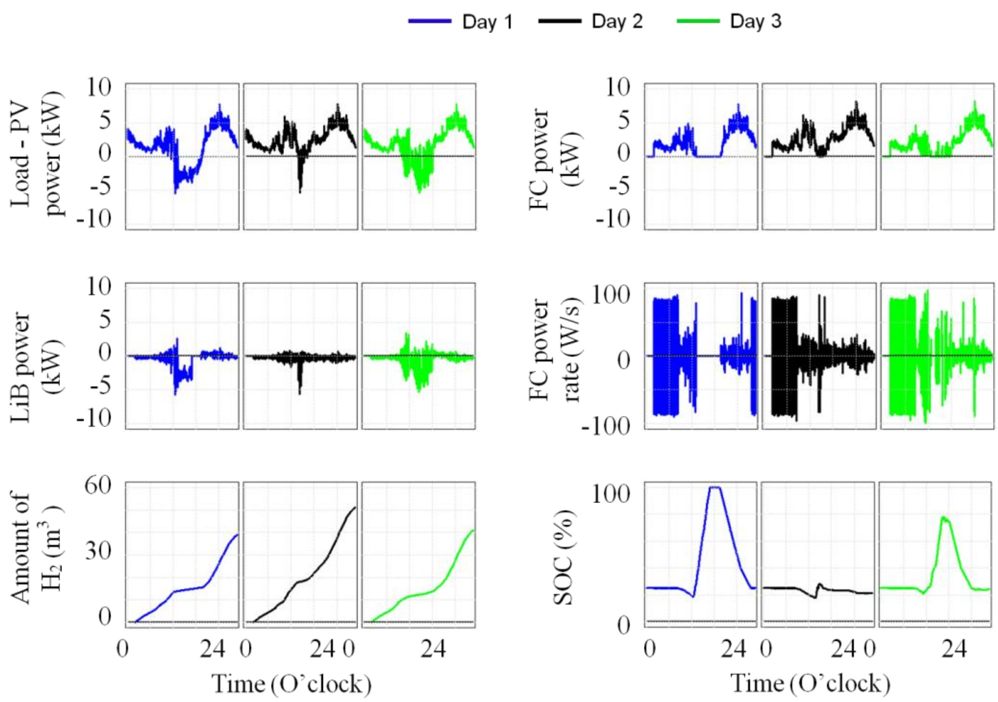

Figure 2. 24: The performance of the system during 3 typical days under KF – PMS with $Q = 10^{-9}$

Figure 2.24 shows the performance of the system in the case of $Q = 10^{-9}$ in 3 typical days: the FC power and its power changing rate, the LiB power, the amount of hydrogen used and the SOC of battery in each day. From the results, it can be realized that the power designated to the FC changes little while the power for the LiB strongly fluctuates. This is due to the application of the trend-AR model and KF-based control method which can predict the trend-power that varies slightly. In other words, the power will be divided into 2 parts, one gradually changes which will be forecasted by KF and generated by FC and the other one drastically fluctuates which will be covered by LiB. Therefore, each device can contribute its part to generate the needed power depending on its dynamic characteristic. With the selection of the Q of 10^{-9}, the FC power changing rate is close to 100 W/s, thus FC can operate without any problems. In addition, it remains keeping the initial value of 25% over the 4 days, so the LiB can operate in a long time.

2.2.3.2. Efficiency of energy conversion

In order to evaluate the effectiveness of the proposed trend-prediction PMS, a comparison of the overall efficiency of the system was conduct using no-prediction PMS and KF-PMS.

The overall efficiency of the system can be calculated as below:

$$\eta_{sys} = \frac{\int_0^T P_L dt}{\int_0^T P_{PV} dt + E_{H_2} + E_{LiB}^{initial} - E_{LiB}^{final}} \tag{2.18}$$

in which P_L, P_{PV} denotes the load and PV power, respectively. E_{H2} is the equivalent energy of hydrogen used during the time period T, which is calculated using equation (2.2). $E_{LiB}^{initial}, E_{LiB}^{final}$ represents the initial and final energy in the battery respectively.

We simulated in 3 cases:

- No-prediction PMS.
- No-prediction PMS and the *offset*.
- Trend-prediction PMS and *offset*.

The result of the amount of consumed hydrogen and corresponding efficiency for each day in 1 year using no-prediction PMS with *offset* = 400 and KF PMS with *offset* = 250 was illustrated in Figure 2.25. It can be seen that in almost all days of the year, using KF-PMS consumed less hydrogen than the case of no-prediction PMS, leading to higher efficiency of energy conversion. The total amount of hydrogen and the overall efficiency was shown in Table 2.6. In the case of using no-prediction PMS, we also compared the case of using the same offset with KF-PMS and bigger offset to keep SOC_{min} during the year not to be deeply discharged ($SOC_{min} = 0$). The results show that when the no-prediction PMS was used, using small offset or without offset resulted in deeply discharged situation. When the *offset* was selected to keep SOC the same with KF-PMS, the total amount of hydrogen in this case was higher and consequently the overall efficiency was slightly smaller as well.

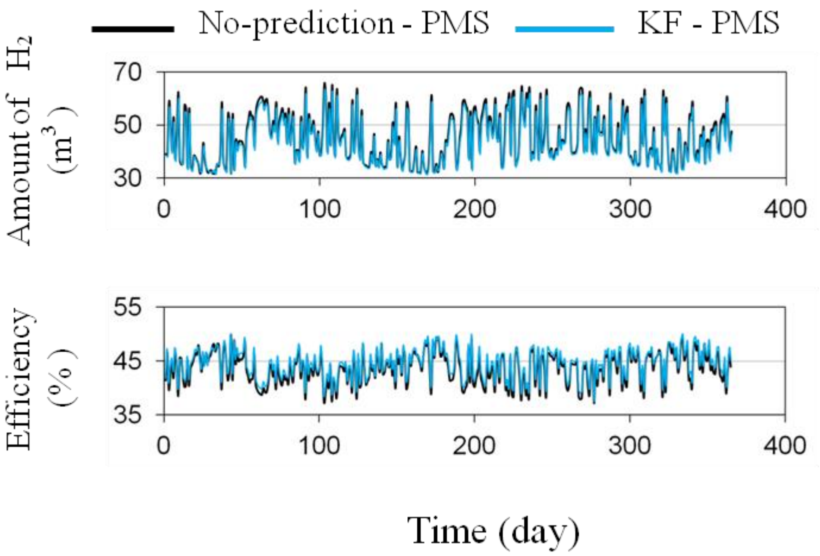

Figure 2. 25: The amount of consumed hydrogen and the corresponding efficiency for each day in 1 year using KF – PMS (*offset* = 250) and no – prediction PMS (*offset* = 400)

Table 2.6: Comparison of simulation result of the amount of hydrogen used and the overall efficiency using different PMS.

Method	SOC_{min} , %	m_{H2}, Nm^3	Overall efficiency (%)
No – prediction + no offset PMS	0		
No – prediction +(*offset* = 250) PMS	0		
No – prediction +(*offset* = 400) PMS	3.21	16456	43.527
KF PMS (*offset* = 250)	3.45	16030	44.385

2.2.3.3. System stability

Voltage is an important parameter to assess a power system quality. Therefore, DC bus voltage was examined to evaluate the effectiveness of the proposed control method. For simplicity, the load was considered as a resistor and represented by a resistance R which is calculated by V_{DC}^2 / P_L . The DC bus voltage was then simulated by the following equation:

$$V = \sqrt{(P_{PV} + P_{LiB} + P_{FC}) \times R} = V_{DC} \times \sqrt{(P_{PV} + P_{LiB} + P_{FC}) / P_L} \tag{2.19}$$

Figure 2.26 shows the DC bus voltage in 3 typical days using 2 PMSs. Assumed that PV power changes from one value to another in a short time *Δt* then keeping this value in a sampling time of 3s before changing to other one as shown in Figure 2.26 (a). With the maximum *ΔP* of 1860 W (in the 3rd day), the DC bus voltage when the sudden change of power occurs in short time *Δt* = 100 ms was within a range of ± 10% which is the acceptable range for DC/AC converter working to supply to the

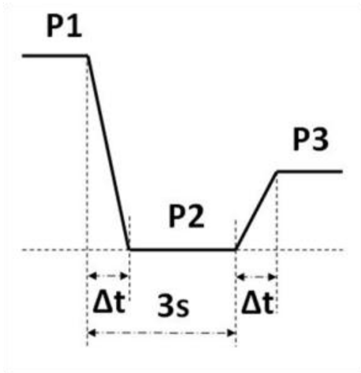

(a)

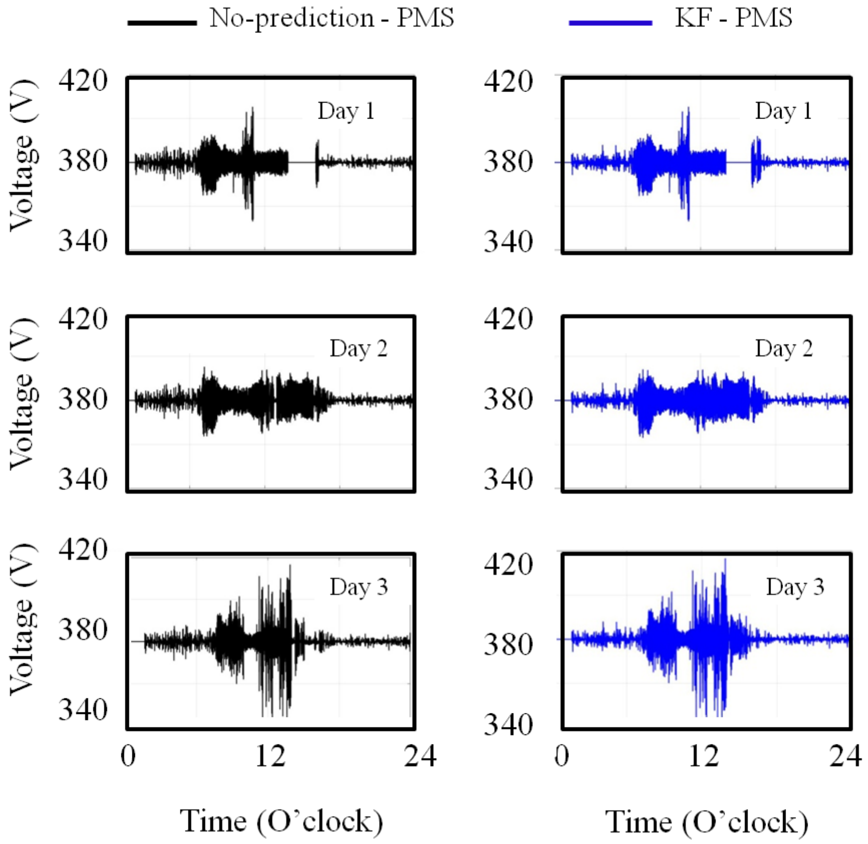

(b)

Figure 2. 26: The voltage of DC bus during 3 typical days using no – prediction PMS and KF – PMS.

load. The shorter the changing time Δt is, the larger the voltage will be. With higher changing power, longer occurring time is needed. This voltage changing was occurred due to the transient characteristic of DC/DC converter for LiB. To diminish the voltage fluctuation, it needs to boost up this characteristic. This can be done by using simple controller such as PID (proportional – integral – derivative) or MPC (Model Predictive Controller). The simulation results for other days shows that under both 2 PMSs, the DC bus fluctuated slightly and can supply to the load stably. As mentioned above, these sudden changes were caused by the sudden change of power that was assumed by error. However, with this unexpected change, the DC bus voltage was still within its accepted working voltage range (± 10%). Comparing 2 cases of methods, there is no considerable difference between the DC voltages in general.

2.3 Downsizing the required capacity of battery for PV/H_2 system by trend-prediction and its improved PMS

2.3.1 Trend-prediction PMS and its improvement for downsizing the battery

In the previous part, we proposed a new trend-prediction PMS for a PV/FC/Battery system and applied it to CNES project as a case study. The stochastic power would be decomposed into trend and fluctuating components. When there is a shortage of power supplying to demand, FC will generate the trend-prediction value. LiB takes the responsibility of compensating the deviation of the prediction and the actual power, which is unexpected fluctuation. Because the capacity of LiB in this system was considerably high, it would operate not only as a compensator but also as storage. The proposed method has the advantage in comparison with no-prediction based PMS. The proposed PMS, however, was applied to an existing system with available storages; the battery capacity requirement was not examined. It can be obviously seen that, the higher the capacity of the battery is, the more power it can store and provide against the variation. On the other hand, due to its high cost, the estimation of the least battery capacity requirement for compensating any potential fluctuations becomes necessary. In this case, battery is used for only one function of compensating the deviation between the supply and the demand. Because Kalman Filter can predict the trend of the stochastic and separate the drastically changing part of the stochastic time series as expected, the proposed PMS can be possibly effective.

However, when the fluctuation distribution is asymmetric or when the efficiency of charging/discharging process of battery is taken into account, the evolution of the energy in battery may increase or decrease continuously, consequently requiring higher capacity or stopping the operation of battery when it is fully charged or deeply discharged. Therefore, the PMS would be improved by combination of KF with the control of the state of charge (SOC) of battery to adjust the battery power in such a way that the power alternates between charge and discharge meanwhile the allowed maximum power changing rates of FC and EL are secured. By adjusting the symmetry of battery power distribution, the required capacity of battery could be smaller.

In this part, we focused on determination of the battery capacity requirement in the hybrid PV/hydrogen system which is shown in Figure 2.27 by allocating the power to battery as alternately positive and negative value while the allowed maximum power changing rate of hydrogen system and the efficiency of charging/discharging process are also taken into consideration. From the analysis of the simulation results, the required capacity of storage could be estimated. The effectiveness in reducing the necessary capacity of battery of the proposed PMSs was evaluated by the comparison with the no-prediction PMS.

2.3.1.1. Trend-prediction PMS

It can be noted that the purpose of the trend-prediction PMS is a slightly different from the proposed PMS in the previous part because battery is responsible for covering the deviation to smooth out the fluctuation only. The trend-prediction

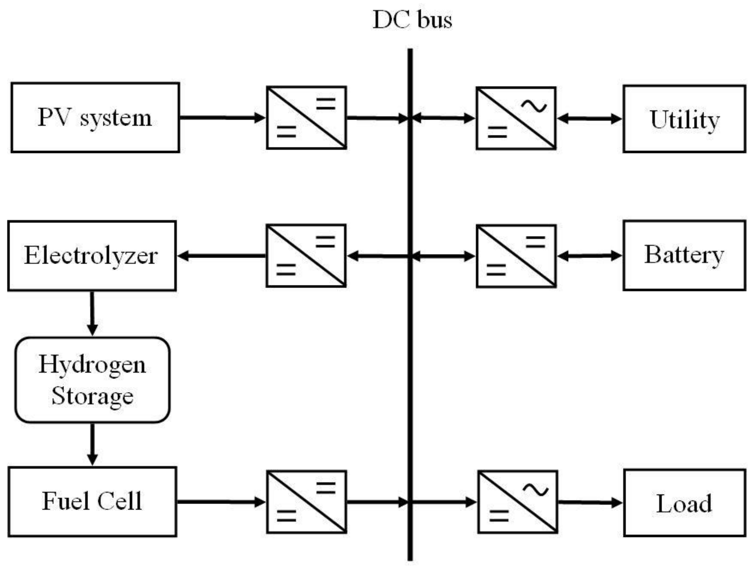

Figure 2. 27*:* Block diagram of the PV/hydrogen system based MG.

value of shortage or surplus power will be designated to FC and EL due to their slow transient response while battery which has the fast dynamic characteristic will cover the rest stochastic variation. In order to estimate the minimum required capacity, the battery only works to compensate the slowness in the dynamic characteristics of EL and FC without being used as storage.

Figure 2.28 shows the algorithm for battery input/output control of PMS1. The difference between load and PV power is calculated, $P = P_L - P_{PV}$, and predicted through KF, P_{pre}. If the predicted value P_{pre} is positive indicating the predicted shortage power, it will be generated by the FC. On the contrary, in the case of negative predicted power, the EL will consume this value. Battery will compensate the difference between the actual P and the power generated or consumed by the FC or the EL respectively.

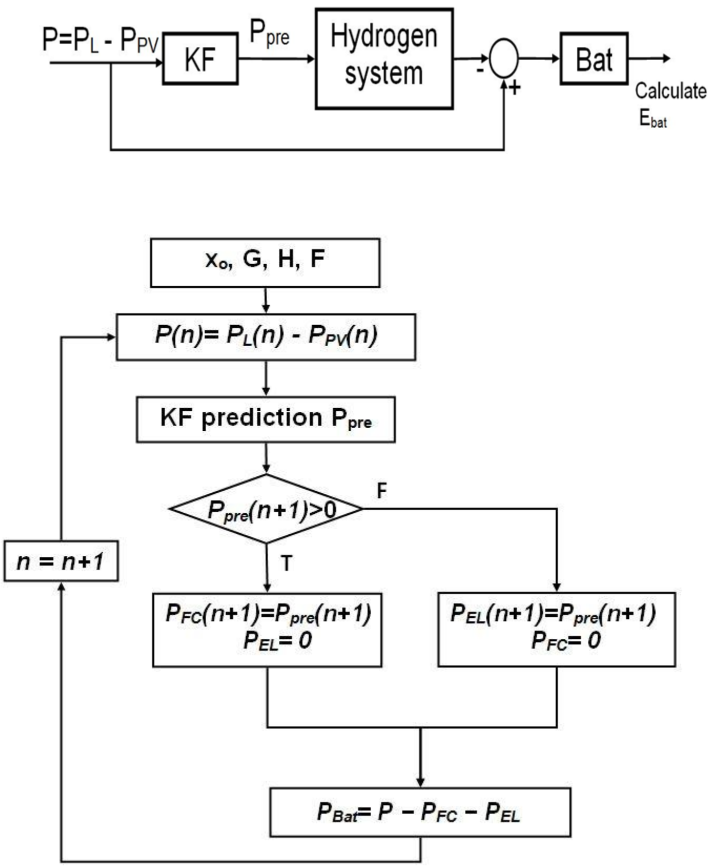

Figure 2. 28: The block and algorithm of battery input/output control in KF trend-prediction PMS (PMS1).

2.3.1.2. Improved trend-prediction PMS

In some cases, the power for battery is continuously positive before changing to negative, thus it tends to be charged or discharged consecutively, resulting in high capacity requirement. In some other cases, the power distribution is asymmetric or when the efficiency of charging/discharging process was taken into account, the charged energy will not be enough to compensate the discharged energy, and thus energy in battery will decrease. In addition, the trend component derived from the filter and designated to hydrogen system, not in almost cases, reaches the allowed maximum changing rate. Hence, it is possible to adjust the power for battery as expected whilst the limit of power changing rate for EL and FC are still secured. The

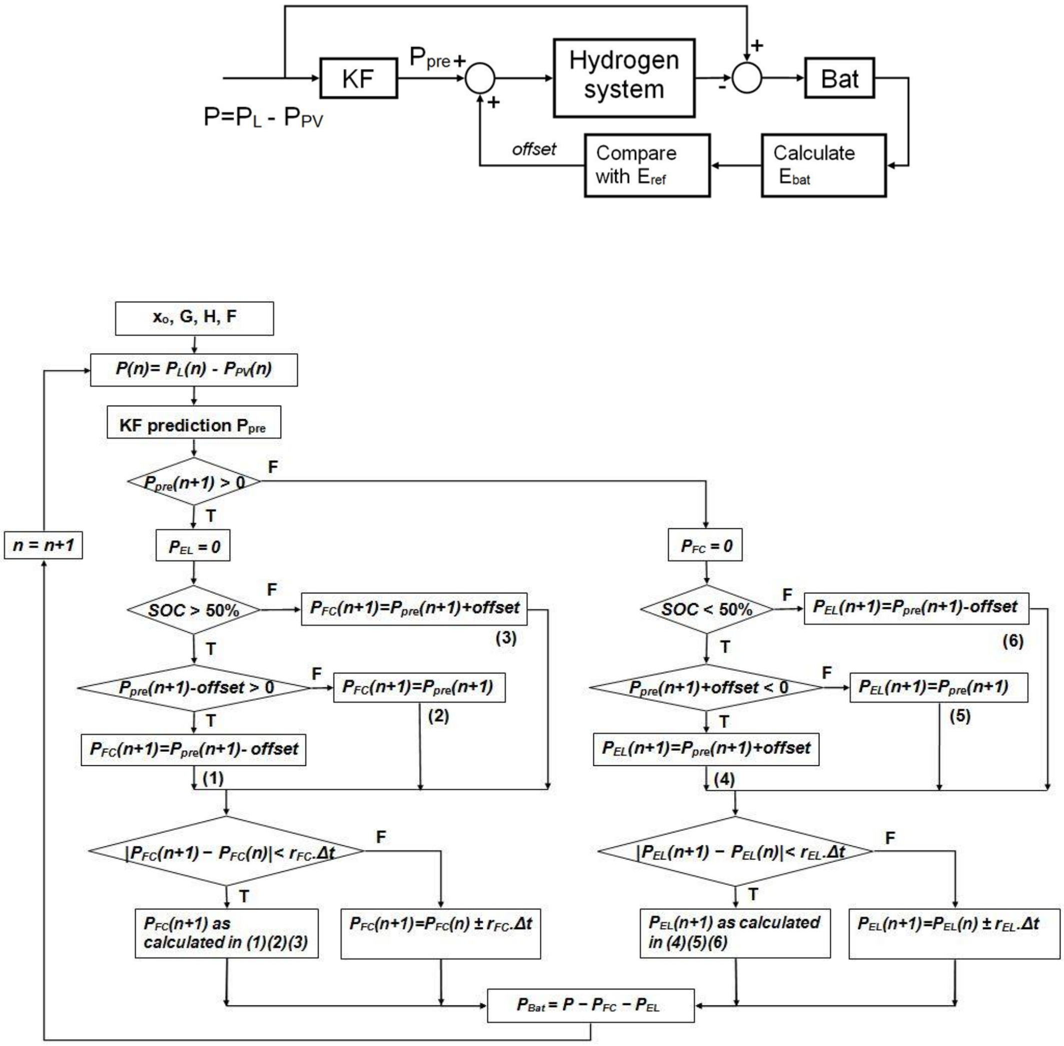

Figure 2. 29: The block and algorithm of battery input/output control in improved KF trend-prediction PMS (PMS2)

PMS1 could be improved by using offset to adjust the battery power which is called PMS2 and shown in Figure 2.29. *Offset* value is decided based on the SOC of the battery and the power for hydrogen system is still adjustable within its limited changing rate:

$$offset = K \times (SOC_{\mathrm{bat}} - SOC_{\mathrm{keep}}) \tag{2.20}$$

where K is the adjustment coefficient. In order to downsize the battery capacity, the SOC is controlled to keep stable around 50% (SOC_{keep}) to cover the upward and downward fluctuations. The advantage of PMS2 over the PMS1 is that it can adjust the power of battery in such a way that the battery will charge and discharge alternately; making the energy to fluctuate around the reference value. As a result, the required capacity will be smaller.

2.3.2 Determination of battery capacity

Battery is a device used to cover all the difference between the real power and the power of FC or EL due to its ability of changing power quickly. It is connected to the DC bus through DC/DC converter. The parameter needed to define is rated energy. The energy in battery can be calculated as a function of the power of battery by the following equations:

$$E_{\mathrm{Bat},n} = E_{\mathrm{Bat},n-1} + \left(P_{n-1}^{\mathrm{Bat.ch}} \times \eta^{\mathrm{ch}} - \frac{P_{n-1}^{\mathrm{Bat.disch}}}{\eta^{\mathrm{disch}}} \right) \times \Delta n \tag{2.21}$$

where $E_{\mathrm{Bat},n}$ is the energy in battery at time n, $P_{n-1}^{\mathrm{Bat.ch}}$, $P_{n-1}^{\mathrm{Bat.disch}}$ are the charge power and discharge power designated for battery at DC bus side of DC/DC converter at time n – 1, η^{ch} and η^{disch} are efficiency of charge and discharge process, respectively.

To determine the capacity of battery, we assumed the initial of energy in battery is 0 and corresponding to the SOC_{keep} which is the value of state of charge needed to be kept during operation of battery. Therefore, the needed capacity of battery will be:

$$E_{\mathrm{need}} = \max\left(\frac{E_{\mathrm{Batmax}}}{1 - SOC_{\mathrm{keep}}}, \frac{|E_{\mathrm{Batmin}}|}{SOC_{\mathrm{keep}}} \right) \times M_{\mathrm{Bat}} \tag{2.22}$$

in which E_{need} is the needed battery energy, E_{Batmax}, E_{Batmin} are the maximum and minimum energy of battery during the considered time, respectively. M_{Bat} is the margin coefficient which is usually chosen from 1 to 3 [20].

With SOC_{keep} = 50%, it will be estimated capacity of battery will be:

$$E_{\mathrm{need}} = 2 \times \max(E_{\mathrm{Batmax}}, |E_{\mathrm{Batmin}}|) \times M_{\mathrm{Bat}} \tag{2.23}$$

2.3.3 Simulation and discussion

The PV data were collected from real 15 kW – class PV systems in 2013 (365 samples of PV data) in University of Tsukuba, Japan. In order to normalize the data, the PV power used in simulation was divided by rated power of PV. The solar irradiance and the histogram of normalized PV power changing rate were shown in Figure 2.30. The system was supposed to supply to domestic load. In this study, we used the real load of several household demands in Tsukuba. Figure 2.31 shows the normalized load sample under the study. The simulation was carried out with the assumption that the normalized limited changing rate of hydrogen system was 1%/s.

A comparison between the estimated capacity of battery with $M_{\mathrm{Bat}} = 2$ [20] using KF-based PMS1 and without prediction (no-prediction-based PMS1) was carried out. First of all, the dependence of the needed energy of battery on the Q was investigated. For each sample of PV data, we changed the covariance of process noise Q of KF and examined the evolution of battery power and energy. Figure 2.32 shows the changing process of power and energy in battery using the PMS1 in the case of efficiency of charging and discharging process is of 1 ($\eta^{\mathrm{ch}} = \eta^{\mathrm{disch}} =1$) for 1 sample of PV data in March 18th 2013. The results reveal that using KF with different Q can change the power allocated to battery, which causes the difference in the evolution of energy. The needed energy in battery to cover the difference between the supply and the consumption in 1 day $E_{\mathrm{need}}^{\mathrm{1day}}$ and the normalized power changing rate $P_{\mathrm{rate}}^{\mathrm{1day}}$ allocated to hydrogen system can be estimated corresponding to each Q. The required energy $E_{\mathrm{need\text{-}all}}$ and P_{rate} of all days were determined by the accumulative probability of 99.7% of all days' values and illustrated in Figure 2.33. It can be noted that with the constraint of limited changing rate of hydrogen system, $P_{\mathrm{rate}}^{\mathrm{limit}}$, the power changing rate $P_{\mathrm{rate}} \leq P_{\mathrm{rate}}^{\mathrm{limit}}$ when $Q \leq Q_o$. Therefore, we can choose Q_o and estimate

$E_{\text{need-all}}$ based on $P_{\text{rate}}^{\text{limit}}$. With the assumed normalized $P_{\text{rate}}^{\text{limit}}$ is of 1%/s, a suitable Q_o was selected as $Q_o = 10^{-9}$ and the corresponding E_{need} in 1 year is 0.064.

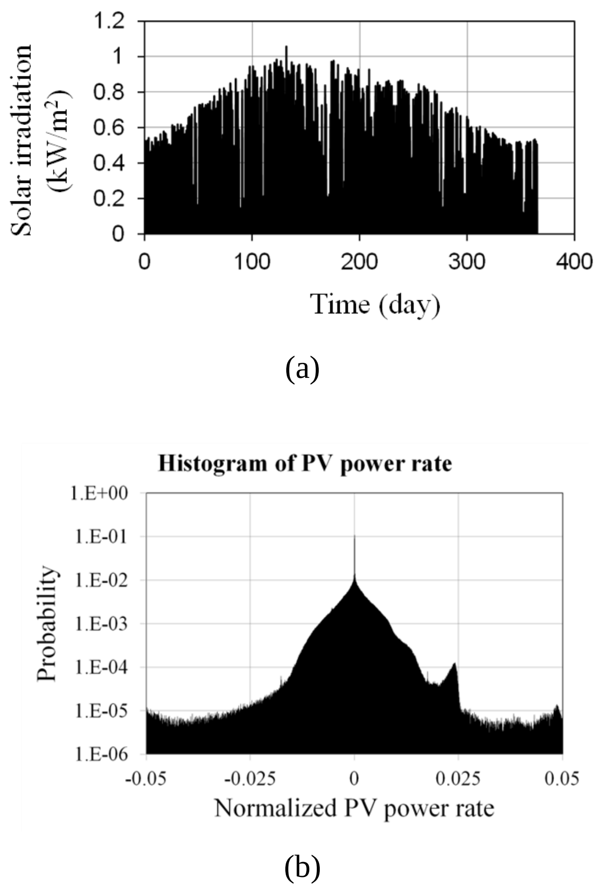

Figure 2. 30: The solar irradiance and the histogram of normalized PV power changing rate in 1 year.

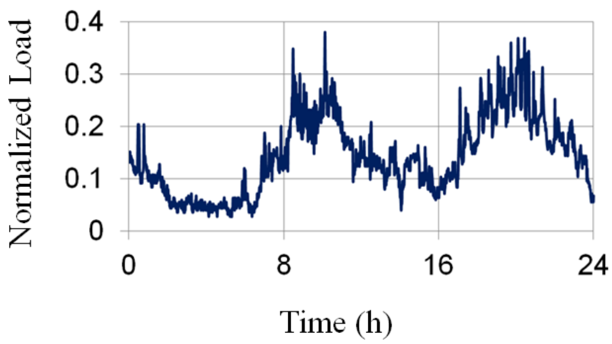

Figure 2. 31: The normalized domestic load.

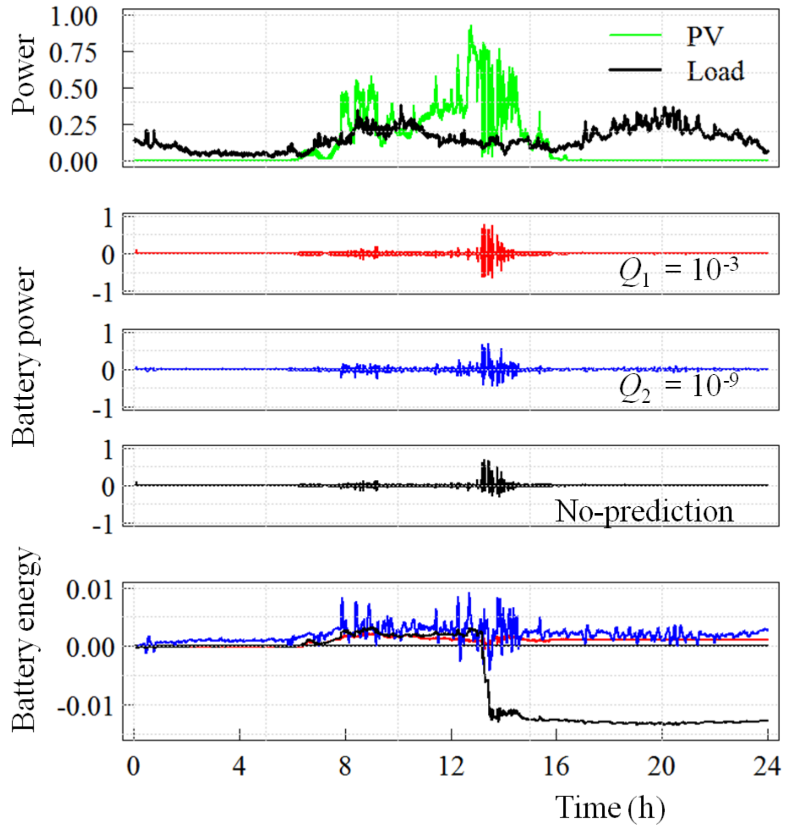

Figure 2. 32: Evolution of PV power, load, power and energy of battery using KF ($Q_1 = 10^{-3}$, $Q_2 = 10^{-9}$) and no prediction PMS1 during one example day (March 18th 2013).

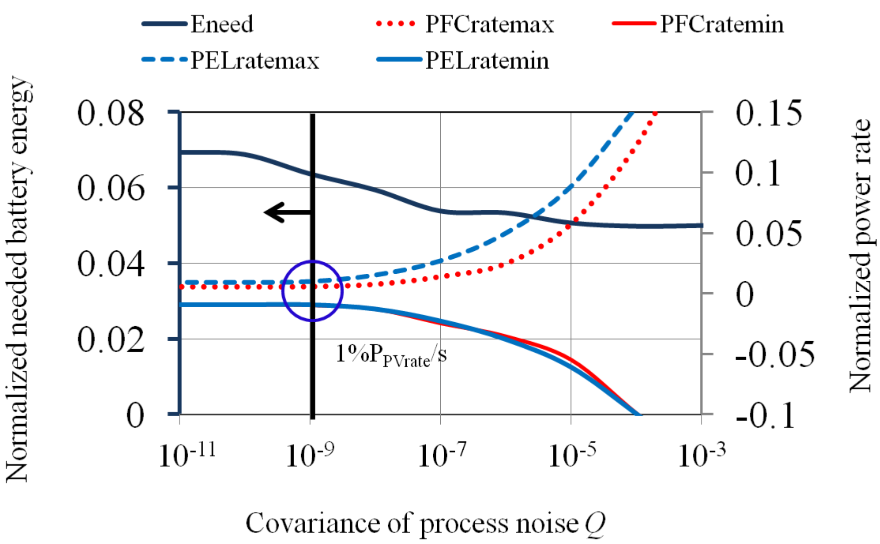

Figure 2. 33: The normalized needed energy and power changing rate of EL/FC depending on covariance noise Q for all days.

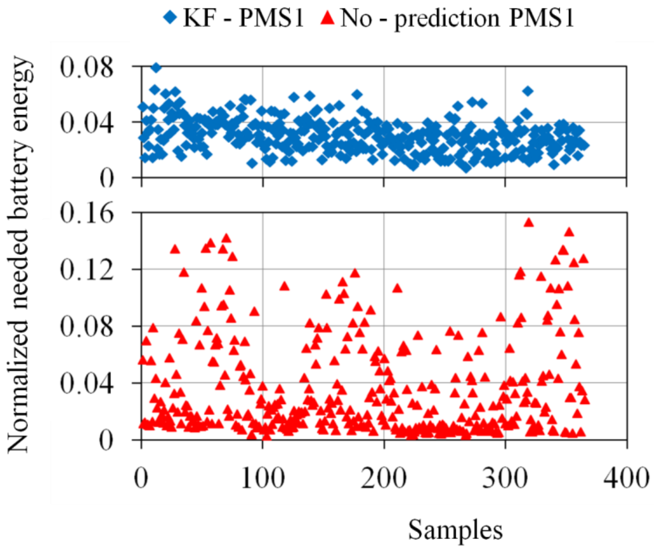

Figure 2. 34: Comparison of the required battery energy for 365 samples of PV power using KF and no prediction in the case of PMS1.

Figure 2.34 compares $E_{\text{need}}^{\text{1day}}$ for all 365 days using PMS1 with and without trend-prediction method corresponding to Q_o = 10^{-9} and $\eta^{\text{ch}} = \eta^{\text{disch}}$ =1. The result shows that in general, no-prediction PMS would required higher $E_{\text{need}}^{\text{1day}}$ in all days than using KF. Summary for 1 year, E_{need} in the case of using KF is smaller than that of no-prediction method of up to 56% (0.0064 compared with 0.146). The result can be explained by the ability of KF to filter the symmetrical fluctuation part of the stochastic waveform as expected. In addition, by adjusting the noise covariance Q, the more symmetric fluctuating component which was covered by battery could be drew out. The energy was kept fluctuating around one value by consecutively increasing and decreasing due to charge and discharge process which results in smaller capacity of battery.

When the distribution of fluctuation of PV power is asymmetric as shown in Figure 2.30 (b) and when the efficiency of charging and discharging process was taken into account, the offset was introduced into the PMS algorithm (PMS2). The simulation for PMS2 was carried out with different coefficients K and different efficiency. Figure 2.35 illustrates the evolution of energy in battery using KF-PMS1 and PMS2 in March 18th 2013 with $Q = 10^{-9}$ when $\eta^{ch} = \eta^{disch} = 1$ and $K = 10$. The evolution energy in this day using PMS2 (purple line) fluctuated around 1 value, that is more stable than that of using KF-PMS1. It also needed $E_{\text{need}}^{\text{1day}}$ in PMS2 case smaller than in KF-PMS1. The comparison of $E_{\text{need}}^{\text{1day}}$ for all samples is depicted in Figure 2.36 corresponding to $\eta^{ch} = \eta^{disch} =1$ and $K = 0$ (PMS1) and $K = 10$ (PMS2). In this case, for each day, $E_{\text{need}}^{\text{1day}}$ is considerably smaller than in PMS1. The required energy for all days $E_{\text{need-all}}$ in PMS2 decreases about 14% comparing to KF-PMS1 (0.055 compared with 0.064). For each efficiency $\eta^{ch} = \eta^{disch} = \eta$, we changed the adjustment coefficient K and find out with which K the required energy would be smallest. Figure 2.37 shows the suitable K that obtained the minimum $E_{\text{need-all}}$ corresponding to different efficiency. When charging/discharging efficiency is high, the adjustment of power needs small coefficient K and resulting in small required battery, and vice versa, when it is low, the suitable K and corresponding E_{need} will be higher.

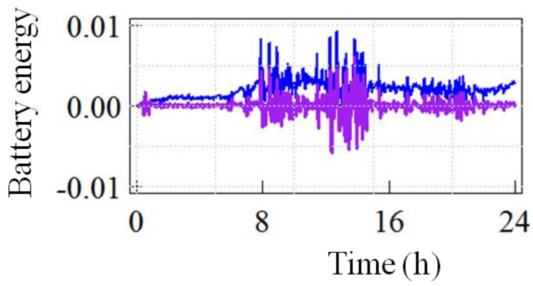

Figure 2. 35: Evolution of E_{Bat} using KF – PMS1 ($Q = 10^{-9}$, $K = 0$) and improved PMS2 ($Q = 10^{-9}$, $K = 10$) in the case of $\eta = 1$

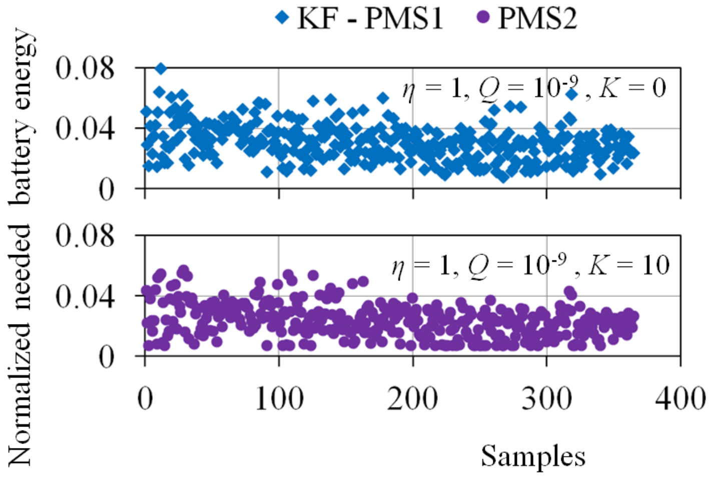

Figure 2. 36: Comparison of the needed battery energy for 365 samples of PV power using KF – PMS1 and PMS2.

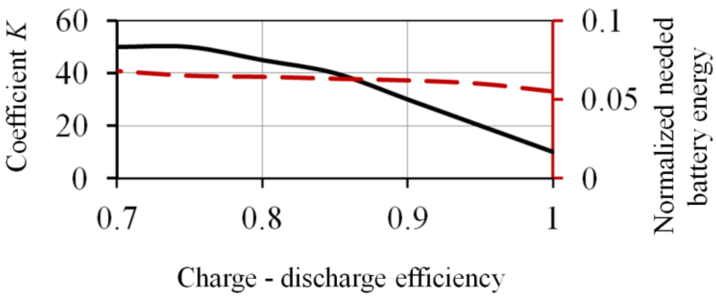

Figure 2. 37: Suitable K and corresponding needed battery energy depending on the efficiency of charging/discharging process using PMS2.

2.4 Conclusions

In this chapter, we proposed a new trend-prediction PMS for a PV based MG to obtain stable and sustainable operation. The proposed PMS was based on the dynamic characteristics of the devices in the system to allocate the power. The trend of the difference between PV power and load demand would be predicted using Kalman Filter and designate to hydrogen system which has slow dynamic characteristics.

Battery with fast transient response would cover the deviation between the actual power and the power consumed/generated by hydrogen system.

Firstly, the proposed PMS was applied in the PV/FC/LiB in CNES in Tsukuba, Japan. Because the battery in the system has large capacity, it is operated not only as a compensator to respond to the fast fluctuation but also as energy storage. The dynamic characteristics of FC and LiB was identified through experiment and modelled. We can choose the suitable covariance Q of KF to adapt the limited changing rate of FC. Simulation results show that with suitable KF parameter, the proposed control method can be applied to the PV system for stable operation in short time as well as in long time. In comparison with conventional PMS, the proposed PMS consume less hydrogen, resulting in higher energy conversion efficiency.

Secondly, we applied the proposed PMS to estimate and downsize the required battery capacity for an existing PV/hydrogen system. In this case, the battery is responsible for covering the fluctuation only. KF can separate the stochastic waveform into trend and fluctuated components as expected, then it can be possibly effective in allocate the symmetric fluctuated component to battery, resulting in smaller energy capacity requirement. Through simulation, the proposed trend-prediction PMS shows its ability in decreasing the necessary capacity of battery of up to 56% in comparison with conventional no-prediction PMS. Considering the asymmetric distribution of power changing rate and the efficiency of the charging/discharging process, the PMS was then improved by combining KF with offset to adjust the power for battery within the limited changing rate of hydrogen system. The proposed improved PMS can decrease the required capacity of up to 14%.

2.5 References

[1] Pragya Nema, R.K. Nema, Saroj Rangnekar, A current and future state of art development of hybrid energy system using wind and PV-solar: A review, Renewable and Sustainable Energy Reviews 13 (2009) 2096–2103.

[2] R. Banos, F. Manzano – Agugliaro, F.G. Montoya, C. Gil, A. Alcayde, J. Gómez, Optimization methods applied to renewable and sustainable energy: A review, Renewable and Sustainable Energy Reviews 15 (2011) 1753–1766

[3] Annabel Yadoo, Heather Cruickshank, The role for low carbon electrification technologies in poverty reduction and climate change strategies: A focus on renewable energy mini-grids with case studies in Nepal, Peru and Kenya, Energy Policy 42 (2012) 591–602

[4] Arif Hepbasli, A key review on exergetic analysis and assessment of renewable energy resources for a sustainable future, Renewable and Sustainable Energy Reviews 12 (2008) 593–661

[5] M. Iqbalb, M. Azam, M. Naeem, A.S. Khwaja, A. Anpalagan, Optimization classification, algorithms and tools for renewable energy: A review, Renewable and Sustainable Energy Reviews 39 (2014) 640–654

[6] Omar Ellabban, Haitham Abu-Rub, Frede Blaabjerg, Renewable energy resources: Current status, future prospects and their enabling technology, Renewable and Sustainable Energy Reviews 39 (2014) 748–764

[7] J.E. Paiva, A.S. Carvalho, Controllable hybrid power system based on renewable energy sources for modern electrical grids, Renewable Energy 53 (2013) 271-279

[8] Anurag Chauhan, R.P. Saini, A review on Integrated Renewable Energy System based power generation for stand-alone applications: Configurations, storage options, sizing methodologies and control, Renewable and Sustainable Energy Reviews 38 (2014) 99–120

[9] Xingguo Tan, Qingmin Li, Hui Wang, Advances and trends of energy storage technology in Microgrid, Electrical Power and Energy Systems 44 (2013) 179–191

[10] P.G. Arul, Vigna K. Ramachandaramurthy, R.K. Rajkumar, Control strategies for a hybrid renewable energy system: A review, Renewable and Sustainable Energy Reviews 42 (2015) 597–608

[11] O. Alsayegh, S. Alhajraf, H. Albusairi, Grid-connected renewable energy source systems: Challenges and proposed management schemes, Energy Conversion and Management 51 (2010) 1690–1693

[12] Abdelkafi, Lotfi Krichen, Energy management optimization of a hybrid power production unit based renewable energies, Electrical Power and Energy Systems 62 (2014) 1–9

[13] Dimitris Ipsakis, Spyros Voutetakis, Panos Seferlis, Fotis Stergiopoulos, Costas Elmasides, Power management strategies for a stand-alone power system using renewable energy sources and hydrogen storage, International Journal of Hydrogen Energy 34 (2009) 7081-7095

[14] M. Hattia, A. Meharrarb, M. Tioursi, Power management strategy in the alternative energy photovoltaic/PEM Fuel Cell hybrid system, Renewable and Sustainable Energy Reviews 15 (2011), 5104-5110

[15] Mohammad Sadigh Behzadi, Mohsen Niasati, Comparative performance analysis of a hybrid PV/FC/battery stand-alone system using different power management strategies and sizing approaches, International Journal of Hydrogen Energy 40 (2015) 538-548

[16] Erkan Dursun, Osman Kilic, Comparative evaluation of different power management strategies of a stand-alone PV/Wind/PEMFC hybrid power system, Electrical Power and Energy Systems 34 (2012) 81–89

[17] Vaishalee Dash, Prabodh Bajpai, Power management control strategy for a stand-alone solar photovoltaic-fuel cell–battery hybrid system, Sustainable Energy Technologies and Assessments 9 (2015) 68–80

[18] O.C. Onara, M. Uzunoglu, M.S. Alam, Modeling, control and simulation of an autonomous wind turbine/photovoltaic/fuel cell/ultra-capacitor hybrid power system, Journal of Power Sources 185 (2008) 1273–1283

[19] Øystein Ulleberg, The importance of control strategies in PV–hydrogen systems, Solar Energy 76 (2004) 323–329.

[20] Keliang Zhou, J.A. Ferreira, S.W.H. de Haan, Optimal energy management strategy and system sizing method for stand-alone photovoltaic-hydrogen systems, International Journal of Hydrogen Energy 33 (2008) 477– 489

[21] Ipsakis, D., Voutetakis, S., Seferlis,P., Stergiopoulos, F., Papadopoulou,S., Elmasides, C., The effect of the hystereris band on power management strategies in a stand – alone power system, Energy 33 (2008) 1537-1550

[22] Roberto Carapellucci, Lorena Giordano, Modeling and optimization of an energy generation island based on renewable technologies and hydrogen storage systems, International Journal of Hydrogen Energy 37 (2012) 2081-2093

[23] M. Trifkovic, M. Sheikhzadeh, K. Nigim and P. Daoutidis, “Modeling and Control of a Renewable Hybrid Energy System with Hydrogen Storage”, Control Systems Technology, IEEE Transactions on Vol. 22, Issue 1 (2014), pp. 169-179.

[24] Chrysovalantou Ziogou, Dimitris Ipsakis, Costas Elmasides, Fotis Stergiopoulos, Simira Papadopoulou, Panos Seferlis, Spyros Voutetakis, Automation infrastructure and operation control strategy in a stand – alone power system based on renewable energy sources, Journal of Power Sources 196 (2011), 9488– 9499.

[25] Benjamin Guinot, Benedicte Champel, Florent Montignac, Elisabeth Lemaire, Didier Vannucci, Sebastien Sailler, Techno-economic study of a PV – hydrogen – battery hybrid system for off-grid power supply: Impact of performances' ageing on optimal system sizing and competitiveness, International Journal of Hydrogen Energy 40 (2015) 623- 632

[26] Rodolfo Dufo-Lopez, Jose L. Bernal-Agustin, Javier Contreras, Optimization of control strategies for stand – alone renewable energy systems with hydrogen storage, Renewable Energy 32 (2007) 1102–1126

[27] Rihab Jallouli, LotfiKrichen, Sizing, techno-economic and generation management analysis of a stand-alone photovoltaic power unit including storage devices, Energy 40 (2012) 196-209

[28] Manuel Castaneda, Antonio Cano, Francisco Jurado, Higinio Sanchez, Luis M. Fernandez, Sizing optimization, dynamic modeling and energy management strategies of a stand-alone PV/hydrogen/battery-based hybrid system, International Journal of Hydrogen Energy 38 (2013) 3830-3845

[29] J.P. Torreglosa, P. García, L.M. Fernández, F. Jurado, Hierarchical energy management system for stand – alone hybrid system based on generation costs and cascade control, Energy Conversion and Management 77 (2014) 514–526

[30] A. Tascikaraoglu, O. Erdinc, M. Uzunoglu, A. Karakas, An adaptive load dispatching and forecasting strategy for a virtual power plant including renewable energy conversion units, Applied Energy 119 (2014) 445–453

[31] Xiaonan Wang, Ahmet Palazoglu, Nael H. El – Farra, Operational optimization and demand response of hybrid renewable energy systems, Applied Energy 143 (2015) 324–335.

[32] Giorgio Cau, Daniele Cocco, Mario Petrollese, Søren Knudsen Kær, Christian Milan, Energy management strategy based on short-term generation scheduling for a renewable Microgrid using a hydrogen storage system, Energy Conversion and Management 87 (2014) 820–831

[33] Pablo García – Trivino, Francisco Llorens – Iborra, Carlos A. García – Vazquez, Antonio J. Gil – Mena, Luis M. Fernandez – Ramírez, Francisco Jurado, Long-term optimization based on PSO of a grid-connected renewable energy/battery/hydrogen hybrid system, International Journal of Hydrogen Energy 39 (2014) 10805-10816.

[34] Kehe Wu, Huan Zhou, Sicheng An, Ting Huang, Optimal coordinate operation control for wind-photovoltaic-battery storage power-generation units, Energy Conversion and Management 90 (2015) 466–475

[35] Nakayama, T., Yagai, T., Tsuda, M., Hamajima, T., Optimization of SMES compensation capacity for stochastic power using Kalman Filter, Journal of Cryogenics and Superconductivity Society of Japan, 45 (2010) 99-106

[36] Nakayama, T.: PhD Dissertation, University of Tohoku, Japan, (2011)

[37] http://en.wikipedia.org/w/index.php?title=File:Solid_oxide_fuel_cell_protonic.svg&page=1

[38] Hong Sun, Guangsheng Zhang, Liejin Guo, Hongtan Liu, A Study of dynamic characteristics of PEM fuel cells by measuring local currents, International Journal of Hydrogen Energy, 34 (2009) 5529 – 5536

[39] Yongping Hou, Zhihua Yang, Xue Fang, An experimental study on the dynamic process of PEM fuel cell stack voltage, Renewable Energy 36 (2011) 325-329

[40] Marcos V. Moreira, Gisele E. da Silva, A practical model for evaluating the performance of proton exchange membrane fuel cells, Renewable Energy 34 (2009) 1734–1741

[41] Yerramalla Sampath, Davari Asad, Feliachi Ali, Biswas Tamal, Modeling and simulation of the dynamic behavior of a polymer electrolyte membrane fuel cell, Journal of Power Sources 124 (2003) 104- 113

[42] Chen Falin, Wen Ying-Zhi, Chu Hsin-Sen, Yan Wei-Mon, Soong Chyi-Yeou, Convenient two-dimensional model for design of fuel channels for proton exchange membrane fuel cells, Journal of Power Sources 128 (2004) 125-134

[43] Ceraolo M, Miulli C, Pozio A, Modelling static and dynamic behaviour of proton exchange membrane cells on the basis of electro-chemical description, Journal of Power Sources 113 (2003) 131-144.

[44] Pathapati PR, Xue X, Tang J. A new dynamic model for predicting transient phenomena in a PEM fuel cell system. Renewable Energy 30 (2005) 1-22.

[45] Wang Y, Wang C-Y, Transient analysis of polymer electrolyte fuel cells, Electrochim Acta, 50 (2005) 1307-1315.

[46] M. Boaventura, J.M. Sousa, A. Mendes, A dynamic model for high temperature polymer electrolyte membrane fuel cells, International Journal of Hydrogen Energy 36 (2011) 9842 – 9854

[47] M.J. Khan, M.T. Iqbal, Dynamic modeling and simulation of a small wind–fuel cell hybrid energy system, Renewable Energy 30 (2005) 421–439

[48] J. Kim, J. Je, M. Kaviany, S. Y. Son, M. H. Kim, Fuel crossover and internal current in polymer electrolyte membrane fuel cell from water visualization using X-ray radiography, Journal of Power Sources 196 (2011) 8398–8401

[49] P. Costamagna, A. Selimovic, M. D. Borghi, G. Agnew, Electrochemical model of the integrated planar solid oxide fuel cell (IP-SOFC), Chemical Engineering Journal 102 (2004) 61–69

[50] S.H. Chan, K.A. Khor, Z.T. Xia, A complete polarization model of a solid oxide fuel cell and its sensitivity to the change of cell component thickness, Journal of Power Sources 93 (2001) 130-140

[51] Rui Xiong, Xianzhi Gong, Chunting Chris Mi, Fengchun Sun, A robust state–of–charge estimator for multiple types of lithium-ion batteries using adaptive extended Kalman Filter, Journal of Power Sources 243 (2013) 805-816

[52] Kumar, C. S., Jain, Y. Kr., Kapoor, H., Bapi, R. S., Yadaiah, N., Negi, A., Rao V. S., Deekshatulu B. L, State Estimation and Tracking Problems: A Comparison Between Kalman Filter and Recurrent Neural Networks, Neural Information Processing, Lecture Notes in Computer Science 3316 (2004) 275-281

[53] Ishikawa, M., Moriyama, T., Prediction of time series by a structural learning of neural networks, Fuzzy Sets and Systems 82 (1996) 167-176

[54] Zemouri, R., Gouriveau, R., Zerhouni, N., Defining and applying prediction performance metrics on a recurrent NARX time series model", Neurocomputing 73 (2010) 2506–2521

[55] Li, G., Shi, J., On comparing three artificial neural networks for wind speed forecasting, Applied Energy 87 (2010) 2313–2320

[56] Liu H., Tian H., Li Y., Comparison of two new ARIMA-ANN and ARIMA- Kalman hybrid methods for wind speed prediction, Applied Energy 98 (2012) 415–424

Chapter 3: Optimal capacity design of PV system by minimizing levelized cost of energy (LCE) and development of rapid estimation formula for grid dependency (GD)

3.1 Introduction

In chapter 2, we considered a PV – based MG in the aspect of the PMS for an existing system. The proposed trend-prediction PMS considering the dynamic charactersitics of the devices shows its efficiency in stable performance and more effective than conventional PMS. However, the optimal sizing of the system has not considered. Due to the high capital cost of the RE systems, it is essential to define the proper sizing of the systems to use the RE more efficiently and economically [1] . Numerous studies on sizing optimization have been reported [2-19]. Almost the researches solved the problem by examining the optimization functions which were based on minimizing the cost of the system [2-5], the levelized cost of energy (*LCE*) [6-10] or maximizing the net present value (*NPV*) of the system [11] and assessed the system reliability by several indices such as loss of power supply probability (*LPSP*) [3,6-9,12], loss of load expected (*LOLE*), loss of energy expected (*LOEE*) or Expected Energy not Supplied (*EENS*) and Equivalent Loss Factor (*ELF*), etc. [13]. There have been many methods used so far to solve the optimization functions, such as probabilistic, analytical and iterative methods [6]. The probabilistic method which was based on the weather average value [12, 14] or the worst scenarios [15] was considered as a simple approach. Yang et al. developed and applied the so-called typical meteorological year (TMY) for probability study on an hourly basis to analyze the system performance [12]. However, the designs achieved by this method seem to be over-sized or inaccurate. In analytical method, the system performance assessment can be computed using a set of possible system configurations or a particular size of the components [6, 7, 11]. Other methods that have been developed and inspired by biology are Genetic Algorithm (GA) [8, 13, 16], Particle Swarm Optimization (PSO) [17–19], Artificial Neural Network (ANN) [20]. These methods do not require deep knowledge of the system; however, the calculation is relatively complicated.

On the other hand, the system reliability has been assessed considering the weather data in a typical year or an assumed solar irradiance waveform for a certain location [12, 14, 15]. Thus, the optimization process must be reconducted at a different location. According to our knowledge, there has been no empirical formula showing the dependence of the system reliability on the weather conditions and the devices' capacities. Such empirical formula not only illustrates the relationship between them but also makes the optimization problem simpler and easier. Hence, this research aims at establishing a formula which can be used to quantify the effect of the weather conditions to the system reliability as well as optimize the sizing capacity. In our previous work, the sizing of a PV/battery system was investigated [21]. The system reliability, namely the grid dependency (*GD*), defined as the dependence of the system on the grid when the system cannot supply to the load and receive the shortage power from the grid, was found to be dependent on the annual total solar insolation [21]. However, the battery was used as a single storage for the PV system. In this work, the research is further expanded with the integration of a hydrogen system. The optimal capacity of PV and the storages can be obtained using a simple iterative method based on the required *GD* and the minimum *LCE*. We calculated the *GD*, using the 25 – year weather data at 9 locations throughout Japan, aiming to find out a general relationship between the *GD* and other parameters. After obtaining such empirical relationship, the system reliability in any Japan's location can be quickly calculated from the formula.

3.2 Model of the system

A block diagram of hydrogen based RES system with battery is depicted in Figure 2.27 in previous chapter. The system is composed of PV arrays, battery and hydrogen system supplying power to the load. All the devices are combined together to a DC bus through DC/DC converters. The system also connects to the grid through AC/DC converter. The grid is responsible for receiving the excess power or supplying the shortage power of the hybrid RES system if necessary.

3.2.1. PV power:

The PV output power is highly influenced by the weather conditions, especially the solar irradiance and the temperature. It can be estimated as below,

$$P_{\mathrm{PV}}(t) = C_{\mathrm{PV}} \times \frac{S(t)}{\mathrm{S_{STD}}} \times \eta_{\mathrm{loss}}(t) \times \eta_{DC/DC}^{PV} \tag{3.1}$$

where $P_{\mathrm{PV}}(t)$, $C_{\mathrm{PV}}(t)$ are the output power and the rated power of PV (kW), respectively. $S(t)$, $\mathrm{S_{STD}}$ are the real solar irradiance at the tilted surface of PV panels (kW/m^2) and the standard solar irradiance (1 kW/m^2), respectively. $\eta_{DC/DC}^{PV}$ is the efficiency of the DC/DC converter. η_{loss} is the efficiency standing for the loss due to the temperature increase,

$$\eta_{\mathrm{loss}}(t) = 1 - \lambda\left(T_{\mathrm{cell}}(t) - 25\right) \tag{3.2}$$

$$T_{\mathrm{cell}}(t) = T_{\mathrm{a}}(t) \times \frac{S(t)}{0.8} \times \left(\mathrm{T_{NOCT}} - 20\right) \tag{3.3}$$

where λ represents the temperature coefficient (0.00485/°C), $T_{\mathrm{cell}}(t)$, $T_{\mathrm{a}}(t)$ and $\mathrm{T_{NOCT}}$ are the temperature of the PV cell, the ambient temperature [°C] and the nominal operating cell temperature (45°C), respectively.

The solar irradiance depends on the location, the tilted surface of the PV panels. In the present work, the model of solar irradiance on the tilted surface presented in Ref. [22, 23] was used. In general, the solar irradiance on the titled surface includes three components: the direct beam, the diffuse radiation, and the reflected light. The more detail of the model for these elements can be found in Ref. [22, 23].

3.2.2. Battery

Battery is modeled by stored energy that could be calculated as a function of the battery power at the DC bus side during the charge and discharge process as below,

$$E_{Bat}(t) = E_{Bat}(t-1)\times(1-\sigma) + (P_{DCside}^{Bat.ch}(t-1)\times\eta^{ch}\times\eta_{DC/DC}^{Bat} - \frac{P_{DCside}^{Bat.disch}(t-1)}{\eta^{disch}\times\eta_{DC/DC}^{Bat}})\times\Delta t \tag{3.4}$$

where $E_{BA}(t)$ is the energy in the battery at time t, $P_{DCside}^{BA.ch}$, $P_{DCside}^{BA.disch}$ is the charge and discharge power allocated to the battery at DC bus side of DC/DC converter, σ is the self-discharge rate of the battery (0.0046 /day=0.0046/24h), Δt is time step (1h). η^{ch} and η^{disch} are the efficiencies of the charge and discharge process, respectively ($\eta^{ch} = \eta^{disch} = 0.9$), $\eta_{DC/DC}^{BA}$ is the DC/DC converter efficiency ($\eta_{DC/DC}^{BA} = 0.9$).

3.2.3. Hydrogen system:

Hydrogen system includes an electrolyzer (EL), a fuel cell (FC) with inverse functions and operation, and a hydrogen tank. EL will consume electrical power in the case of surplus power to produce hydrogen which is then stored in the hydrogen tank. FC is contrary which uses the hydrogen from the tank to generate electrical power during the period of shortage power. It can be noted that due to the inverse functions, FC and EL will not work at the same time. For this system, the optimization variables will be the EL and FC capacity. In numerous previous studies, the electrolyzer's output is directly injected into a hydrogen tank [13, 17, 24–27]. In some cases, a compressor may be integrated into the hydrogen system to pressurize the hydrogen to increase its density [28, 29]. However, in Japan, a very high-pressure (35 MPa) electrolyzer without a gas compressor has been developed by Honda Motor Co., Ltd. [30, 31]. For this reason, we assumed that the electrolyzer is directly connected to the hydrogen tank without a gas compressor.

The hydrogen system is modeled using a parameter of the equivalent energy of hydrogen in the hydrogen tank. The equivalent energy in the hydrogen tank will decrease when the FC works and vice versa, increase when the EL operates.

$$E_{\text{tank}}(t) = E_{\text{tank}}(t-1) + (P_{DCside}^{EL}(t-1) \times \eta_{\text{EL}} \times \eta_{\text{DC/DC}}^{\text{EL}} - \frac{P_{DCside}^{FC}(t-1)}{\eta_{\text{FC}} \times \eta_{\text{DC/DC}}^{\text{FC}} \times \eta_{\text{storage}}}) \times \Delta t \tag{3.5}$$

in which $E_{\text{tank}}(t)$ is the equivalent energy in the hydrogen tank at time t (kWh), $P_{\text{DCside}}^{\text{EL}}(t-1)$ and $P_{\text{DCside}}^{\text{FC}}(t-1)$ represent the power at the DC bus side of the EL and the FC, η_{EL}, η_{FC}, are the efficiencies of the energy conversion of the EL and the FC. η_{tank} expresses the efficiency of the hydrogen tank, ($\eta_{\text{EL}} = 0.6$, $\eta_{\text{FC}} \times \eta_{\text{tank}} = 0.5$) [9], $\eta_{\text{DC/DC}}^{\text{EL}}$ and $\eta_{\text{DC/DC}}^{\text{FC}}$ are the DC/DC converters' efficiencies ($\eta_{DC/DC}^{EL} = \eta_{DC/DC}^{FC} = 0.9$).

3.2.4. Load profile:

In this study, the system is supposed to supply to 2 kinds of load patterns: a network of domestic household load (pattern 1) and a constant load (pattern 2) which are shown in Fig. 3.1. It can be realized that there are uncertainties associated with the load and the PV power. We consider the uncertainties of the PV power and adopt the determined smooth average load. The results will be affected but insignificantly because the uncertainties of the load if any can be assumed in the uncertainties of the PV power. The hourly mean value of the load has been used as input data of the optimization problems in the literature [6, 25, 32–35]. In fact, the criteria for system evaluation can not be exactly determined due to those uncertainties. The calculation considering the uncertainties of the load is still a relative result. Thus, the use of average load can be acceptable in this case. Moreover, it should be noted that the load was created to generalize the work so that the total daily consumed energy is 1kWh.

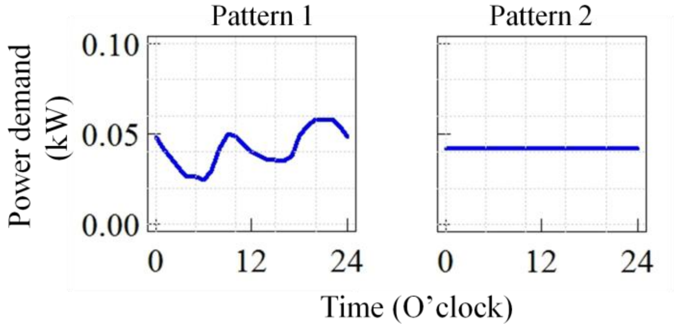

Figure 3. 1: The load profile for domestic household (pattern 1) and hospital (pattern 2)

3.2.5. Weather data:

As mentioned above, the weather data, namely the hourly solar irradiance and the temperature during the past 25 years (from 1990 to 2014) at 9 locations (except Tokyo) around Japan obtained from a database of Japan Meteorological Agency [36] are used. The nine selected cities scatter around Japan, from the north to the south, the west to the east of Japan, as illustrated in Fig. 3.2a. An example of the collected weather data in 1999 in Osaka is shown in Fig. 3.2b. In addition, the meteorological data of Tokyo during this period is also acquired for the verification of the established formula.

3.2.6. Power management strategy:

Power management strategy is a control method to ensure the energy balance of the system. The chosen PMS in this work is similar to the strategy in Ref. [24] and shown in Fig. 3.3. In this strategy, the on/off switch of the EL/FC will be dependent on the level of the energy in the battery as well as in the hydrogen tank.

In general, the insufficient power from PV to the load will be supplied from the storages and/or the grid if necessary. Otherwise, the excess power from the RE system can be stored in the battery/hydrogen system or sold to the grid. However, when the penetration of the PV increases further, the utilities/grids may order the output restriction or curtail the available RE input to maintain the system security [37, 38]. In fact, several utilities in Japan recently ordered the plants to reduce the output due to the agile solar development in recent years. Hence, we consider the PV system in the case that the grid will not buy the excess energy [39]. The excess energy will be stored in the battery and the hydrogen system or using dump load. Although the efficiency of the hydrogen system is quite low, when it is introduced into the system, we can combine the electricity and the heat generation, which may result in improving the efficiency of the system. However, this is of different scope and objective and is not considered in this research.

The allocation of the power to the storages will be decided based on the difference between the power produced by PV, $P_{PV,}$ and the demand P_D:

When $\Delta P = P_{PV} - P_D < 0$, the necessary power to satisfy the load is provided by the battery if it is not deeply discharged. It will partly or fully supply the shortage power depending on the energy in the battery. If the battery cannot supply all the shortage, the FC will be considered to operate based on the equivalent energy in the hydrogen tank. In the final case, if no storages can provide to the load or just provide partly, the grid will be responsible for the shortage. The received power from the grid can be calculated as following,

$$P_{\mathrm{grid}} = P_{\mathrm{D}} - P_{\mathrm{PV}} - P_{\mathrm{BA}} - P_{\mathrm{FC}} \tag{3.6}$$

when $\Delta P > 0$, the excess power will be charged for the battery if it is not full. In the case of fully charged battery, this surplus energy will be consumed by the EL depending on its rated power and the limited equivalent energy in the hydrogen tank or dumped if all storages are full.

The detail of the algorithm can be found in Ref. [24].

3.3 Optimal sizing criteria

3.3.1. System reliability criterion:

In this study, the criterion for evaluating the reliability of the RES system is the grid dependency (*GD*) which is defined as the dependence of the RES on the grid in supplying to the load in the case of shortage power. The value of the *GD* is a number from 0 to 1. The *GD* of 0 means that the RES system can fully supply to the load without the grid. In other words, it can operate in stand-alone mode. In contrast, the *GD* of 1 means that the load will completely receive the power from the grid. The *GD* is defined as the ratio of the total energy receiving from the grid when the RES system cannot meet the demand to the expected load energy in 1 year,

$$GD = \frac{\sum_{t=1}^{8760}\left(P_{\mathrm{grid}}(t)\times 1\right)}{E_{\mathrm{Dyear}}} \tag{3.7}$$

where $P_{\mathrm{grid}}(t)$ (kW) stands for the power receiving from the grid at time t, $E_{\mathrm{Dyear}} = \sum_{t=1}^{8760} P_{\mathrm{D}}(t)$ is the total energy of the load in 1 year.

As analyzed in the above subsection, the excess energy will be stored in the storages or dump load. If the grid agrees to buy the excess energy, this value can be used as a criterion to design the system capacity, together with the grid dependency. In this case, the grid dependency will not be changed because it is defined by the shortage power receiving from the grid. It is unreasonable if the *GD* is defined including both the shortage and the excess energy receiving from or selling to the grid because it will be zero if the shortage and the excess energy are equal, but in this case, the system still depends on the grid.

(a)

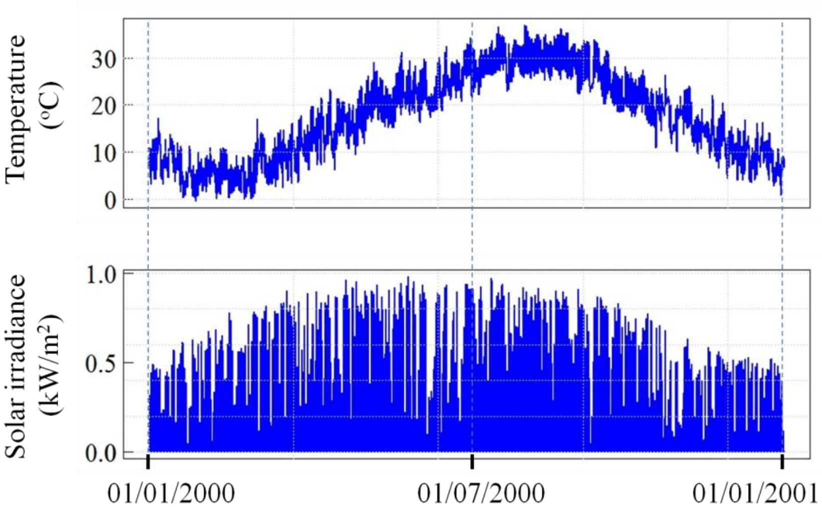

(b)

Figure 3. 2: (a) The typical climate locations throughout Japan (Sapporo, Sendai, Niigata, Wajima, Osaka, Hiroshima, Kochi, Kagoshima, and Naha) and (b) example of the ambient temperature and the solar irradiation in 1999 in Osaka

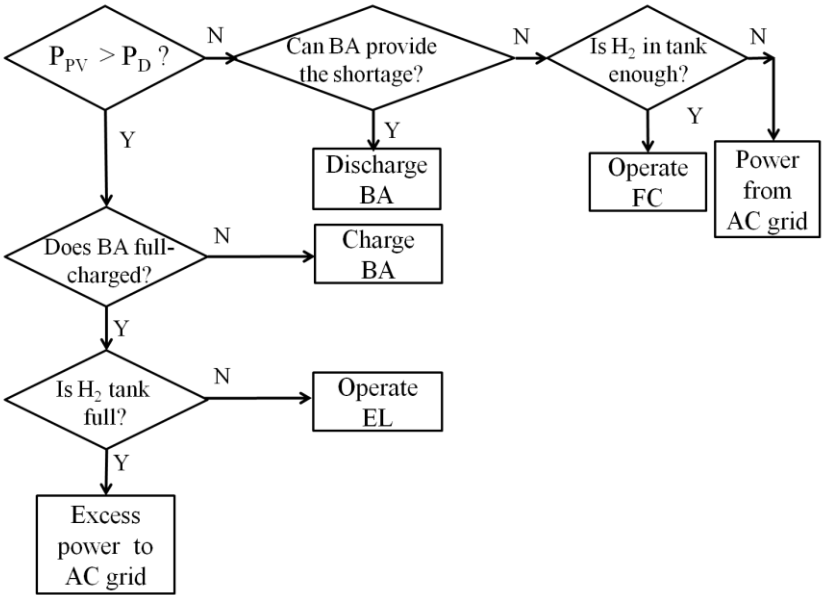

Figure 3. 3: The general PMS for the system under study [24]

The calculation of the *GD* corresponding to each configuration of the system can be carried out according to the following procedure. The power allocation to the devices in one location in a certain year can be determined based on the proposed PMS, the models of the devices, and the assumed load which were expressed in section 3.2. Then the *GD* can be calculated using equation (3.7) based on the shortage power receiving from the grid in one year.

3.3.2. Economic criterion:

It is evident that the economic issue plays an important role in any project. While designing the optimal capacity of a RES system, the economic analysis should be conducted. The *LCE* is widely considered in sizing optimization [6–10] because it is a simple but effective way for the economic assessment of a RES system [9]. It can be defined as the constant price per unit of energy as the following equation:

$$LCE = \frac{AC_{sys} + AC_{grid}}{E_{Dyear}} \tag{3.8}$$

where LCE (¥/kWh) is the levelized cost of energy, AC_{sys} (¥) and AC_{grid} (¥) are the annual cost of the system and the annual cost of purchasing power from the grid, respectively. These two kinds of cost can be calculated as below,

$$AC_{\mathrm{sys}} = \left(PC_{\mathrm{equip}} + PC_{\mathrm{aux}} + PC_{\mathrm{rep}}\right) \times \mathrm{CRF} + AC_{\mathrm{O\&M}} \tag{3.9}$$

$$AC_{\mathrm{grid}} = E_{\mathrm{Dyear}} \times GD \times \mathrm{k}_{\mathrm{grid.u}} \tag{3.10}$$

Where annual cost of the system AC_{sys} includes the main equipment cost PC_{equip}, the auxiliary equipment cost PC_{aux}, the total replacement cost PC_{rep}, the annual operation and maintenance cost $AC_{\mathrm{O\&M}}$. $k_{\mathrm{grid.u}}$ (¥/kWh) represents the electricity price purchased from the grid and is assumed to be constant. CRF is the capital recovery factor used to change the present capital cost to the annual capital cost:

$$CRF = \frac{i(1+i)^N}{(1+i)^N + 1} \tag{3.11}$$

where i is the interest rate, N is the project lifetime. The number of years has been used in numerous previous works to assess the life expectancy of the system as well as the storages [3, 6, 13, 25, 32–34, 40]. We assumed that the system lifetime is the life of the PV module (20 years) [34, 40], the battery lifetime is 4 years [6, 32, 34], and the lifetime of the FC/EL/converters is 10 years [25, 32, 33]. Thus they need to be replaced one or several times during the project lifetime [25, 40].

The above components of the cost can be estimated by equation (3.12) – (3.15)

$$PC_{\text{equip}} = \text{k}_{\text{PV.u}} \times C_{\text{PV}} + \text{k}_{\text{BA.u}} \times C_{\text{BA}} + \text{k}_{\text{EL.u}} \times C_{\text{EL}} + \text{k}_{\text{FC.u}} \times C_{\text{FC}} + \text{k}_{\text{DC/DC.u}} \times (C_{\text{PV}} + C_{\text{BA}} + C_{\text{EL}} + C_{\text{FC}}) \tag{3.12}$$

$$PC_{\text{aux}} = PC_{\text{equip}} \times \text{r}_{\text{aux}} \tag{3.13}$$

$$AC_{\text{O\&M}} = (PC_{\text{equip}} + PC_{\text{aux}}) \times \text{r}_{\text{O\&M}} \tag{3.14}$$

$$\begin{aligned} PC_{rep} = {} & k_{BA.u} \times C_{BA} \times \sum_{n=1}^{y_{BA}} \frac{1}{(1+i)^{n \times L_{BA}}} + k_{FC.u} \times C_{FC} \times \sum_{m=1}^{y_{FC}} \frac{1}{(1+i)^{m \times L_{FC}}} \\ & + k_{EL.u} \times C_{EL} \times \sum_{j=1}^{y_{EL}} \frac{1}{(1+i)^{j \times L_{EL}}} \\ & + k_{DC/DC.u} \times (C_{PV} + C_{BA} + C_{EL} + C_{FC}) \times \sum_{j=1}^{y_{DC/DC}} \frac{1}{(1+i)^{j \times L_{DC/DC}}} \end{aligned} \tag{3.15}$$

where $k_{\text{PV.u}}$, $k_{\text{BA.u}}$, $k_{\text{EL.u}}$, $k_{\text{FC.u}}$, and $k_{\text{DC/DC.u}}$ represent the unit price, C_{PV}, C_{BA}, C_{EL}, and C_{FC} are the capacity of the devices, respectively. r_{aux} is the ratio of the auxiliary equipment cost to the main equipment cost; $r_{\text{O\&M}}$ is the ratio of the operation and maintenance cost to the equipment cost. L_{BA}, L_{FC}, L_{EL}, $L_{\text{DC/DC}}$ are the lifetime of the battery, the FC and the EL. y_{BA}, y_{FC}, y_{EL}, $y_{\text{DC/DC}}$ are the number of replacements of these components during the project lifetime [13, 29, 32].

The data for the economic evaluation [6, 13, 20, 25, 32, 34, 40] are shown in Table 3.1.

Table 3.1: Data for economic assessment.

Components	PV	Battery	EL	FC	Converter
Lifetime (years)	20	4	10	10	10
Unit price (10^4 ¥/kW or 10^4 ¥/kWh)	55	7	40	40	10
$\text{k}_{\text{grid.u}}$ (¥/kWh)	23		$\text{r}_{\text{O\&M}}$	0.01	
i	0.04		r_{aux}	0.10	

3.3.3. Objective function and constraint:

In the sizing optimization problem, the system needs to be designed to meet the requirement of the system reliability while minimizing the cost. The sizing problem is constructed to determine the optimal capacity of PV (C_{PV}), the battery (C_{BA}), the EL (C_{EL}), the FC (C_{FC}) that can satisfy the load at a specific *GD* at the minimum *LCE*. Because the price of the hydrogen tank is quite small in comparison with the cost of the EL/FC [35], we assume that the hydrogen tank is relatively large to store the hydrogen produced from the EL (E_{tankmax} = 5 kWh).

The optimization problem is described as follows:

$$LCE = f(C_{PV}, C_{BA}, C_{EL}, C_{FC}) \rightarrow \min$$

$$\text{Subject to } GD \leq GD_{required}$$

In which, the *LCE* is calculated using equations (3.8–3.15). The *GD*, which is defined as in equation (3.7), will be estimated based on an empirical formula depending on the weather data and the devices' capacities which is developed in the next section.

3.4 Proposed empirical *GD* formula

In order to obtain the *GD* for solving the optimal sizing problem, in this section, we develop an empirical formula of the *GD* depending on the weather conditions and the devices' capacities. Firstly, the *GD* of the system will be determined for each system configuration (C_{PV}, C_{BA}, C_{EL}, C_{FC}) and the real weather data at 1 location in 1 year.

Fig. 3.4 shows an example of the calculation of the equivalent energy in the hydrogen tank with 3 system configurations in Osaka in 1999: case 1) (red line) C_{PV} = 0.50 kW, C_{BA} = 0.60 kWh, C_{EL} = 0.20 kW, C_{FC} = 0.05 kW, case 2) (green line) C_{PV} =

0.50 kW, C_{BA} = 0.60 kWh, C_{EL} = 0.10 kW, C_{FC} = 0.05 kW, case 3) (black line) C_{PV} = 0.20 kW, C_{BA} = 0.20 kWh, C_{EL} = 0.20 kW, C_{FC} = 0.02 kW (a). It can be noted that the needed hydrogen tank depends on the capacity of the PV and the electrolyzer. The selection of a small storage will significantly affect the ability to store energy and then affect the *GD*. On the other hand, a hydrogen tank with too large volume is unnecessary because it has a slight impact on the *GD*. Moreover, the cost of the hydrogen tank is quite small than that of other devices [35]. Thus, we assume the maximum equivalent energy in the tank is considerably large to store almost all the produced hydrogen from the electrolyzer ($E_{tankmax}$ = 5 kWh). The change of the *GD* is small with a higher hydrogen tank volume. For example, when the maximum energy of the tank is set to be 10 kWh, the *GD* is almost the same with that of the case 5 kWh when the devices' capacities are small and about 0.5% smaller when PV capacity is high. The power receiving from the grid P_{grid} in case 1 is calculated and illustrated in Fig. 3.4b. The *GD* is calculated of 0.112 in this case.

Considering the real hourly weather data at 9 locations throughout Japan in 25 years with a broad range of C_{PV}, C_{BA}, C_{EL}, and C_{FC}, we calculate all the *GD* of the system corresponding to these parameters. Then, the dependence of the *GD* on the weather as well as on the devices' capacities will be analyzed.

3.4.1. GD formula development and the accuracy:

Generally, the *GD* will depend on the waveform of the PV output power, or in other words, rely on the waveform of the solar irradiance and temperature. In this research, the weather data are collected in 25 years at 9 locations. The results of the *GD* show that corresponding to a specific value of (C_{PV}, C_{BA}, C_{EL}, C_{FC}), the *GD* linearly depends on the annual total solar insolation S_{total} (MWh/m^2) as shown in Fig. 3.5. Despite the different waveforms and different locations, the *GD* receives nearly identical value at the same device capacity (C_{PV}, C_{BA}, C_{EL}, C_{FC}) and corresponding to the same S_{total}. Therefore it is possible to determine the *GD* based on the S_{total} without

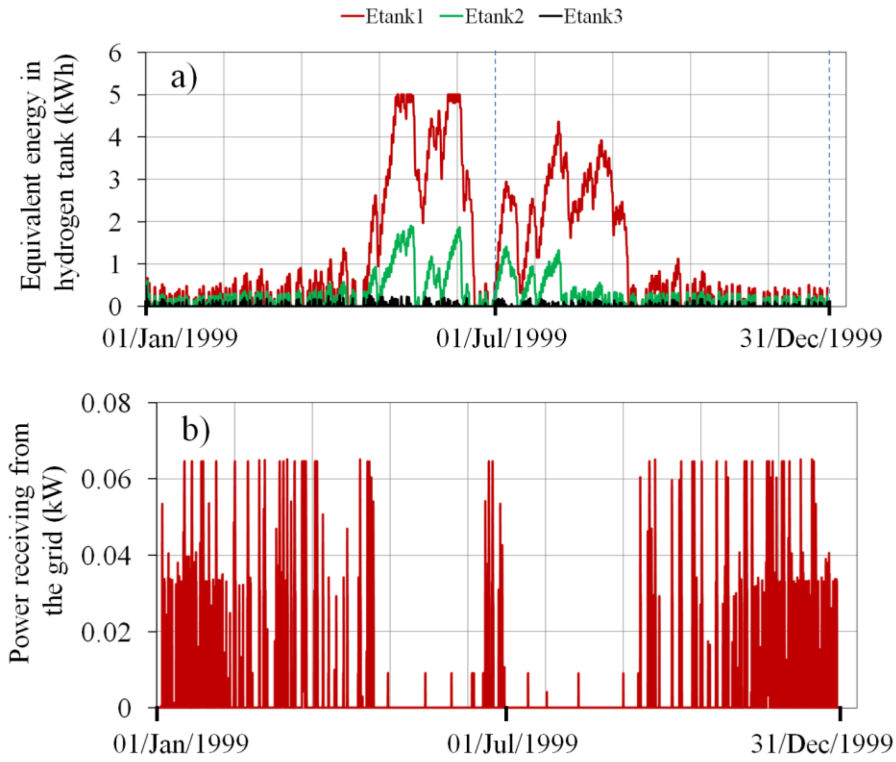

Figure 3. 4: (a) Example of the equivalent energy in the hydrogen tank with 3 system configurations in Osaka in 1999: case 1) (red line) C_{PV} = 0.50 kW, C_{BA} = 0.60 kWh, C_{EL} = 0.20 kW, C_{FC} = 0.05 kW, case 2) (green line) C_{PV} = 0.50 kW, C_{BA} = 0.60 kWh, C_{EL} = 0.10 kW, C_{FC} = 0.05 kW, case 3) (black line) C_{PV} = 0.20 kW, C_{BA} = 0.20 kWh, C_{EL} = 0.20 kW, C_{FC} = 0.02 kW and (b) the power receiving from the grid P_{grid} in case 1.

taking the waveform into consideration. This result leads to the simplification and the considerable decrease of calculation in the sizing optimization problem because the selection of S_{total} to estimate the *GD* is much easier and requires less time than calculating based on a series of a long time weather data.

For the purpose of developing the *GD* formula, firstly the relationship of the *GD* and a certain parameter will be considered, and then the next step is to find out the dependence of the coefficients of this first relationship on the second parameter. The process continues until the sub-coefficients depend on the last parameter.

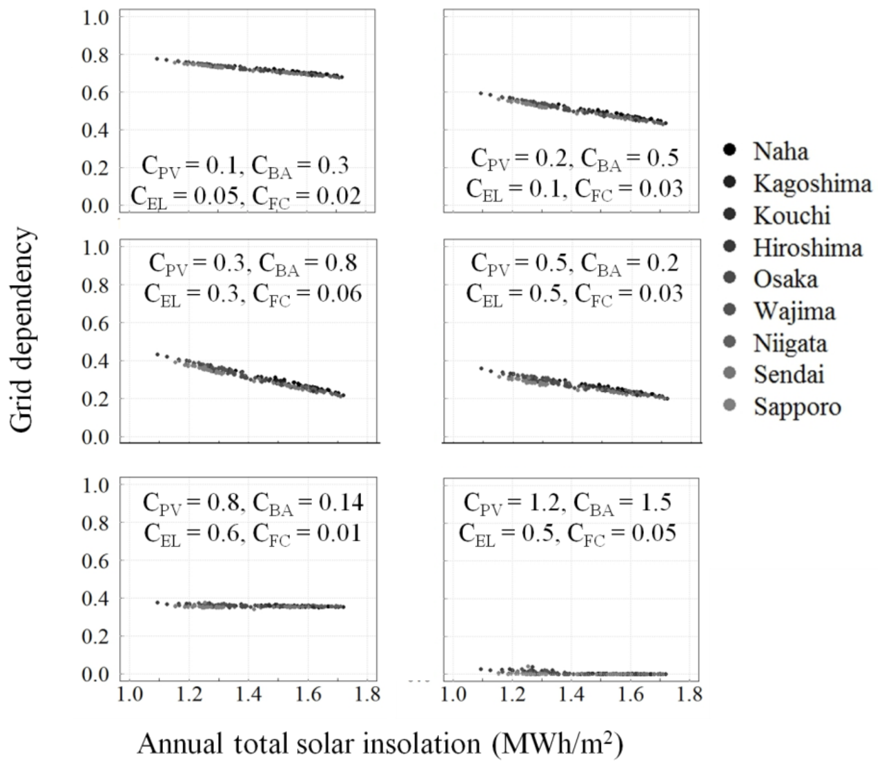

Figure 3. 5: Dependence of the *GD* on the annual total solar insolation at 9 locations corresponding to the specific value of the capacity of devices.

There is a high possibility that the *GD* of the system will depend on the annual total PV energy that is approximately calculated by (3.16):

$$E_{PV} = C_{PV} \times \mathrm{S}_{\mathrm{total}} \quad (3.16)$$

Figure 3.6 displays the relationship between *GD* and the annual PV energy E_{PV} with different value of storage capacities (pattern 1). It can be realized that *GD* is exponentially proportional to E_{PV} according to the following function:

$$GD(E_{PV}) = A \times e^{B \times E_{PV}} + 1 - A \quad (3.17)$$

Corresponding to each set of (C_{BA}, C_{EL}, C_{FC}), the coefficient *A* and *B* can be determined by using regressive analysis and least squared fitting. For example, with

C_{BA} = 0.20 kWh, C_{EL} = 0.15 kW, C_{FC} = 0.015 kW, the coefficient A = 0.745 and B = –3.283 was found. The coefficient of determination of the fitting in this case R^2 was 0.998 meaning that the fitting is relatively accurate. The coefficients A and B will depend on (C_{BA}, C_{EL}, C_{FC}).

The relationship between coefficient A and C_{EL} is also according to exponential function.

$$A(C_{EL}) = A_1 \times e^{A_2 \times C_{EL}} + A_3 \tag{3.18}$$

Similarly, the sub – coefficients A_1, A_2, A_3 are also exponentially proportional to C_{FC}

$$A_i(C_{FC}) = A_{i1} \times e^{A_{i2} \times C_{FC}} + A_{i3} \quad (i = 1, 2, 3) \tag{3.19}$$

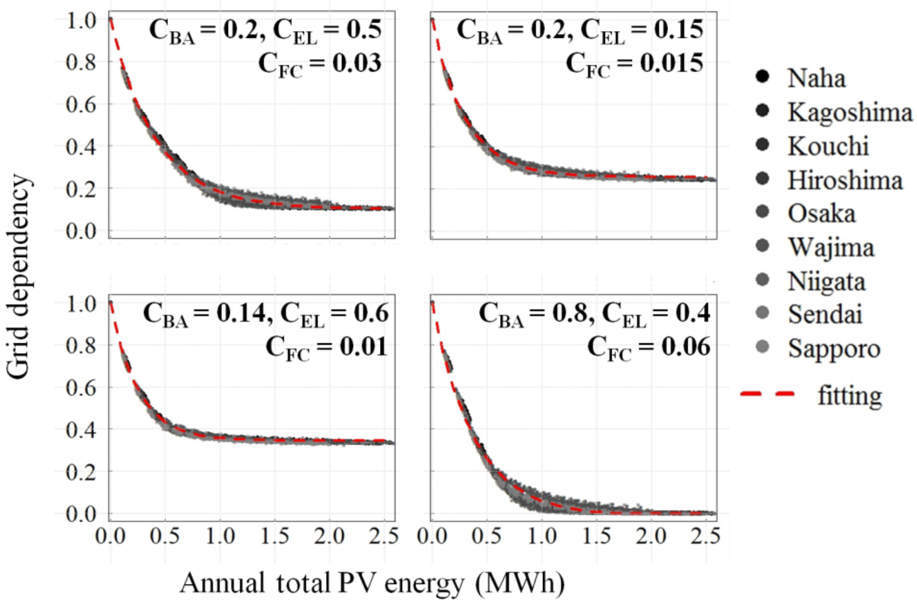

Figure 3. 6: Dependence of the *GD* on the annual PV energy at 9 locations.

Finally, the sub – coefficients A_{ij} (i, j = 1 to 3) nonlinearly depends on C_{BA}. The results of fitting process were given in Table 3.2.

As for the coefficient B, the same fitting procedures were conducted to found the relationship between B and C_{BA}, C_{EL}, C_{FC}. The results were shown in Table 3.2.

$$B = \begin{cases} B_1 \times C_{\mathrm{BA}}^2 + B_2 \times C_{\mathrm{BA}} + B_3 & (C_{\mathrm{BA}} \le 0.8) \\ B_4 \times C_{\mathrm{BA}} + B_5 & (0.8 < C_{\mathrm{BA}}) \end{cases} \tag{3.20}$$

$$B_m(C_{EL}) = B_{m1} \times e^{B_{m2} C_{EL}} + B_{m3} \quad (\mathrm{m} = 1,2,.., 5) \tag{3.21}$$

In a similar way, the *GD* of system in the case of load pattern 2 was estimated based on the coefficients *A*, *B* and their sub – coefficients that were fitted and shown in Table 3.3.

Table 3.2: The sub – coefficients of A and B used in GD formula for pattern 1.

$A_{11}=\begin{cases}-0.8679\times C_{BA}+0.6926 & (C_{BA}\le 0.8)\\ 0.3339\times e^{-2.1782\times C_{BA}}+0.0036 & (0.8<C_{BA})\end{cases}$
$A_{12}=\begin{cases}-68.93\times C_{BA}^2-7.0014\times C_{BA}-38.218 & (C_{BA}\le 0.6)\\ -44.584\times C_{BA}^4+268.05\times C_{BA}^3-585.67\times C_{BA}^2+546.97\times C_{BA}-237.77 & (0.6<C_{BA})\end{cases}$
$A_{13}=\begin{cases}0.8036\times C_{BA}-0.6482 & (C_{BA}\le 0.8)\\ -0.3263\times e^{-2.1934\times C_{BA}}-0.0035 & (0.8<C_{BA})\end{cases}$
$A_{21}=\begin{cases}-250.13\times C_{BA}^2-3.0704\times C_{BA}-70.376 & (C_{BA}\le 0.6)\\ -667.789\times e^{-3.362\times C_{BA}}-69.119 & (0.6<C_{BA})\end{cases}$
$A_{22}=\begin{cases}563.18\times C_{BA}^3-535.29\times C_{BA}^2+43.013\times C_{BA}-117.2 & (C_{BA}\le 0.58)\\ -1617.447\times e^{-5.404\times C_{BA}}-98.652 & (0.58<C_{BA})\end{cases}$
$A_{23}=8.069\times C_{BA}^3-20.439\times C_{BA}^2-3.0667\times C_{BA}-5.502$
$A_{31}=\begin{cases}0.7969\times C_{BA}-0.6495 & (C_{BA}\le 0.8)\\ -0.3415\times e^{-2.1924\times C_{BA}}-0.0041 & (0.8<C_{BA})\end{cases}$
$A_{32}=\begin{cases}-62.869\times C_{BA}^2-10.092\times C_{BA}-38.826 & (C_{BA}\le 0.6)\\ -45.628\times C_{BA}^4+274.75\times C_{BA}^3-601.76\times C_{BA}^2+561.91\times C_{BA}-242.33 & (0.6<C_{BA})\end{cases}$
$A_{33}=\begin{cases}0.157\times C_{BA}^2-0.1513\times C_{BA}+1.054 & (C_{BA}\le 0.6)\\ -0.0163\times e^{-1.4597\times C_{BA}}+1.0244 & (0.6<C_{BA})\end{cases}$
$B_{11}=3.723\times e^{-45.935\times C_{FC}}-3.657$
$B_{12}=-24.463\times e^{-71.432\times C_{FC}}-5.272$
$B_{13}=-3.492\times e^{-47.310\times C_{FC}}+1.245$
$B_{21}=-8.278\times e^{-48.951\times C_{FC}}+7.948$
$B_{22}=-43.481\times e^{-79.656\times C_{FC}}-6.897$
$B_{23}=8.023\times e^{-49.230\times C_{FC}}-2.530$
$B_{31}=4.222\times e^{-50.706\times C_{FC}}-3.998$
$B_{32}=-142.845\times e^{-112.556\times C_{FC}}-8.374$
$B_{33}=-4.154\times e^{-50.557\times C_{FC}}-1.451$
$B_{41}=0.0699\times e^{-70.2965\times C_{FC}}\times\cos(-80.9382\times C_{FC})+0.1051\times e^{-70.2965\times C_{FC}}\times\sin(-80.9382\times C_{FC})-0.0699$
$B_{42}=-23.03\times e^{-137.66\times C_{FC}}-16.99$
$B_{43}=0.0598\times e^{-76.323\times C_{FC}}\times\cos(52.7156\times C_{FC})+0.2082\times e^{-76.323\times C_{FC}}\times\sin(52.7156\times C_{FC})-0.0945$
$B_{51}=-0.1833\times e^{-79.805\times C_{FC}}\times\cos(91.85\times C_{FC})+0.125\times e^{-79.805\times C_{FC}}\times\sin(91.85\times C_{FC})+0.1833$
$B_{52}=-22.21\times e^{-146.5\times C_{FC}}-17.79$
$B_{53}=0.0645\times e^{-80.2824\times C_{FC}}\times\cos(-56.8941\times C_{FC})+0.4069\times e^{-80.2824\times C_{FC}}\times\sin(-56.8941\times C_{FC})-2.6259$

Table 3.3: The sub – coefficients of *A* and *B* used in *GD* formula for pattern 2.

$A_{11} = \begin{cases} -0.8566 \times C_{BA} + 0.6756 & (C_{BA} \le 0.8) \\ 0.3115 \times e^{-2.1208 \times C_{BA}} + 0.0032 & (0.8 < C_{BA}) \end{cases}$
$A_{12} = \begin{cases} -20.051 \times C_{BA}^2 + 0.9358 \times C_{BA} - 43.076 & (C_{BA} \le 0.7) \\ -15.04 \times C_{BA}^4 + 92.386 \times C_{BA}^3 - 208.05 \times C_{BA}^2 + 201.24 \times C_{BA} - 119.45 & (0.7 < C_{BA}) \end{cases}$
$A_{13} = \begin{cases} 0.7867 \times C_{BA} - 0.6258 & (C_{BA} \le 0.8) \\ -0.3014 \times e^{-2.1457 \times C_{BA}} - 0.0033 & (0.8 < C_{BA}) \end{cases}$
$A_{21} = \begin{cases} -39.636 \times C_{BA}^2 - 153.91 \times C_{BA} - 65.842 & (C_{BA} \le 0.6) \\ -280.766 \times e^{-2.233 \times C_{BA}} - 63.961 & (0.6 < C_{BA}) \end{cases}$
$A_{22} = \begin{cases} 718.39 \times C_{BA}^3 - 420.82 \times C_{BA}^2 + 15.09 \times C_{BA} - 120.67 & (C_{BA} \le 0.42) \\ -138.533 \times e^{-2.465 \times C_{BA}} - 88.263 & (0.42 < C_{BA}) \end{cases}$
$A_{23} = 7.8914 \times C_{BA}^3 - 19.62 \times C_{BA}^2 - 3.7255 \times C_{BA} - 5.562$
$A_{31} = \begin{cases} 0.7891 \times C_{BA} - 0.6357 & (C_{BA} \le 0.8) \\ -0.319 \times e^{-2.1353 \times C_{BA}} - 0.0036 & (0.8 < C_{BA}) \end{cases}$
$A_{32} = \begin{cases} -15.759 \times C_{BA}^2 - 0.9266 \times C_{BA} - 43.75 & (C_{BA} \le 0.7) \\ -14.533 \times C_{BA}^4 + 90.442 \times C_{BA}^3 - 206.36 \times C_{BA}^2 + 200.58 \times C_{BA} - 119.23 & (0.7 < C_{BA}) \end{cases}$
$A_{33} = \begin{cases} 0.1322 \times C_{BA}^2 - 0.1269 \times C_{BA} + 1.0482 & (C_{BA} \le 0.6) \\ -0.0152 \times e^{-1.42151 \times C_{BA}} + 1.0241 & (0.6 < C_{BA}) \end{cases}$
$B_{11} = 3.936 \times e^{-97.083 \times C_{FC}} - 3.791$
$B_{12} = -95.062 \times e^{-129.737 \times C_{FC}} - 5.354$
$B_{13} = -3.614 \times e^{-98.592 \times C_{FC}} + 1.282$
$B_{21} = -8.194 \times e^{-66.447 \times C_{FC}} + 7.827$
$B_{22} = -44.13 \times e^{-82.568 \times C_{FC}} - 6.843$
$B_{23} = 7.872 \times e^{-66.112 \times C_{FC}} - 2.519$
$B_{31} = 4.072 \times e^{-54.168 \times C_{FC}} - 3.83$
$B_{32} = -95.164 \times e^{-87.027 \times C_{FC}} - 8.017$
$B_{33} = -4.005 \times e^{-53.993 \times C_{FC}} - 1.489$
$B_{41} = 0.0724 \times e^{-43.667 \times C_{FC}} \times \cos(-109.898 \times C_{FC}) + 0.0401 \times e^{-43.667 \times C_{FC}} \times \sin(-109.898 \times C_{FC}) - 0.0724$
$B_{42} = -22.13 \times e^{-134.93 \times C_{FC}} - 17.92$
$B_{43} = 0.0553 \times e^{-54.2583 \times C_{FC}} \times \cos(61.0683 \times C_{FC}) + 0.1435 \times e^{-54.2583 \times C_{FC}} \times \sin(61.0683 \times C_{FC}) - 0.0917$
$B_{51} = -0.1871 \times e^{-62.9937 \times C_{FC}} \times \cos(115.2762 \times C_{FC}) + 0.0254 \times e^{-62.9937 \times C_{FC}} \times \sin(115.2762 \times C_{FC}) + 0.1871$
$B_{52} = -21.41 \times e^{-143.2 \times C_{FC}} - 18.61$
$B_{53} = 0.0568 \times e^{-53.4477 \times C_{FC}} \times \cos(-67.5995 \times C_{FC}) + 0.2649 \times e^{-53.4477 \times C_{FC}} \times \cos(-67.5995 \times C_{FC}) - 2.6491$

The accuracy of the fitting method was examined by the mean absolute error (MAE). In statistics, MAE is quantity to measure the average magnitude of the error between the real and the predicted value, which is given by:

$$\mathrm{MAE} = \frac{\sum_{i=1}^{n} |e_i|}{n} = \frac{\sum_{i=1}^{n} |y_i - f(x_i)|}{n} \tag{3.22}$$

where $|e_i|$ is the absolute error, y_i is the true value, $f(x_i)$ is the prediction.

Applying the above function to calculate the *MAE* for the fitted formula is conducted as followings: corresponding to each specific set of (C_{BA}, C_{EL}, C_{FC}), the *GD* is calculated by using the real weather data at 9 locations during 25 years (y_j) and estimated by the formula ($f(x_j)$) depending on the real E_{PV}. The average of the absolute error between them is the *MAE* corresponding to (C_{BA}, C_{EL}, C_{FC}).

Figure 3.7 depicts the *MAE* with various values of (C_{BA}, C_{EL}, C_{FC}) for the formula of pattern 1 (Fig. 3.7a), pattern 2 (Fig. 3.7b), and some detail images of the *MAE* depending on two of 3 parameters (C_{BA}, C_{EL}, C_{FC}) while other parameters is fixed (Fig. 3.7c, 3.7d, and 3.7e). From the results, it can be seen that the *MAE* ranges from 0.007 to 0.045, in which it mainly varies between 0.015 and 0.025. High *MAE* values occur at some points, for example, the *MAE* of about 0.045 at (C_{FC} = 0 & C_{BA} = 0.8). It is noticeable that these points are the margin points when C_{BA} = 0.8 which is the chosen value to change the function. Another formula can separately fit these special marginal cases to increase the accuracy. However, the supplement of more functions for special cases will increase the complexity of the fitted functions. In addition, if the function is used to estimate the *GD* for the purpose of sizing optimization, the error can be acceptable.

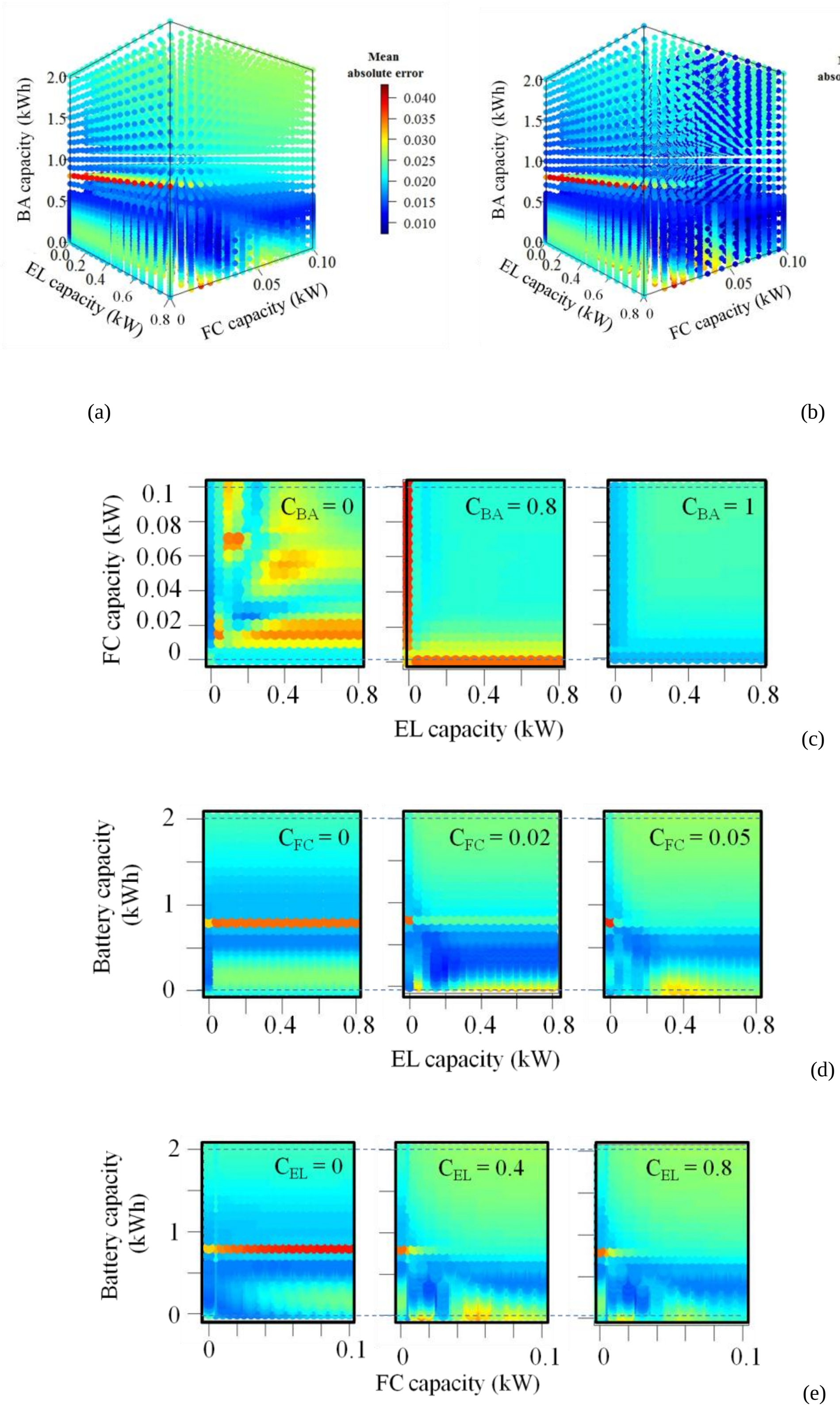

Figure 3. 7: The mean absolute error of the *GD* calculated by the formula and by using real 25 – year weather data in 9 chosen locations depending on three storages capacities for pattern 1 (a), pattern 2 (b) and depending on two parameters while one parameter is fixed (c, d, e)

3.4.2. Formula verification:

In order to verify and demonstrate the effectiveness and the advantages of the developed *GD* formula, the formula is applied to calculate the *GD* of the system assumedly supplying to a group of several households in Tokyo that consumes 8 kWh/day with a particular configuration of C_{PV}, C_{BA}, C_{EL}, and C_{FC}. The results then will be compared with the *GD* obtained by using 25 – year weather data.

It is noted that the formula was established in the case of the load of 1 kWh/day. Therefore, when using the formula to estimate the *GD* for the case of the load of a certain consumed energy E_{1day}, the obtained formula will be applied to the value of (C_{PV}, C_{BA}, C_{EL}, C_{FC}) divided by E_{1day}.

Moreover, an important parameter in the empirical formula that needs to be determined is the annual total insolation S_{total}. The selection of the S_{total} will be based on the probability of its occurrence. Based on the statistics of the S_{total} during 25 years in Tokyo, the histogram of the S_{total} is calculated and shown in Fig. 3.8. During this period, it ranges from 1.170 to 1.593 MWh/m^2. It could be seen that the *GD* is negatively proportional with the S_{total}. Thus, the selection of a small S_{total} will guarantee the calculated *GD* not to be much smaller than expected. In this work, we chose the value of the S_{total} at the probability of 0.95 meaning that the selected value of the S_{total} surely occurs in reality with a probability of 95%. From the cumulative probability of the S_{total} in Fig. 3.8, the values of the S_{total} can be determined $S_{\mathrm{total}}^{95\%} = 1.1859$ MWh/m^2. Taking a set of capacity (C_{PV} = 4.00 kW, C_{BA} = 4.00 kWh, C_{EL} = 2.40 kW, C_{FC} = 0.16 kW) as an example, the *GD* calculated by the empirical formula corresponding to the $S_{\mathrm{total}}^{95\%}$ is 0.2430.

Meanwhile, the distribution of the *GD* calculated directly from the weather data of 25 years shows that it ranges from 0.1298 to 0.2410. It can be obviously realized that the *GD* obtained by the formula is similar to the maximum value in reality. The comparison is also carried out with some different values of capacities of the devices and the S_{total} at the guaranteed probability of 0.95, 0.96, 0.97, 0.98 as in Table 3.4. The results show that there is an insignificant difference between the *GD* at the guaranteed probability of 95% to 98% and the maximum real *GD* derived from the weather data series. As a result, the developed formula and the selected S_{total} of 95% can be applied to calculate the *GD* in a simple way with high accuracy.

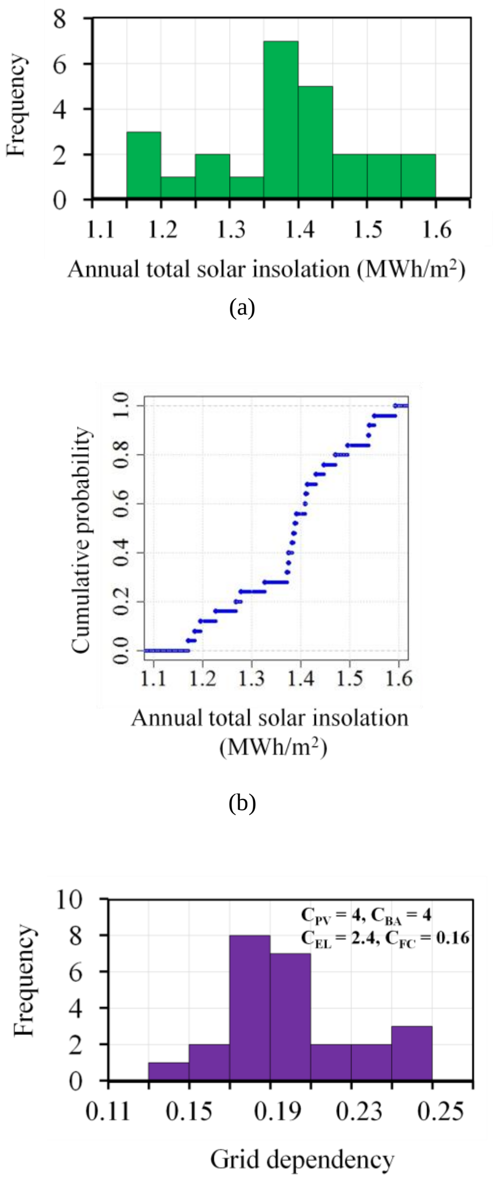

(c)

Figure 3. 8: (a) The distribution of annual total solar insolation in Tokyo during 25 years, (b) the cumulative probability of annual total solar insolation, (c) the distribution of *GD* calculated by normal method using 25 – year weather data corresponding to (C_{PV} = 4.00 kW, C_{BA} = 4.00 kWh, C_{EL} = 2.40 kW, C_{FC} = 0.16 kW)

Table 3.4: The comparison of the *GD* obtained by the established formula using different guarantied probability (95%-98%) and directly calculated by using 25 – year weather data corresponding to several set of capacity of devices.

C_{PV} kW	C_{BA} kWh	C_{EL} kW	C_{FC} kW	*GD* (by formula)				*GD* (by real weather data)	
				$S_{total}^{95\%}$ =1.1859	$S_{total}^{96\%}$ =1.183	$S_{total}^{97\%}$ =1.1798	$S_{total}^{98\%}$ =1.1765	min	max
0.3	0.2	0.2	0.035	0.4961	0.4969	0.4977	0.4986	0.4051	0.4966
0.5	0.5	0.3	0.020	0.2432	0.2439	0.2447	0.2456	0.1298	0.2511
0.6	0.5	0.3	0.035	0.1766	0.1772	0.1781	0.1789	0.06050	0.1713
0.7	0.5	0.5	0.040	0.1276	0.1282	0.1289	0.1297	0.02570	0.1211

3.5 Optimization results

Aiming at applying the developed empirical *GD* formula into the optimization problem, the S_{total}, the required *GD*, and the expected energy consumed by the load in one day should be identified. As analyzed in the previous section, the S_{total} of 95% can be used with an acceptable accuracy in estimation of the *GD*. It is noticeable that the formula of the *GD* is not asymptotic at 0; it would be set of 0 when it receives the negative value.

A simple iterative method is applied to determine the optimal sizing. Among the configurations satisfying the requirement of $GD_{required}$, the optimal configuration is the one that has the minimum *LCE*. The diagram of the iterative method is shown in Fig. 3.9.

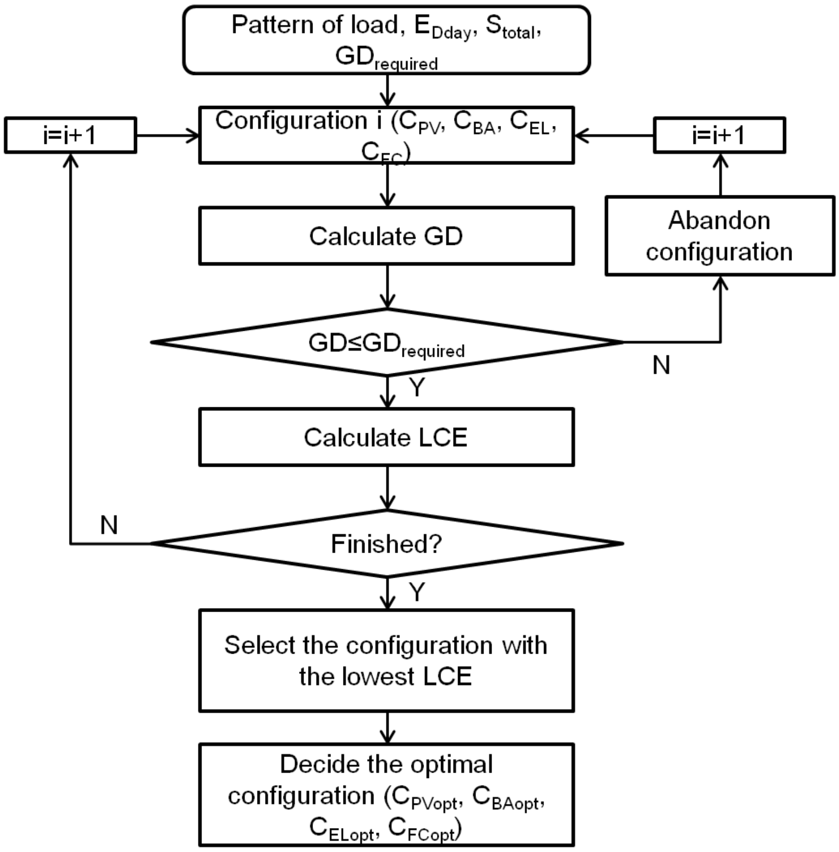

Figure 3. 9: The diagram to select the optimal configuration corresponding to GD_{required}

Table 3.5: The result of optimal capacity corresponding to several GD_{required}

C_{PV} kW	C_{BA} kWh	C_{EL} kW	C_{FC} kW	GD_{cal}	GD_{require}	LCE Yen/kWh
10.72	6.40	0.32	0.304	0	0	329
7.20	6.40	0	0	0.04890	0.05	268
5.60	6.40	0	0	0.09950	0.10	227
4.16	6.24	0	0	0.1997	0.20	172
3.36	3.36	0	0	0.3990	0.40	124
2.24	0.64	0	0	0.5990	0.60	71.0

Assuming the system supply to a network of residential households of 8 kWh/day in Tokyo, the optimal capacity corresponding to the required *GD* from 0 to 1 is found. Table 5 displays the optimal configurations which have the minimum *LCE* and meet the requirement of the GD_{required}, Fig. 3.10 shows the result of the minimum *LCE* corresponding to each required *GD* from 0 to 1.

- The *LCE* will reach the highest value of 328 ¥/kWh in the case $GD_{\text{required}} = 0$ with the optimal configuration: $C_{\text{PV}} = 10.72$ kW, $C_{\text{BA}} = 6.40$ kWh, $C_{\text{EL}} = 0.32$ kW, $C_{\text{FC}} = 0.304$ kW, the system does not depend on the system.
- When the GD_{required} increases from 0 to 0.20, the *LCE* decreases considerably. It can be explained that when the required grid dependency is too small, the increase of devices capacity has little effect on the *GD*. Therefore, a slight change of the GD_{required} will need a significant change of the *LCE*.
- When the GD_{required} increases from 0.20 to 0.60, the *LCE* nearly linearly reduces because, in this range of the GD_{required}, the changes in the devices' capacities have a relatively considerable effect on the *GD*. Thus the optimal configurations include PV and the storages.
- When the GD_{required} increases from 0.60 to 1.00, the *LCE* slightly decreases because the requirement of the *GD* is pretty high, the changes of the devices' capacities significantly affects the *GD*. In this range, the use of the storages is unnecessary; the optimal configurations include PV only.
- When the system totally depends on the grid ($GD_{\text{required}} = 1$), the *LCE* is 23 ¥/kWh that is the price of purchasing electricity from the grid.

The optimization result is calculated based on the empirical formula of the *GD* for the system with or without battery and hydrogen system. In the case of without hydrogen system, meaning that only PV and battery, the established formula is still applicable with $C_{\text{EL}} = C_{\text{FC}} = 0$ and the optimal configuration can be designed.

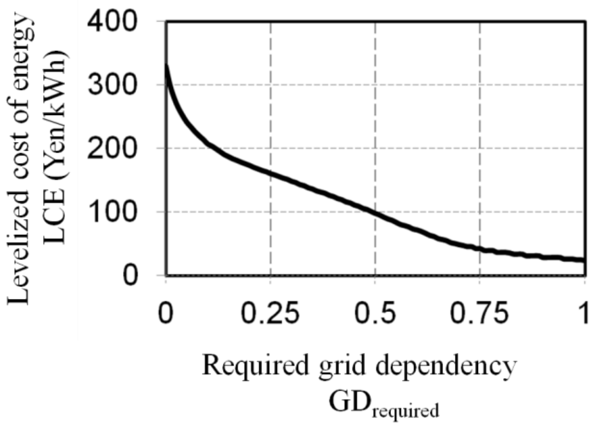

Figure 3. 10: The minimum *LCE* corresponding to the required *GD* calculated by the established formula (pattern 1)

The sensitivity analysis is carried out to investigate the change of the *LCE* according to the variations of several parameters: the cost of the PV systems, the battery, the EL and the FC, the interest rate and the lifetime of the battery. Different scenarios compared with the basic case are created as followings:

- PV cost: the cost of PV increases +50% and decreases –50%
- Battery cost: the cost of battery increases (+25%, +50%, +75%, +100%) and decreases (–25%, –50%)
- FC cost: the cost of FC increases +50% and decreases –50%
- EL cost: the cost of EL increases +50% and decreases –50%
- Interest rate: the interest rate increases (+25%, +50%) and decreases (–25%, –50%)
- Battery lifetime: the lifetime of the battery increases +50% and decreases –50%

Figure 3.11 shows the sensitivities analysis results corresponding to the parameters variations. It can be seen that the *LCE* of the optimal configurations changes inconsiderably with the variation of the FC/EL cost. However, the *LCE* changes significantly when the cost of PV, the cost of the battery, the interest rate and the lifetime of the battery increase or decrease. The optimal configurations also change depending on the change of parameters.

A deep investigation in the case of the battery cost variation is conducted. Fig. 3.12 illustrates the optimal configurations of the system corresponding to the GD_{required} when the battery cost increases +50% and decreases –50%. The battery will dominate over the hydrogen system when its cost decreases. When the battery cost increases, on the contrary, the combination of the battery and the hydrogen system will be more efficient. Moreover, it can be seen from the figure that when the GD_{required} is small, the battery capacity of a certain value without increasing will be optimal configurations. This can be explained by looking into the empirical formula of the *GD*, it is noticeable that when the capacity of the battery increases to a certain value, for example, 6.40 kWh corresponding to the case of supplying to the load of 8 kWh/day, the increase of the battery capacity will not considerably affect the *GD*. Therefore, with a small GD_{required}, the increase of the PV capacity and the combination of the battery with the hydrogen system will be more economical. In contrast, when the GD_{required} is high, the use of the only PV will be more efficient. In the case of $GD_{\text{required}} = 0$, when the battery cost changes, the optimal configuration remains unchanged.

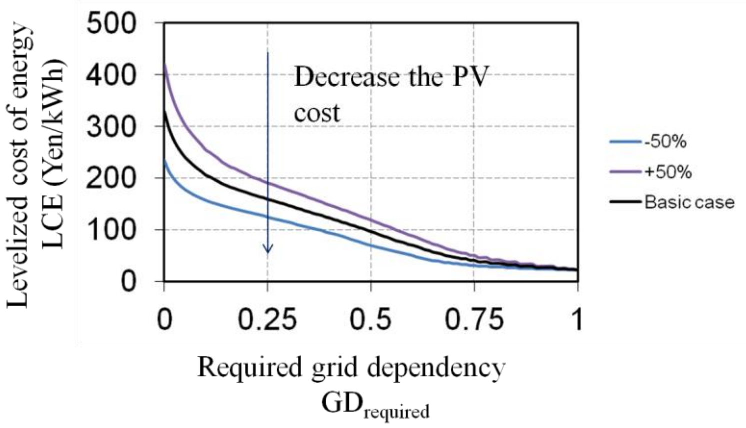

(a) PV cost variation

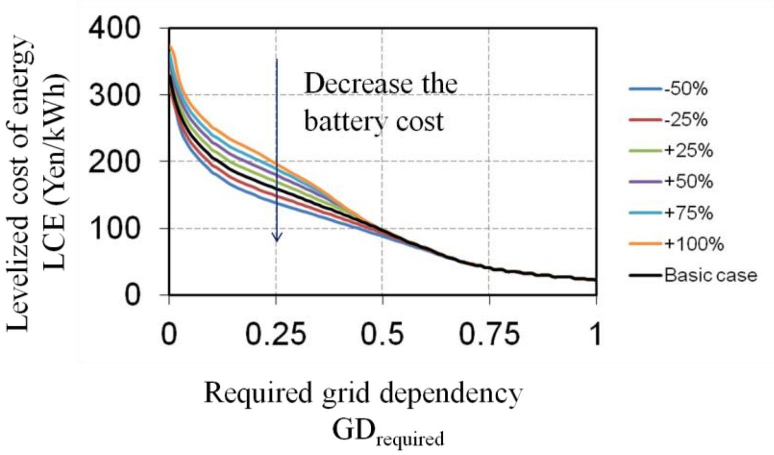

(b) Battery cost variation

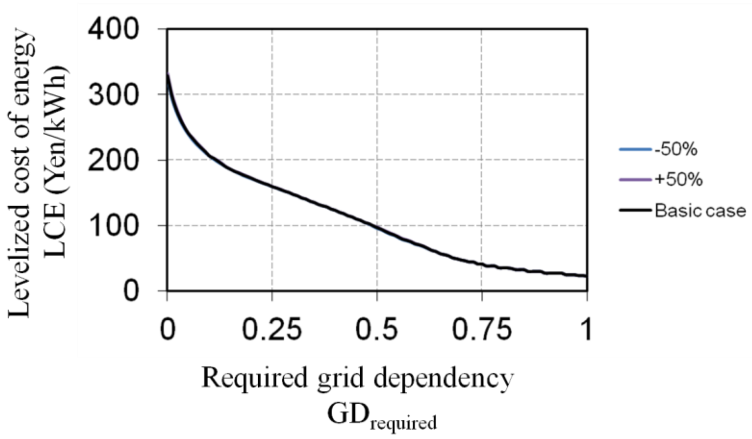

(c) FC cost variation

Figure 3.11: Sensitivities analysis results.

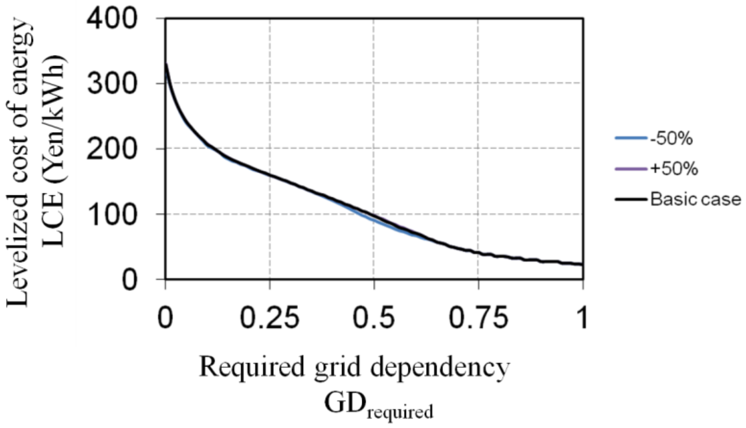

(d) EL cost variation

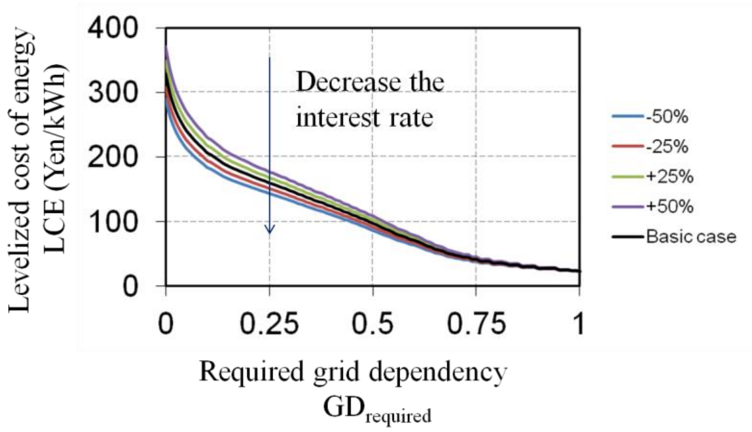

(e) Interest rate variation

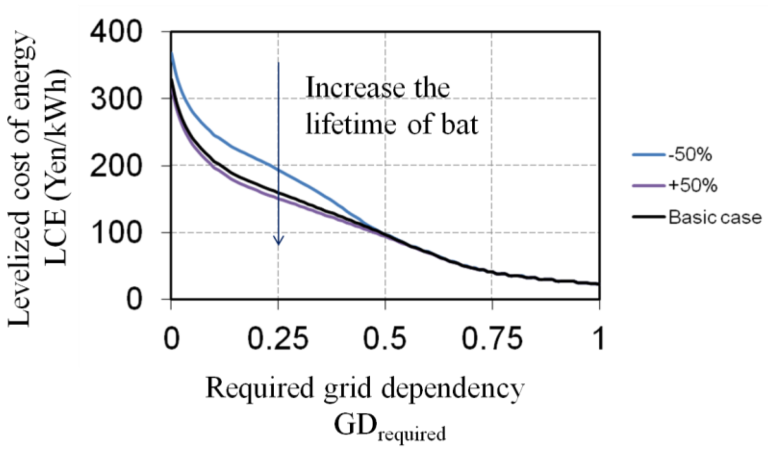

(f) Lifetime of battery variation

Figure 3. 11: Sensitivities analysis results.

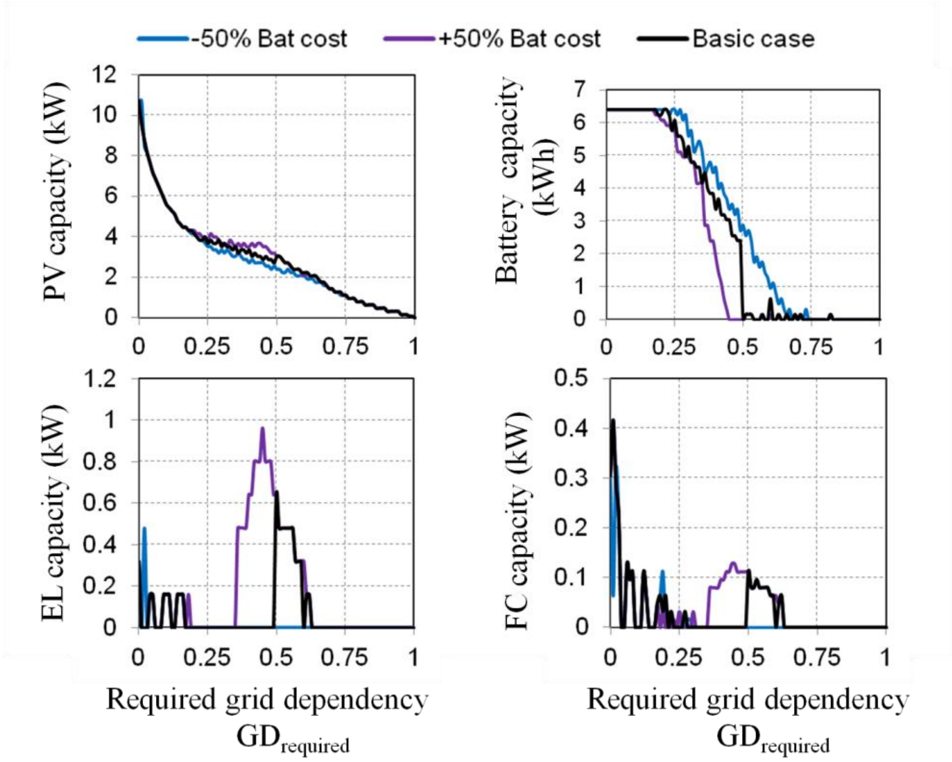

Figure 3. 12: The optimal configurations of the system corresponding to the GD_{required} when the battery cost increases +50% and decreases -50%

3.6 Optimization using trend-prediction PMS

In this chapter we optimized the size of the system using the conventional PMS with hourly time interval. Additionally, the obtained *GD* formula was established based on the assumed smooth load pattern. Therefore, in this section, we optimized the system based on the trend-prediction PMS proposed in chapter 2 using the fluctuated load pattern and then compared the results with the case of using empirical formula, conventional PMS, and smooth load pattern.

Figure 3.13 shows the real solar irradiation in 2013 in Tsukuba with the time interval of 3 seconds. The normalized load power of the real domestic pattern corresponding to is shown in Figure 3.14 with the sampling time of 1min.

Applying the trend-prediction PMS into the system to calculate the *GD* with and without using the established *GD* formula and then minimizing the *LCE* based on the required *GD*, we could obtain the optimal LCE curve corresponding to GD_{required}. It can be noted that due to the error during the calculation of the *GD* by formula, we calculated the *LCE* based on the *GD* formula and *GD* ± error (0.04). In Figure 3.15, the black line depicts the optimal LCE obtained by GD formula, the blue and purple lines are for the plus and minus error, the red line is the direct calculation using real stochastic PV power, domestic load and trend-prediction PMS.

The results reveal that the *LCE* by direct calculation with real fluctuated data is a little bit higher than the one by the *GD* formula. However, it still lies in the area of the results by the formula and its errors. Therefore, the optimal result can be obtained using the *GD* formula and validated by error.

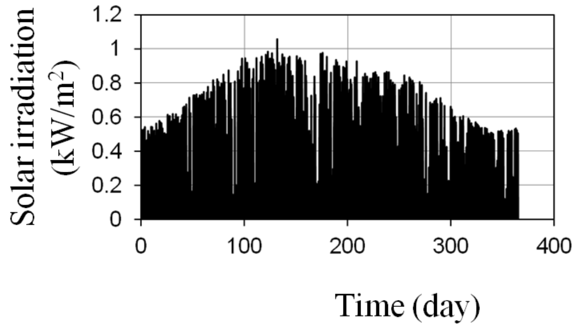

Figure 3. 13: The solar irradiation in 2013 in Tsukuba.

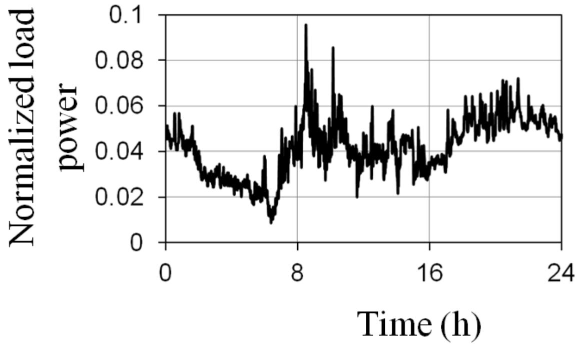

Figure 3. 14: The stochastic domestic demand.

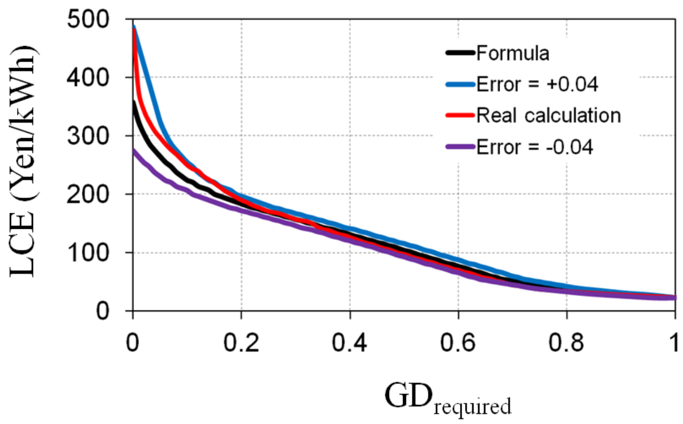

Figure 3. 15: Comparison of the optimal *LCE* obtained by using *GD* formula, *GD* ± error and using *GD* directly calculated by trend-prediction PMS with real stochastic PV and load data

3.7 Conclusions

In this research, a simple but highly accurate formula of the *GD* is developed aiming at giving a fast tool to estimate the *GD*, then the optimal sizing of the system can be rapidly obtained by using an uncomplicated iterative technique to minimize the *LCE*. The *GD* is found to depend on the annual total solar insolation without taking the waveform of the weather data into consideration. The accuracy, as well as the application of the developed *GD* formula, is demonstrated and compared with the normal calculation. The results show that the formula can be applied in estimating the *GD* of the system quickly and precisely. Based on the estimated *GD* and the *LCE*, the optimal capacity of the system is determined. Also, the sensitivities analysis is conducted to investigate how the *LCE* changes when the parameters take other values. The results indicate that the *LCE* is more sensitive to the variation of the PV cost, the battery cost, the battery lifetime and the interest rate than the variation of the EL/FC cost. Moreover, when these parameters change, the optimal configurations remain unchanged with high GD_{required}, insignificantly change with small GD_{required} and considerably change for the GD_{required} of about from 0.20 to 0.70. The uncertainties of the load and the proposed trend-prediction PMS are also considered to calculate the *GD* and the *LCE*. The empirical formula of the *GD* with the validation of the error is revealed to be still applicable in this case.

3.8 References

[1] R. Luna-Rubio, M. Trejo-Perea, D. Vargas-Vazquez, G.J. Rıos-Moreno, Optimal sizing of renewable hybrids energy systems: A review of methodologies, Solar Energy 86 (2012) 1077–1088

[2] Zhang Beihong, Long Weiding, An optimal sizing method for cogeneration plants, Energy and Buildings 38 (2006) 189–195

[3] Yang Hongxing, Lou Chengzhi, Optimal design and techno-economic analysis of a hybrid solar-wind power generation system, Applied Energy 86 (2009) 163–169

[4] J.K. Kaldellis, D. Zafirakis, Optimum sizing of stand-alone wind-photovoltaic hybrid systems for representative wind and solar potential cases of the Greek territory, Journal of Wind Engineering and Industrial Aerodynamics 107–108 (2012) 169–178

[5] Xiongwen Zhang, Siew-Chong Tan, Guojun Li, Jun Li, Zhenping Feng, Components sizing of hybrid energy systems via the optimization of power dispatch simulations, Energy 52 (2013) 165–172

[6] Diaf, D. Diaf, M. Belhamel, M. Haddadi, A. Louche, A methodology for optimal sizing of autonomous hybrid PV/wind system, Energy Policy 35 (2007) 5708–5718

[7] Diaf, G. Notton, M. Belhamel, M. Haddadi, A. Louche, Design and techno–economical optimization for hybrid PV/wind system under various meteorological conditions, Applied Energy 85 (2008) 968–987

[8] Hongxing Yang, Lin Lu, Wei Zhou, A novel optimization sizing model for hybrid solar-wind power generation system, Solar Energy 81 (2007) 76–84

[9] Zachariah Iverson, Ajit Achuthan, Pier Marzocca, Daryush Aidun, Optimal design of hybrid renewable energy systems (HRES) using hydrogen storage technology for data center applications, Renewable Energy 52 (2013) 79–87

[10] Benjamin Guinot, Benedicte Champel, Florent Montignac, Elisabeth Lemaire, Didier Vannucci, Sebastien Sailler, Techno-economic study of a PV-hydrogen-battery hybrid system for off-grid power supply: Impact of performances' ageing on optimal system sizing and competitiveness, International Journal of Hydrogen Energy 40 (2015) 623–632

[11] Rodolfo Dufo-Lopez, Jose L. Bernal-Agustın, Franklin Mendoza, Design and economical analysis of hybrid PV-wind systems connected to the grid for the intermittent production of hydrogen, Energy Policy 37 (2009) 3082–3095

[12] H.X. Yang, L. Lu, J. Burnett, Weather data and probability analysis of hybrid photovoltaic-wind power generation systems in Hong Kong, Renewable Energy 28 (2003) 1813–1824

[13] A. Kashefi Kaviani, G.H. Riahy, SH.M. Kouhsari, Optimal design of a reliable hydrogen-based stand-alone wind/PV generating system, considering component outages, Renewable Energy 34 (2009) 2380–2390

[14] Ali Naci Celik, Techno-economic analysis of autonomous PV-wind hybrid energy systems using different sizing methods, Energy Conversion and Management 44 (2003) 1951–1968

[15] Protogeropoulos, C., Brinkworth, B.J., Marshall, R., Sizing and techno-economical optimization for hybrid solar PV-wind power systems with battery storage, International Journal of Energy Research 21 (1997) 465–479

[16] Eftichios Koutroulis, Dionissia Kolokotsa, Antonis Potirakis, Kostas Kalaitzakis, Methodology for optimal sizing of stand-alone photovoltaic/wind-generator systems using genetic algorithms, Solar Energy 80 (2006) 1072–1088

[17] S.M. Hakimi, S.M. Moghaddas-Tafreshi, Optimal sizing of a stand-alone hybrid power system via particle swarm optimization for Kahnouj area in south-east of Iran, Renewable Energy 34 (2009) 1855–1862

[18] Masoud Sharafi, Tarek Y. ELMekkawy, Multi-objective optimal design of hybrid renewable energy systems using PSO-simulation based approach, Renewable Energy 68 (2014) 67–79

[19] Ce Shangdipti Srinivasan, Thomas Reindl, An improved particle swarm optimisation algorithm applied to battery sizing for stand-alone hybrid power systems, Electrical Power and Energy Systems 74 (2016) 104–117

[20] L. Hontoria, J. Aguilera, P. Zufiria, A new approach for sizing stand alone photovoltaic systems based in neural networks, Solar Energy 78 (2005) 313–319.

[21] Mineno Katsuya, Master Dissertation, University of Tsukuba, 2013

[22] N.Z. Al-Rawahi, Y.H. Zurigat and N.A. Al-Azri, Prediction of Hourly Solar Radiation on Horizontal and Inclined Surfaces for Muscat/Oman, The Journal of Engineering Research 8 (2) (2011) 19–31

[23] Robert Foster, Majid Ghassemi, Alma Cota, (2010), Solar Energy: Renewable Energy and the Environment, CRC Press, Taylor & Francis Group

[24] Adel Brka, Yasir M. Al-Abdeli, Ganesh Kothapalli, The interplay between renewables penetration, costing and emissions in the sizing of stand-alone hydrogen systems, International Journal of Hydrogen Energy 40 (2015) 125–135

[25] Akbar Maleki, Alireza Askarzadeh, Comparative study of artificial intelligence techniques for sizing of a hydrogen-based stand-alone photovoltaic/wind hybrid system, International Journal of Hydrogen Energy 39 (2014) 9973–9984

[26] Mariem Smaoui, Achraf Abdelkafi, Lotfi Krichen, Optimal sizing of stand-alone photovoltaic/wind/ hydrogen hybrid system supplying a desalination unit, Solar Energy 120 (2015) 263–276

[27] D.B. Nelson, M.H. Nehrir, C. Wang, Unit sizing and cost analysis of stand-alone hybrid wind/PV/fue*LCE*ll power generation systems, Renewable Energy 31 (2006) 1641–1656

[28] Raquel S. Garciaa, Daniel Weisser, A wind-diesel system with hydrogen storage: Joint optimisation of design and dispatch, Renewable Energy 31 (2006) 2296–2320

[29] Øystein Ulleberg, The importance of control strategies in PV-hydrogen systems, Solar Energy 76 (2004) 323–329

[30] Koji Nakazawa, Hisashi Nagaoka, Jun Takeuchi, Frank Moburg, Ikuya Yamashita, Masanori Okabe, Introduction of high differential pressure water electrolysis-type solar hydrogen station (SHS2), Honda R&D Technical Review 22 (2) (2010) 28–35

[31] Hisashi Nagaoka, Nobuyoshi Yoshida, David Cun, Ikuya Yamashita, Masanori Okabe, Verification test of high differential pressure water electrolysis-type solar hydrogen station (SHS2), Honda R&D Technical Review 24 (2) (2012) 74–81

[32] A. Kaabeche, M. Belhamel, R. Ibtiouen, Sizing optimization of grid-independent hybrid photovoltaic/wind power generation system, Energy 36 (2011) 1214–1222

[33] R. Carapellucci, L. Giordano, Modeling and optimization of an energy generation island based on renewable technologies and hydrogen storage systems, International Journal of Hydrogen Energy 37 (2012) 2081–2093

[34] Abdolvahhab Fetanat, Ehsan Khorasaninejad, Size optimization for hybrid photovoltaic-wind energy system using ant colony optimization for continuous domains based integer programming, Applied Soft Computing 31 (2015) 196–209

[35] Zhuomin Zhou, Doctoral Dissertation, University of Tsukuba, 2013

[36] http://www.data.jma.go.jp/obd/stats/etrn/index.php

[37] T. Estermann a, M. Newborough, M. Sterner, Power-to-gas systems for absorbing excess solar power in electricity distribution networks, International Journal of Hydrogen Energy 41 (2016) 13950–13959

[38] E. Troncoso, M. Newborough, Implementation and control of electrolyzers to achieve high penetrations of renewable power, International Journal of Hydrogen Energy 32 (2007) 2253–2268

[39] Woojin Cho, Janghyun Kim, Kwan-Soo Lee, Combined heat and power unit capacity for high-heat to power ratio buildings without selling excess electricity to the grid, Energy 38 (2012) 354–361

[40] Akbar Maleki, Morteza Gholipour Khajeh, Mehran Ameri, Optimal sizing of a grid independent hybrid renewable energy system incorporating resource uncertainty, and load uncertainty, Electrical Power and Energy Systems 83 (2016) 514–524

Chapter 4: Conclusion

The main goal of this research was to study and develop a PV generation – based Microgrid with stable, sustainable and economical performance. The system can be connected to or disconnected from the main grid to work in dependent or off – grid mode, respectively. The research would solve 2 aspects of the MG which are: i) the control method to operate the system considering the dynamic characteristics of the devices and against the fluctuation of the PV generation and load demand and ii) the sizing optimization of the devices in the system.

In chapter 2, we proposed a trend-prediction PMS using Kalman Filter to allocate the power to battery and hydrogen system. We carried out the experiments on the dynamic characteristics of the storages including the DC/DC converter in the Carbon Neutral Energy Supply system (CNES) in Tsukuba, Japan and modeled them. The experiment results show that fuel cell is slow in responding to the input power changing while the battery can quickly respond to fluctuated power. Therefore, the trend-prediction PMS was proposed based on the dynamic characteristics of the devices to designate power. The trend of the difference between load and PV power will be predicted to adapt the slow transient response of the hydrogen system. Kalman Filter can predict the trend and separate the stochastic time series into trend and fluctuation components. The parameter of KF can be selected for the trend prediction value satisfying the limited changing rate of the hydrogen system. The simulations results show that with suitable value of KF parameter, the proposed control method can be applied to the PV system for stable operation in short time as well as in a long time. In comparison with conventional no-prediction PMS, the overall energy conversion using trend-prediction PMS is slightly higher.

In addition, based on the proposed PMS, the requirement of battery capacity was also estimated. Because the KF can filter the symmetrical fluctuation part of the stochastic waveform as expected, using KF with suitable parameter can reduce the necessary energy of battery. The simulation results show that the proposed PMS can decrease the required capacity of battery comparing to conventional no-prediction PMS. When the asymmetric distribution of power changing rate and the efficiency of the charging/discharging process were taken into account, the PMS was improved by using *offset* to control the charging and discharging energy of battery within the limited changing rate of hydrogen system, leading to the decrease of the required capacity. The proposed improved PMS can decrease the required capacity of up to 14% in comparison with trend-prediction PMS.

In chapter 3, the research focuses on the optimal sizing of the system. When the economic criterion was considered to assess a project, the optimal capacity of system components becomes necessary. In this study, the optimization problem was solved by minimizing the *LCE* and satisfying the required *GD*. A *GD* formula depending on the annual total solar insolation and the devices capacity was developed. The accuracy as well as the application of the developed *GD* formula was demonstrated and compared with the normal calculation. The results show that the formula can be applied to highly accurately estimate *GD* of the system in any location in Japan with assumed load pattern. Additionally, the sensitivities analysis was conducted to investigate how the *LCE* changed when the parameters take other values. Moreover, when the dynamic load and the trend-prediction PMS is considered, the results show that the *GD* formula can be still applied to calculate the *GD* and then the optimal sizing of the system.

In conclusion, the research provides new methods to operate and design a PV – based Microgrid with storages for a stable, sustainable and economical performance to integrate the PV generation into the grid. The research also partly contributes to broaden the application of PV or the RE sources in general into the energy sector, especially in power system.

List of publication

JOURNAL PAPERS

1, Thu Thi Hoai Nguyen, Tomonori Nakayama, Masayoshi Ishida: Power Control Method Using Kalman Filter Prediction for Stable Operation of PV/FC/LiB Hybrid Power System Based on Experimental Dynamic Characteristics, Journal of the Japan Institute of Energy, 94 (2015) 532-541.

2, Thi Hoai Thu Nguyen, Tomonori Nakayama, Masayoshi Ishida: Optimal capacity design of Battery and Hydrogen system for the DC grid with photovoltaic power generation based on the rapid estimation of grid dependency, International Journal of Electrical Power and Energy Systems 89 (2017) 27-39.

CONFERENCES

1, Thu Thi Hoai Nguyen, Tomonori Nakayama, Masayoshi Ishida: A Proposal for Stable and Smooth Power Supply Control Method of the Photovoltaic/Fuel Cell/Lithium-ion Battery System Based on the Experimental Dynamic Characteristics of the Components, IEEJ student conference, Tokyo 2013 (oral)

2, Thu Thi Hoai Nguyen, Tomonori Nakayama, Masayoshi Ishida: Power Control Method Using Kalman Filter Prediction for Stable Operation of PV/FC/LiB Hybrid Power System Based on Experimental Dynamic Characteristics, Grand Renewable Energy, Tokyo 2014, CDROM proceedings.

3, Thu Thi Hoai Nguyen, Tomonori Nakayama, Masayoshi Ishida, Downsizing the Battery Capacity Requirement of Photovoltaic/Hydrogen Systems by Adjusting the Asymmetric Time Series Using Improved Prediction - Based Power Management

Strategy, 51st International Universities' Power Engineering Conference (UPEC) 6-9 September 2016, Coimbra, Portugal, Proceedings.

4, Tomonori Nakayama, Katsuya Mineno, Thu Thi Hoai Nguyen, Masayoshi Ishida: A method for capacity designing of a photovoltaic power generation with a battery using annual total amount of solar radiation analysis model, 51st International Universities' Power Engineering Conference (UPEC) 6-9 September 2016, Coimbra, Portugal, Proceedings.

Acknowledgement

Undertaking this PhD has been a truly life-changing and memorable experience for me and it would not have been possible to do without the support and guidance that I received from many people. I would like to give many thanks to all these people.

First of foremost, I would like to express my sincere gratitude to my supervisors, Prof. Masayoshi Ishida (University of Tsukuba) for all the support and encouragement he gave me during the PhD course. He has been a tremendous mentor for me. I have learned a lot from him, without his help I could not have finished my dissertation successfully. His advices on research as well as on my career have been invaluable. The patience and motivation from him take me to overcome a series of difficulties in scientific research.

I would like to say a special thanks to Assistant Prof. Tomonori Nakayama (University of Tsukuba) for his contributions of time and ideas to make my Ph.D. experience productive and stimulating. Many thanks also to Assistant Prof. Nobuko Hanada (University of Tsukuba) for her valuable suggestion and advice during the lab seminar.

I would like to express my sincere thanks to all members in Energy Conversion Lab. of University of Tsukuba. Thanks to the Dr. Liu, Dr. Guo, Mr. Ahn, Mr. Mariano in PhD students group for talking, sharing experience, and sometimes having lunch/dinner together. Thanks to Mr. Toda, Mr. Mineno, Mr. Tachihara, Mr. Kawai, Mr. Shibata, Mr. Ito, and Mr. Sasaki in the electrical group for their help doing experiments or discussion in group seminar before any conference. I also would like to thank to Mr. Kawato, Mr. Kajino, Mr. Fukutake, Mr. Miyazaki, and many others in the lab for every help and conversation together. The lab has been a source of friendships as well as collaboration. Thanks to Ms. Miki and Ms. Yoshinaga who made all the administrative issues during my study in the lab. The time spent with the lab members during working in lab, the summer/winter trips and many parties was very fun, and will be my beautiful memories forever. They let me to adapt and closer to the real Japan and Japanese student life. The first time climbing to Mt. Fuji or the first time of skiing will be one of my memorable and unforgettable experiences.

I also would like to thank to my very first friends who came to the university at the same time with me for their interesting talk and conversation in Japanese class: Ms. Nora, Ms. Anna, Ms. Muti and Mr. Samuel. I will remember their help during my moving to apartment. All of us finally finished the Master or the Doctoral course.

I wish to say special thanks to Vietnamese friends, Ms. Le Phuong, Ms. Hang, Ms. Thao, Ms. Van, Ms. Hoang Anh, Ms. Le, Ms. Tu, Ms. Duong, Ms. Thuy, Mr. Long and his wife, Ms. Thuy, and many other friends in Vietnamese student community who always help me to overcome the difficulty and encourage me during my life in Japan. I will keep in my mind the memory together such as visiting many parks in spring, holding parties to celebrate lunar New Year, to welcome newcomers or simply to share the homesickness. It is also my fortunate to join the Betoaji cooking class to introduce Vietnamese cuisine.

To my home university, I would like to thank my colleagues in Department of Power Systems, School of Electrical Engineering, Hanoi University of Science and Technology for their undertaking the work in the department, supporting me to study abroad in a long time, encouraging me or giving me some advices when my work was at a standstill.

I would like to thank Japanese Government for the financial support (MEXT Scholarship) during the Doctoral course.

Finally, I would like to say a heartfelt thank you to my family for always believing in me and encouraging me to follow my dream. My parents' unconditional love and care have always been spent for my sister and me. I would not have done the PhD course without them. My sister, to whom I can share every feeling almost every day, has been a best friend all my life, thank her for her consideration. I thank my nephew, who I witnessed the growing up from a baby until I came to Japan; I always miss him very much. I would like to thank to my parents in law for supporting and caring me, and not putting pressure on me although I have had to study in such a long time. And last but not least, I am greatly indebted to my husband, Dr. D.Q. Khanh who has been staying by my side throughout my PhD even when I felt irritable and depressed. The past several years have not been easy, both academically and personally, but he still has faith in me.

Thank you very much. I will do my best and keep going on.

Tôi muốn được gửi lời cảm ơn chân thành tới gia đình, bạn bè và đồng nghiệp đã luôn ở bên cạnh tôi, động viên tôi vượt qua mọi khó khăn trong quá trình học tập tại Nhật Bản để đạt được học vị Tiến sỹ như ngày hôm nay.

Con xin cảm ơn bố mẹ đã luôn tôn trọng và tin tưởng vào các lựa chọn của con, động viên con cố gắng học hành. Thời gian 5 năm ở Nhật đã cho con rất nhiều những trải nghiệm thú vị và những bài học hữu ích, từ cuộc sống hàng ngày đến công việc nghiên cứu. Bên cạnh đó, trong 5 năm ấy, thực sự là đã có những khoảng thời gian rất tệ, nhưng nhờ có bố mẹ, có gia đình mà con đã vượt qua. Con sẽ tiếp tục cố gắng hơn nữa.

Xin cảm ơn mọi người!